공학박사학위논문

직교격자계에서 Cut Cell을 고려한 정확한 주조공정용 유동 해석

Accurate Mold Filling Simulation using Cut Cell in the Cartesian Grid System

2018년 2월

서울대학교 대학원

기계항공공학부

최 영 심

직교격자계에서 Cut Cell을 고려한 정확한 주조공정용 유동 해석

Accurate Mold Filling Simulation using Cut Cell in the Cartesian grid system

지도교수 김 규 홍

이 논문을 공학박사 학위논문으로 제출함

2017년 11월

서울대학교 대학원

기계항공공학부

최 영 심

최영심의 공학박사 학위논문을 인준함

2017년 12월

위 원 장 : 이 관 중

부위원장 : 김 규 홍

위 원 : 이 신 형

위 원 : 황 호 영

위 원 : 강 형 민

Abstract

Accurate Mold Filling Simulation using Cut Cell in the Cartesian Grid System

Youngsim Choi
School of Mechanical and Aerospace Engineering
The Graduate School
Seoul National University

In the field of casting flow analysis, despite good quality analysis results it is difficult to apply body-fitted grid. This is on account of difficulties in grid generation and efficiency. Cartesian grid based numerical techniques for casting flow have been developed to address this issue. However, the Cartesian grid cannot be used to accurately represent complex shapes with many sloped and curved surfaces. A step grid that does not match the precise geometry leads to unsound results in flow analysis, such as loss of momentum during flow and false filling pattern.

In this study, a Cut Cell method based on Partial Cell Treatment is applied to the casting flow analysis in the Cartesian grid system.

The newly developed numerical method is then verified in comparison with

water model experiments and practical casting experiments. The conventional and Cut Cell methods of using the Cartesian grid are also compared. The numerical results of the two methods are compared according to the number of grids, and it is confirmed that the increased number of grids cannot solve the disadvantages of the Cartesian grid. In addition, the practical castings are analyzed for each casting process. It is confirmed that the numerical error in the conventional method can be rectified by the Cut Cell method. Finally, the computational time of the conventional method and the Cut Cell method are compared.

In conclusion, it is confirmed more accurate Cartesian grid based casting flow analysis is possible by using Cut Cell method without Body-Fitted Coordinate. However the Cut Cell method involves a long calculation time. There may be no significant difference between the two methods depending on the shape of castings or the casting process. Therefore, in the analysis of casting flow, it is necessary to selectively use the conventional Cartesian grid method or the Cut Cell method considering the accuracy and efficiency of analysis.

Key words: Casting process, Mold filling simulation, Cut Cell, Cartesian grid system, Accuracy, Filling pattern, Water model experiment

Student Number: 2009-30173

Table of Contents

Abstract I

Table of Contents III

Nomenclature V

List of figures VII

List of tables X

1. Introduction 1

1.1 Casting 1

1.1.1 Casting process 1

1.1.2 Mold filling simulation 6

1.2 Cartesian cut cell approach 10

1.3 Research objectives 12

2. Numerical method 14

2.1 Casting flow analysis 14

2.1.1 Characteristics of molten metal 14

2.1.2 Governing equations 16

2.2 Cut Cell method 20

2.2.1 Partial cell treatment 20

2.2.2 Governing equations 22

3. Experimental and numerical validations 23

3.1 Experimental validation 23

3.1.1 Water model experiment 23

3.1.2 Comparison of experiments with numerical results 26

3.1.3 Comparison with numerical results of the BFC system 48

3.2 Comparison with experimental results by Mampaey 52

3.3 Numerical validation 57
3.3.1 Comparison of energy loss rate by the number of grids 58
3.3.2 Effects of pouring rate change 61
3.3.3 Effects of width reduction 64
4. Simulation results and analysis 68
4.1 Comparison of results according to the number of grids 68
4.1.1 Model with a sloped ingate 69
4.1.2 Model with a circled mold cavity 77
4.2 Application of products by casting process 85
4.2.1 Sand casting 85
4.2.2 Gravity die casting 91
4.2.3 High pressure die casting 97
4.2.4 Low pressure die casting 107
4.3 Computational time 112
5. Conclusion 114
Reference 118
국문초록 124

Nomenclature

English symbols

d	distance
d_C	distance between the cell center
f	volume fraction of fluid
$\vec{g}$	acceleration of gravity
p	pressure
p_n	neighboring pressure
p_s	surface pressure
Re	Reynolds number
T_L	liquidus temperature
T_S	solidus temperature
t	time
$\vec{u}$	velocity vector
u	x-component of velocity
v	y-component of velocity
w	z-component of velocity

Greek symbols

θ	partial cell parameter
ν	kinematic viscosity
ρ	density

Abbreviations

BFC	Body-Fitted Coordinate
CAE	Computer-Aided Engineering
CFD	Computational Fluid Dynamics

DAFA Donor and Acceptor Flux Approximation

DFDM Direct Finite Difference Method

FDM Finite Difference Method

FEM Finite Element Method

FVM Finite Volume Method

PCT Partial Cell Treatment

PSOR Point Successive Over-Relaxation method

S.R.G Sprue-Runner-Ingate

Acronyms

MAC Marker And Cell

SIMPLE Semi-Implicit Method for Pressure-Linked Equations

SMAC Simplified Marker And Cell

SOLA A SOLution Algorithm for transient fluid flow

VOF Volume Of Fluid

List of figures

Fig. 1.1 Schematic illustration of a riser-gated casting 1
Fig. 1.2 Defects of a mold filling stage..... 4
Fig. 1.3 Types of gating system: (a) and (b)..... 5
Fig. 1.4 Original shape and generated meshes 7
Fig. 1.5 Filling sequence of L-curved cavity 9
Fig. 1.6 Sketch of body representation by PCT method..... 11
Fig. 2.1 Cooling curves of alloys 14
Fig. 2.2 Pressure in the free surface cell 17
Fig. 2.3 Volume fraction of molten metal at a cell 18
Fig. 2.4 Cut cells on surface of a circle..... 21
Fig. 3.1 Equipment for water model experiment 25
Fig. 3.2 FASTCAM Viewer..... 25
Fig. 3.3 Drawings..... 27
Fig. 3.4 Acrylic device 28
Fig. 3.5 3D model and meshes..... 28
Fig. 3.6 Experimental results of water model according to pouring time..... 31
Fig. 3.7 Results of the conventional method according to pouring time 33
Fig. 3.8 Results of Cut Cell method according to pouring time..... 33
Fig. 3.9 Close-up results of water model experiment in the runner 36
Fig. 3.10 Close-up results of the conventional method in the runner..... 36
Fig. 3.11 Close-up results of Cut Cell method in the runner 36
Fig. 3.12 Drawings..... 38
Fig. 3.13 Acrylic device 39
Fig. 3.14 3D model and meshes..... 39
Fig. 3.15 Experimental results of water model according to pouring time..... 42
Fig. 3.16 Results of the conventional (left) and Cut Cell (right) methods..... 45
Fig. 3.17 Meshes of BFC for Case 1 49
Fig. 3.18 Meshes of BFC for Case 2 49
Fig. 3.19 Comparison of simulation results for Case 1..... 50
Fig. 3.20 Comparison of simulation results for Case 2..... 51
Fig. 3.21 Dimensions of physical models..... 54

Fig. 3.22 Experimental mold filling sequence 55
Fig. 3.23 Numerical mold filling sequence 55
Fig. 3.24 Experimental mold filling sequence with a curved gating system 56
Fig. 3.25 Numerical mold filling sequence with a curved gating system 56
Fig. 3.26 Dimensions of a sloped runner model 57
Fig. 3.27 Meshes of 1 and 5 times the number of grids 58
Fig. 3.28 Comparison of mass flow error by the number of grids 60
Fig. 3.29 Comparison of momentum loss error by the number of grids 60
Fig. 3.30 Comparison of momentum loss at 30cm/s 62
Fig. 3.31 Comparison of momentum loss at 180cm/s 62
Fig. 3.32 Momentum loss of the conventional method with pouring rate 63
Fig. 3.33 Momentum loss of the Cut Cell method with pouring rate 63
Fig. 3.34 Dimensions of sloped runners with widths of 5 and 10 mm 65
Fig. 3.35 Momentum loss of the two methods at a width of 5 mm 66
Fig. 3.36 Momentum loss of the two methods at a width of 10 mm 66
Fig. 3.37 Momentum loss of the conventional method by width 67
Fig. 3.38 Momentum loss of the Cut Cell method by width 67
Fig. 4.1 3D model of a casting product 70
Fig. 4.2 Coarse meshes 70
Fig. 4.3 Fine meshes 70
Fig. 4.4 Results of conventional method by the coarse meshes 73
Fig. 4.5 Results of Cut Cell method by the coarse meshes 74
Fig. 4.6 Results of conventional method by the fine meshes 75
Fig. 4.7 The velocity color contour of two methods at 30 % 76
Fig. 4.8 3D model of a casting product 78
Fig. 4.9 Coarse meshes 78
Fig. 4.10 Fine meshes 78
Fig. 4.11 Results of conventional method by the coarse meshes 81
Fig. 4.12 Results of Cut Cell method by the coarse meshes 81
Fig. 4.13 Results of conventional method by the fine meshes 82
Fig. 4.14 Results of Cut Cell method by the fine meshes 82
Fig. 4.15 Comparison of the velocity contour with the two methods at 50 % 83
Fig. 4.16 Comparison of the velocity vector with the two methods at 50 % 84

Fig. 4.17 3D model of a casting product 86
Fig. 4.18 Results of the two methods according to the filling rate (1) 88
Fig. 4.19 Results of the two methods according to the filling rate (2) 89
Fig. 4.20 Results of the conventional method by the fine meshes 90
Fig. 4.21 3D model of a propeller 92
Fig. 4.22 Results of the two methods at the 24, 30, 60 % 94
Fig. 4.23 Velocity contour at the 30, 40, 60 % 95
Fig. 4.24 Results of the conventional method by the fine meshes 96
Fig. 4.25 3D model of a casting product 98
Fig. 4.26 Results of the conventional method for air conditioner compressor 100
Fig. 4.27 Results of Cut Cell method for air conditioner compressor 101
Fig. 4.28 Results of the conventional method by the fine meshes 102
Fig. 4.29 Velocity contour of the conventional method at the x-z plane 103
Fig. 4.30 Velocity contour of Cut Cell method at the x-z plane 103
Fig. 4.31 Velocity vector at the cross section of the x-z plane 103
Fig. 4.32 Real castings of an automotive air conditioner compressor 105
Fig. 4.33 Casting design based on the result of Cut Cell method 105
Fig. 4.34 Casting design based on the result of the conventional method 105
Fig. 4.35 Simulation results of Cut Cell method by the casting design 106
Fig. 4.36 3D model of an aluminum alloy wheel 108
Fig. 4.37 Results of the two methods according to the filling rate 110
Fig. 4.38 Velocity contour of the two methods at the 12 %, 30 % and 70 % 111

List of tables

Table 3.1 Experimental data 53
Table 3.2 Work conditions 53
Table 4.1 Analysis conditions 69
Table 4.2 Analysis conditions 77
Table 4.3 Analysis conditions 86
Table 4.4 Analysis conditions 91
Table 4.5 Analysis conditions 97
Table 4.6 Pressurized conditions 107
Table 4.7 Analysis conditions 107
Table 4.8 Computational time (s) for the cases 113

Chapter 1. Introduction

1.1 Casting

1.1.1 Casting process

Casting is a manufacturing process by which molten metal is poured into a mold and solidified. In other words, casting consists of the processes of mold filling and solidification. Obtaining a good casting thus means making a product free of casting defects. There are many factors that lead to casting defects: characteristics of the metal, fluidity of the molten metal in the mold, thermal properties of the mold, shrinkage during solidification etc. Appropriate casting design is essential to produce good quality castings [1]. An unsound casting design leads to many casting defects during the pouring and solidification of the melt [2].

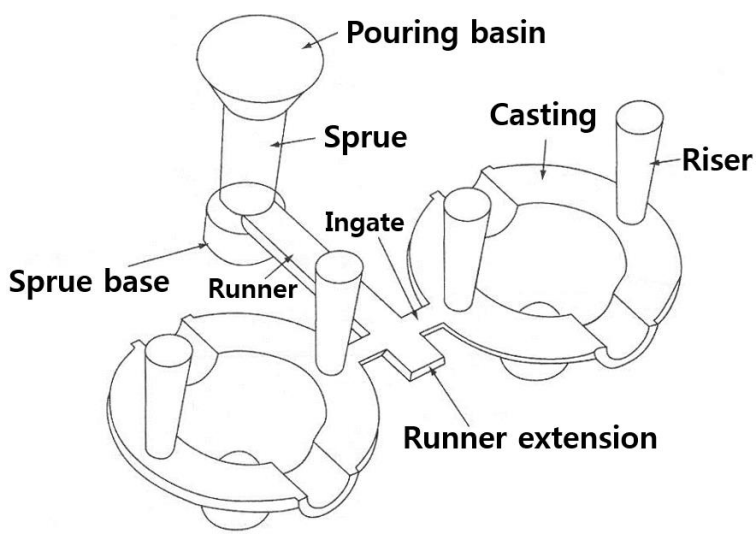

Fig. 1.1 Schematic illustration of a riser-gated casting

J. Campbell et al. investigated the fundamentals of obtaining defect-free castings and introduced well-designed gating systems and major design parameters [3-8]. It is difficult to obtain a complete casting design at the design stage. In the past, gating systems and risers were designed using either theoretically calculated gating ratio or experience. Then, test casting was repeated or prototypes were produced and modified [9]. Computer simulations have been used extensively in the casting industry for decades now, since the introduction of Computer-Aided Engineering (CAE) [10, 11]. The primary purposes of computer simulation of casting are to prevent defects, improve productivity, shorten periods of development, and save energy. Computer simulation of the casting process includes mold filling simulation, solidification simulation, prediction of defects, and optimization of casting design.

In the process of pouring, the flow of molten metal is controlled through gating system design. The important factors in the design of gating system are the fluidity of molten metal in the mold, pouring temperature, pouring time, i.e., pouring velocity, and the gating ratio [1]. Using the casting flow simulation, it is possible to grasp the flow pattern, find the final filling area, and determine the proper temperature to be applied at the time of pouring. Studies on mold filling simulation for each casting process and various physical phenomena of casting flow have been conducted [12-16].

In the process of solidification of the molten metal, a riser design is required to fill the shortage of the molten metal caused by shrinkage. This is also necessary for

inducing directional solidification. Solidification simulation can be used to determine the size and location of the riser. Heat transfer between the casting and the mold plays an important role during the solidification process. Simulation of solidification can be used to obtain temperature distribution of the mold, which is an important factor that can contribute to improved casting quality. Many researchers have studied numerical methods for solidification simulation [17-20].

Flow and solidification simulations can predict casting defects. It is necessary to track gas porosity caused by the isolated air in the cavity or the gas dissolved in the liquid materials during pouring [21]. To predict shrinkage defects during solidification, the best known method is to use the Niyama Criterion [22]. There are various methods to predict casting defects using computer simulations [23-27].

- **Mold filling related defects**

In recent years, the foundry industry is becoming increasingly aware that it is important to develop casting design at the mold filling stage to manufacture castings with sound metallurgical and dimensional accuracy. Mold filling related defects include misruns, cold shuts, gas porosity, and inclusion. A misrun occurs when the molten metal does not completely fill the mold cavity. A cold shut occurs when the melt does not mix completely at the point where it merges. These defects are mainly caused by lack of fluidity of the molten metal in the mold cavity. Gas porosity can occur when inaccurate gating system design leads to isolated space in the cavity. Inclusion defects occur when sand particles, metal oxides, etc. are

mixed into the melt and remain in the product. The types of inclusions vary depending on the cause of the improper process. An accurate gating system design can control defects during this pouring process.

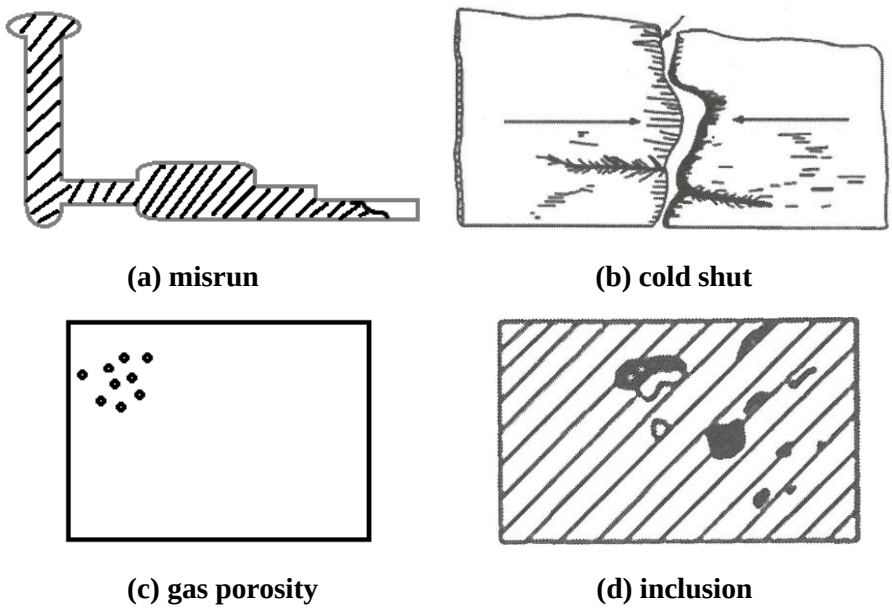

(a) misrun **(b) cold shut**

(c) gas porosity **(d) inclusion**

Fig.1.2 Defects of a mold filling stage

- **Gating system**

Sprue, runner, ingate, etc., which directly control the flow of the molten metal, are the main components of a gating system. A well-designed gating system ensures smooth and complete flow of molten metal from the pouring basin to the mold cavity. The proportion of the cross sectional area of the Sprue-Runner-Ingate (S.R.G) is called the gating ratio. Typically, the cross sectional area of the sprue, the total cross sectional area of the runners, and the total cross sectional area of the

ingates are indicated. The gating systems consist of a pressurized gating system and an unpressurized gating system according to the gating ratio.

Fig. 1.3 (a) shows the pressurized gating system. The total cross sectional area decreases towards the mold cavity. Here, molten metal flows at high velocity leading to greater turbulence and chances of mold erosion. Fig. 1.3 (b) shows the unpressurized gating system. The total cross sectional area increases towards the mold cavity, thus realizing lower velocity and reduced turbulence.

The flow of the molten metal in the mold cavity, the pouring temperature, and the pouring time are very important considerations in the design of the gating system. The pouring time is determined in advance, and gating ratio is determined based on this. If pouring time is prolonged, solidification can start before the mold cavity is filled. If pouring time is too short, problems such as mold erosions and rough casting surfaces will occur.

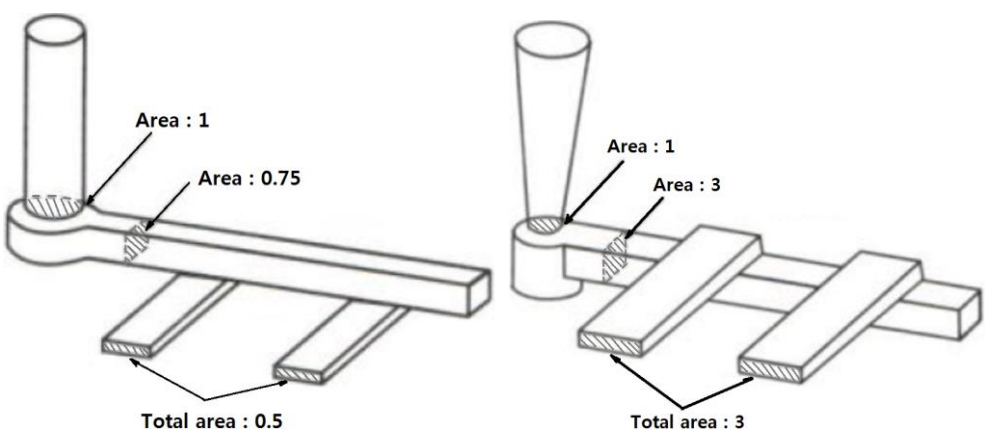

(a) Gating ratio 1:0.75:0.5 **(b) gating ratio 1:3:3**

Fig.1.3 (a) pressurized gating system and (b) unpressurized gating system

1.1.2 Mold filling simulation

The metallurgical integrity of castings is greatly influenced by the design of the gating system. Mold filling simulations, make it possible to assess in advance whether a gating system design is appropriate. In other words, the location, ratio, pouring temperature, and pouring rate of the gating system design can be verified by simulation. In this respect, it is important to accurately carry out the casting flow simulation.

Casting flow is two-phase flow with free surfaces between the molten metal and the air in the mold cavity. The existing numerical models of casting flow simulation that require free interface tracking are mostly based on MAC (Marker And Cell) [28], SMAC (Simplified Marker And Cell) [29] or SOLA-VOF (A SOLution Algorithm for transient fluid flow - Volume Of Fluid) [30]. These algorithms use finite volume techniques or finite difference techniques based on the Cartesian grid system. This grid system generates rectangular shaped grids (in the case of two dimensions) regardless of the appearance of the body, making it easy to generate grids without any particular skill; further, it does not take a long time to generate the grids [32]. If there are both castings and molds in a cell, it is determined as a cast or mold cell depending on the volume ratio of the casting in the cell. When generating grids of products with slopes or curves, grids are generated in a stepped shape, and for such reasons, the generated grids on Cartesian coordinates do not precisely reflect the original geometries (see Fig. 1.4). Therefore, fatal errors occur when considering a curved or thin-walled castings.

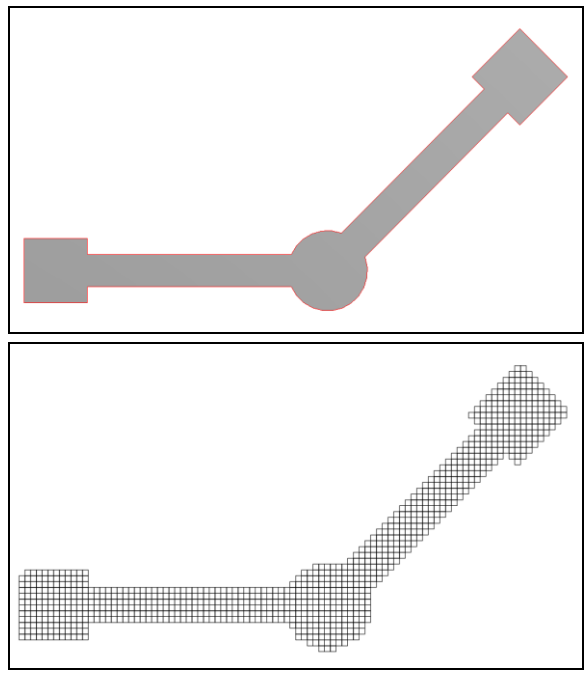

Fig.1.4 Original shape (above) and generated meshes (below)

Mampaey et al. [32] performed a numerical analysis of casting flow based on orthogonal curvilinear coordinates that employ a structured non-orthogonal mesh. Experimental and numerical analyses of castings with curved, straight, and stair shaped gating systems respectively were compared, and it was shown that the orthogonal mesh cannot reflect the casting behavior of the curved gating system accurately. Zhu et al. [33] studied a novel numerical technique based on the Direct Finite Difference Method (DFDM), which uses regular and irregular mixing elements to preserve the advantages of orthogonal meshing. Hetu et al. [34] applied Finite Element Method (FEM) to the analysis of casting flow and solidification. FEM generates meshes using triangular elements as well as tetrahedral elements, so

that the surfaces of the geometry can be expressed well. However, FEM is known to be less efficient in terms of computation time and memory size than FDM (Finite Difference Method) or FVM (Finite Volume Method). Hong et al. [35] developed the SIMPLE-BFC-VOF method based on a Body-Fitted Coordinate (BFC) system. They demonstrated that the simulation of casting shapes with curved and thin-walled surfaces can be accurately analyzed. However, the BFC method requires highly advanced techniques to generate grids. Also, it requires a lot of computational time even for a simple shape model. Furthermore modeling molds and casts at the same time is a very complex process.

Casting is a process that runs very quickly from development to completion, so computational time is an element that is just as important as the accuracy of mold filling simulation. In addition, since most casting products have complex geometries with many slopes and curves, it is very difficult to apply the BFC or FEM methods in casting flow simulation. For such reasons, the Cartesian grid system has been normally used in the casting flow analysis field.

Fig 1.5 shows the flow simulation results of an L-curved cavity by Lee et al. [36]. These results are analyzed by the Cartesian grid system (Fig. 1.5 (a)) and the BFC grid system (Fig 1.5 (b)), respectively. Pouring velocity is 1m/s. As shown in Fig. 1.5 (a), the velocity of molten metal decreases in the L-curved zone. Thus, the molten metal cannot reach the top of the cavity and flows downward. The results of Fig. 1.5 (b), on the other hand, represent that the melt advances upward well without decreasing the velocity. In this way, inaccurate flow results can be

obtained due to stepped grids that do not match the original geometries when performing a numerical analysis without any treatment in the Cartesian grid system. Therefore, special treatment is needed to carry out casting flow simulations in the Cartesian grid system.

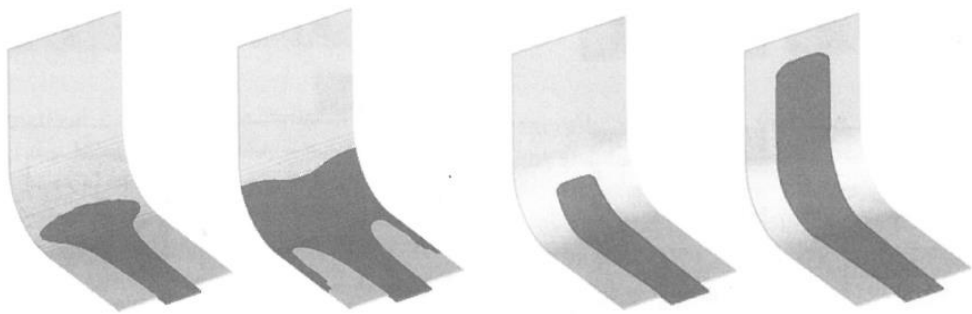

(a) Cartesian grid system **(b) BFC system**

Fig.1.5. Filling sequence of L-curved cavity

1.2 Cartesian cut cell approach

The first step when analyzing numerical properties in computational fluid dynamics (CFD) is to generate a grid in the computational domain. In order to obtain the exact values of the flow fields, it is crucial to generate an appropriate grid that fits the shape to be analyzed. There are a variety of techniques for creating a grid [37], but from a macroscopic point of view, they can be divided into body-fitted grids and shape-independent Cartesian grids [38]. It is difficult to generate a precise grid for complex shapes including sloped and curved surfaces. Traditionally, two approaches have been used: a structured body-fitted mesh [39-40] and an unstructured body-fitted mesh [41-43]. These grid systems can accurately represent the surface of the body, and high quality analytical solutions can be obtained using these systems. However, such a system requires significant efforts to generate a body-oriented grid [44]. Advanced techniques are required to create proper grids, and furthermore it takes a lot of time to generate such grids; sometimes time taken for generating such grids exceeds the computational time for the flow simulation [45].

An alternative to this is the Cartesian grid. The shape is located within the Cartesian grid system. The grids are then simply cut out by the shapes. The biggest disadvantage of the Cartesian grid is that it does not represent sloped and curved surfaces well. Three major strategies for solving these problems have been previously studied [46]: (a) interpolation/extrapolation [47], (b) insertion of local geometry [48], (c) trimming of surface cells. Tucker and Pan [46] proposed a new

hybrid Cartesian cut cell method for incompressible laminar flow. Yang et al. [49, 50] have successfully developed a cut cell method for complex moving shapes, assuming that there is only one cutting plane per every cut-off cell. Ingram et al. [45] applied a Cartesian cut cell method using cell merging technique to handle fluid-body interactions. Chung [51] implemented a two dimensional unsteady viscous incompressible flow with a cut-cell based Cartesian grid method. P. Lin [52] applied a Cartesian cut cell approach to simulate a moving body in a free surface flow in an orthogonal grid system. Volume of Fluid (VOF) method was used to track the free surface flow and partial cell treatment (PCT) was applied in order to consider solid surfaces.

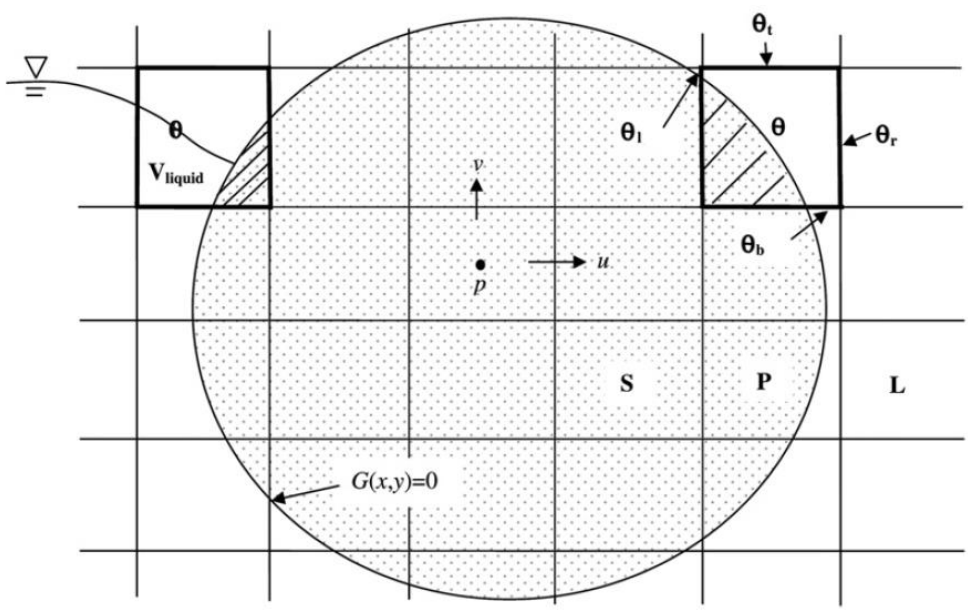

Fig.1.6 Sketch of body representation by PCT method in a staggered mesh system [52]

1.3 Research objectives

From the review of previous research addressed so far, it is seen that the Cartesian grid makes it easy to generate the grid for the flow analysis of the casting process. However, it is difficult to accurately express the shape surfaces, which is the biggest disadvantage. Distorted geometries can lead to incorrect flow analysis results. In particular, numerical analysis of castings with curved thin walls or castings with a curved or a stair shaped gating systems result in a large energy loss due to this stepped grid.

Many previous researchers have implemented BFC based numerical methods for mold filling simulations to solve these problems. However, generating a BFC grid requires advanced skills and much time. Therefore, the body-fitted grid is not a suitable alternative that can overcome this drawback.

Cartesian grid based numerical methods are still used in the casting flow field, and it is creating a large number of grids to avoid shape distortion problems. A Cartesian grid based numerical method requires a special treatment.

In this study, the Cut Cell method developed for accurate representation of geometries in the Cartesian grid is applied to the flow analysis within the casting process. The casting flow simulation reflects a free surface flow in which the molten metal flows through shapes cut by the Cartesian grid system. Using the method proposed by P. Lin [52] and considering the governing equations involving the partial ratio value of the cut-cell, a result similar to that of the body-fitted grid is obtained. Thus this method can provide accurate flow analysis results while

maintaining the advantages of the Cartesian grid system (convenient and fast grid creation).

The present work compares the results of the Cut Cell method with those of the conventional method without special treatments and confirms improvement in the accuracy of the casting flow analysis by the Cut Cell method. Flow analysis is performed for each casting process and how to utilize the Cut Cell method in the casting flow fields is investigated.

Chapter 2. Numerical method

2.1 Casting flow analysis

2.1.1 Characteristics of molten metal

The kinematic viscosity of molten metal is similar to that of water at room temperature, and so is the Reynolds number. In addition, the kinematic viscosity of the molten metal varies greatly with temperature below the liquidus temperature, T_L, but there is little change in the kinematic viscosity depending on temperature above T_L. Fig. 2.1 describes a cooling curve of alloys. Solidification begins at the liquidus temperature and solidification is completed at the solidus temperature, T_S. The liquidus temperature, however, does not mean that the pouring of the liquid metal is completed. During the mold filling process of actual casting, the temperature of the liquid metal may drop below the liquidus temperature.

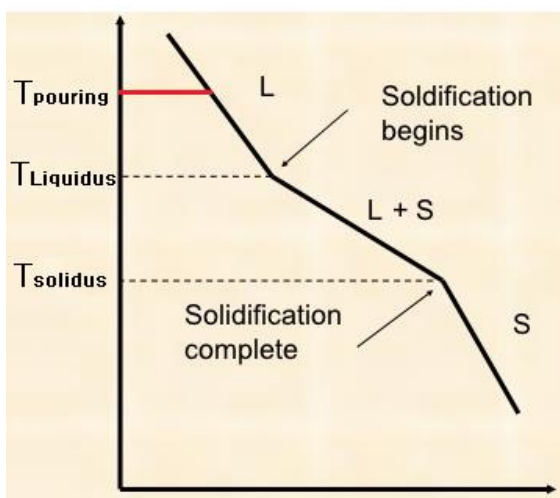

Fig.2.1 Cooling curves of alloys

The physical phenomenon of the mold filling process also includes solidification, but it depends on the shape of the castings and may proceed in a very locally area. Therefore, even though the temperature drops below the liquidus temperature, the kinematic viscosity is assumed to be temperature-independent in the casting flow analysis. The casting flow is assumed to be a three dimensional unsteady incompressible viscous flow with free surfaces.

In this paper, heat transfer analysis is not considered because it focuses on the correction of momentum loss and the flow pattern by applying the Cut Cell method in the Cartesian grid system.

2.1.2 Governing equations

The 3 dimensional unsteady incompressible viscous Navier-Stokes equations and the Volume of Fluid equation for free surface tracking in simulating mold filling have been solved.

Continuity Equation:

$$\nabla \cdot (\vec{u}) = 0 \tag{2.1}$$

Momentum Equation:

$$\frac{\partial(\vec{u})}{\partial t} + \nabla \cdot (\vec{u}\vec{u}) = -\frac{1}{\rho}\nabla p + \nu \nabla^2 \vec{u} + \vec{g} \tag{2.2}$$

Volume of Fluid Equation:

$$\frac{\partial(f)}{\partial t} + \nabla \cdot (f\vec{u}) = 0 \tag{2.3}$$

Here, $\vec{u}$ is the velocity, $\vec{g}$ is acceleration due to gravity, ν is the kinematic viscosity, ρ is the density, p is the pressure and f is the volume fraction of fluid.

For the calculation of flow fields, the SOLA method was used, and the VOF method was used to track the free surface interface of the molten metal. The PSOR (Point Successive Over-Relaxation method) is used to calculate the pressure and velocity fields in the full cell.

■ **Free surface cell boundary condition**

In the SOLA-VOF method, the pressure of a surface cell in Fig. 2.2 is obtained from linear interpolation between a neighboring pressure and a surface pressure.

The interpolation function is given by

$$p_{ij} = (1 - \frac{d_c}{d}) p_n + \frac{d_c}{d} p_s \qquad (2.4)$$

Here, p_n is the neighboring pressure inside the fluid in a direction most nearly perpendicular to the free surface. p_s is the surface pressure computed from surface tension. d_c is the distance between the cell centers and d is the distance between the free surface and the center of the interpolation neighbor cell.

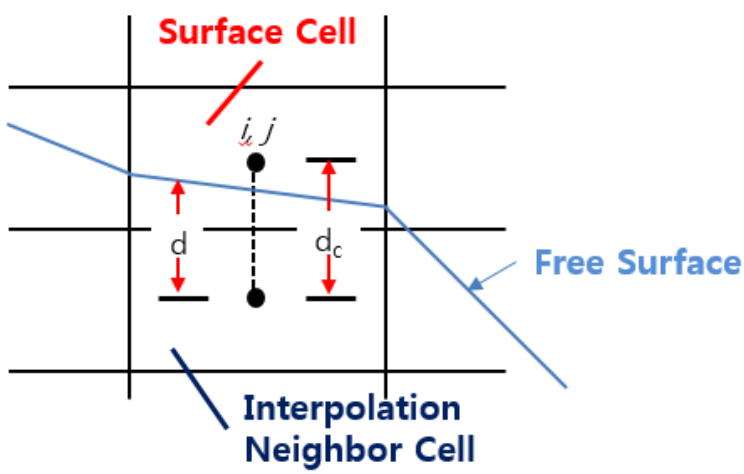

Fig.2.2 Pressure in the free surface cell

■ **VOF method for free surface tracking**

The VOF methods suggested by C. W. Hirt and B. D. Nichols [30] in 1981, one of the oldest multiphase flow analysis methods, uses the volume fraction that one of the fluids occupies in the control volume. The value of the volume fraction function in the VOF method has 0 or 1 in each non-interface cell and a value between 0 and 1 in the cell where surface interfaces exist (see Fig. 2.3).

First, the volume fraction is obtained by reconstructing an interface in the control volume in which surface interfaces exist. Then, the new volume fraction in the next time interval can be obtained from a given velocity field and the reconstructed volume fraction. The interface reconstruction algorithm for tracking free surfaces uses the Donor and Acceptor Flux Approximation (DAFA), which is usually used in the SOLA-VOF method.

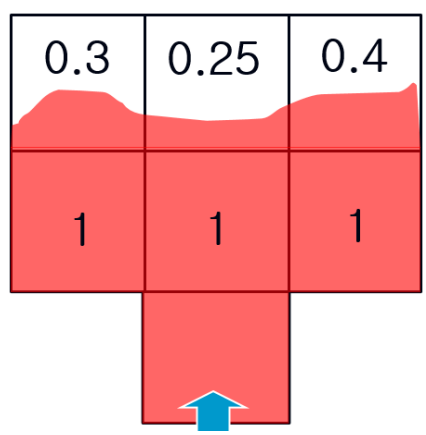

Fig.2.3 Volume fraction of molten metal at a cell

The VOF advection equation is as follows.

$$\frac{\partial f}{\partial t} + u\frac{\partial f}{\partial x} + v\frac{\partial f}{\partial y} + w\frac{\partial f}{\partial z} = 0 \tag{2.5}$$

where u, v, w are the velocity components in the x-, y-, and z-directions respectively; and f is the volume fraction that one of the fluids occupies in each cell.

Since the flow is incompressible, $\vec{u}$ satisfies Eq. (2.1).

A conservation law for the function f is obtained as follows.

$$\frac{\partial f}{\partial t} + \frac{\partial (uf)}{\partial x} + \frac{\partial (vf)}{\partial y} + \frac{\partial (wf)}{\partial z} = 0 \tag{2.6}$$

Eq. (2.6) represents the VOF function in the conservative form, in which volume conservation is equivalent to mass conservation. Due to discontinuous properties on the surface interfaces in multiphase flows, it is difficult to satisfy mass conservation in numerical calculation. In the VOF method, however, the equation itself satisfies mass conservation. This is a major advantage of the VOF method in the analysis of multiphase flows.

2.2 Cut Cell method

2.2.1 Partial cell treatment

The partial cell treatment (PCT) named by Kothe et al. [54] is another branch of Cartesian cut cell approach, and use the volume fraction and line fraction of the cut-off on a cell to represent shapes cut out by Cartesian grid. Compared to the stair-step representation of a curved surface in the Cartesian grid system, the PCT has a better representation of actual body geometry. P. Lin applied this method to simulate a moving solid body in a free surface flow in the Cartesian grid system. In this paper, PCT based the Cut Cell method is applied to simulate a free surface flow within the fixed empty mold.

Fig. 2.4 shows that grids for the model with a circular shape are created in the Cartesian coordinates. Here, the grids which include both casting and mold are defined as Cut Cells. On the other hand, in the Cartesian grid system, the cut cell is determined as the cast or mold cell according to the fraction of the cast in a cell. In Fig. 2.4, two cells in the upper left corner of the grid domain may become mold cells. The wall boundary condition have to be applied to the cell faces, but those cell faces are still exposed to actual velocities. Therefore, a special treatment is required to solve these problems.

In the cut cell, an openness function θ defined for the volume and the area of castings is used. When θ=0, it shows the mold part cell. When θ=1, it shows the cell of the casting part. When 0<θ<1, it shows the cell of the interface between casting and mold. Such a definition is very similar to the method for the Volume of

Fluid (VOF) function defining the free surface interface of molten metal. The difference is that function θ is used not only for the center of the grid, but also defining the ratio of the casting in the grid interfaces as well.

In the Cartesian coordinates, the grids are divided into casting and mold. In other words, they are divided into the flow calculation area and non-calculation area, but in the Cut Cell method, θ is used to calculate the grids treated as non-calculation areas. When taking a look at the cell indicated with bold lines in Fig. 2.4, θ_C shows the volume fraction of the casting at the center of the cell, and that value is used in the continuity equation and VOF equation. θ_R, and θ_L in the x axis and θ_F and θ_K of the y axis show the area fraction of the casting on each of the cell faces. In the case of three dimensions, θ_T and θ_B of the z axis direction were added. These values show the location of the body in the grids and are used in the momentum equation. Using the values of θ, the conservation of mass is calculated for the amount that the actual casting takes up in a cell and the VOF equation is made to calculate the free surface of the molten metal flow.

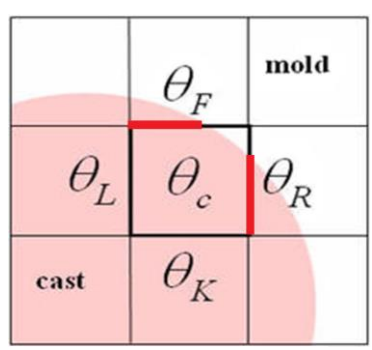

Fig.2.4 Cut cells on surface of a circle

In the Cut Cell method, θ is a variable that shows the original geometrical surface shape information in the calculating grids. Using these values, it is possible to compensate for loss of momentum that occur due to changed shapes or to correct the overload of pressure on the wall boundaries.

2.2.2 Governing equations

The continuity, momentum, and Volume of Fluid (VOF) equation for coupling with the function θ are shown below:

Continuity equation:

$$\nabla \cdot (\theta \vec{u}) = 0 \tag{2.7}$$

Momentum equation:

$$\frac{\partial(\theta \vec{u})}{\partial t} + \nabla \cdot (\theta \vec{u}\vec{u}) = -\frac{\theta}{\rho}\nabla p + \nu\theta\nabla^2 \vec{u} + \theta \vec{g} \tag{2.8}$$

Volume of fluid equation:

$$\frac{\partial(\theta f)}{\partial t} + \nabla \cdot (\theta f \vec{u}) = 0 \tag{2.9}$$

When applying the Cut Cell method in the governing equations, if the θ has sufficiently small value, it can cause an increase in numerical instability, and therefore, it is advised to set the θ value the amount of 0 for analysis.

Chapter 3. Numerical and experimental validations

3.1 Experimental validation

3.1.1 Water model experiment

In the casting process, the molten metal flow is at a high temperature when it is being poured into the mold, making it difficult to observe the inside. Water model experiments can be a useful alternative to casting experiments because these experiments make it possible to directly observe the fluid flow at relatively low cost and accurately identify the formation, movement and final filling position of gas porosity.

Several studies on the use of water models in casting flows have been carried out in the past. These studies concluded that flow behaviors of water and molten metals are similar under certain conditions [55-57]. The kinematic viscosity of liquid metal varies greatly with temperature below the liquidus temperature, but hardly changes above the liquidus temperature. The kinematic viscosity of water at room temperature (20℃) is similar to that of dissolved aluminum alloys [58]. Reynolds number (Re) defines the dynamic behavior of fluid flow. There is similarity between water and liquid metal when Reynolds number is the same [59]. Therefor many researchers are using water model experiments to reduce time and cost in casting design [60-64].

In the present study, water model experiments were conducted to verify the effectiveness of the developed Cut Cell method. Experimental apparatus were fabricated using transparent acrylic plastic with high visibility.

In Case 1, a gravity casting device with two simple cavities is designed. The numerical method is verified by comparing the water model test results with the Cut Cell method results. The symmetry is confirmed by comparing the result of the conventional method with the result of the Cut Cell method.

In Case 2, the casting shaped experimental device is designed by a gating system. The numerical results of the conventional and the Cut Cell methods are compared with the water model test results. The improved accuracy of Cut Cell method compared to the conventional method is confirmed.

The flow pattern is recorded using a high-speed video camera (FASTCAM-1024) from PHOTRON to visualize the water model experiment results (Fig 3.1). The high-speed camera is controlled by FASTCAM Viewer program (Fig. 3.2). Colored water with blue paint is used to improve visibility.

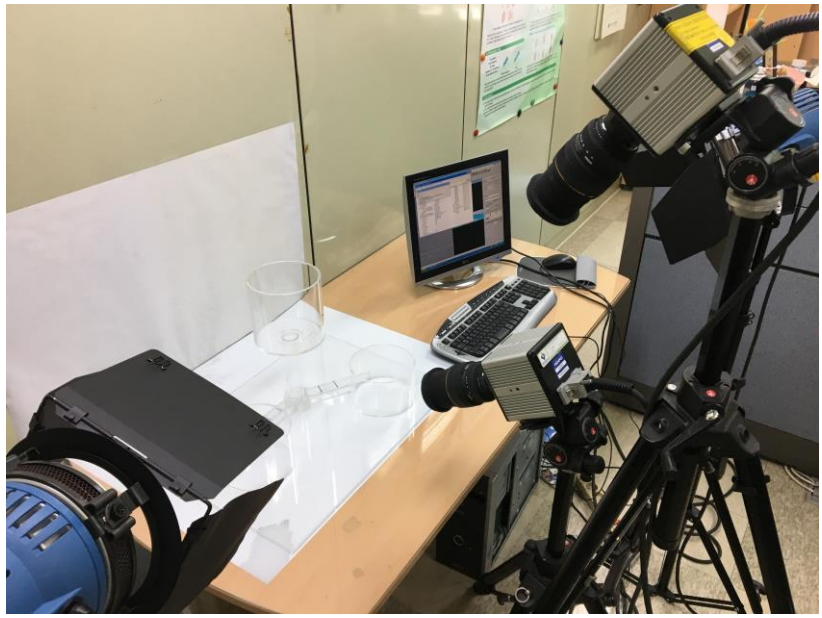

Fig. 3.1 Equipment for water model experiment

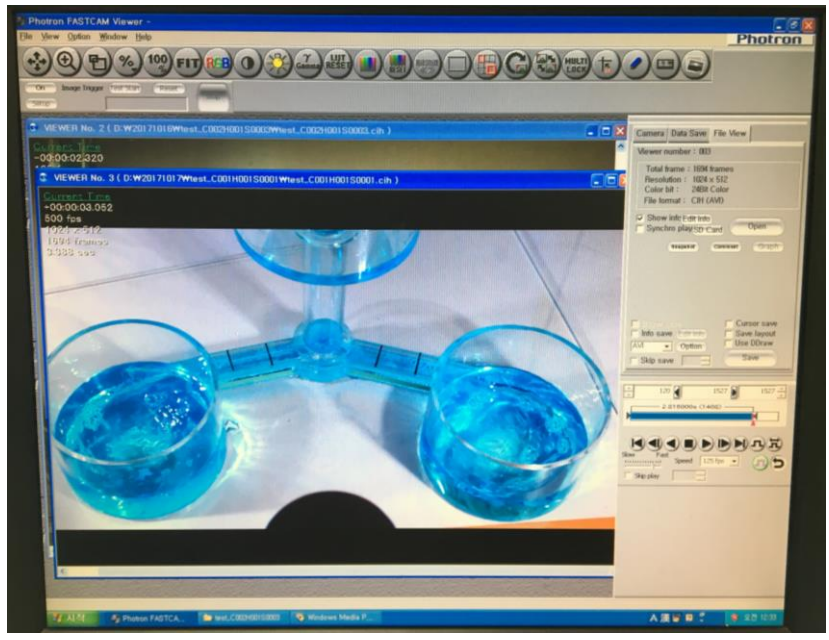

Fig. 3.2 FASTCAM Viewer

3.1.2 Comparison of experimental and numerical results

- **Case 1**

The first verification test uses a gravity casting shaped model with two simple, symmetric cavities. Liquid is poured from the basin, reaches the sprue base, and flows into each cavity through two runners at an angle of 150°. The model is designed to be symmetrical around the sprue. Therefore, it can be predicted that the poured water flows into each cavity at the same speed in the two runners. The pouring basin is filled with 1000 ml of water.

Two high-speed cameras are used. One of them covers the whole experimental device. The resolution of the high-speed video camera is 1024×512, and the flow pattern is stored at 500 frames per second. The other camera captures an enlarged view to confirm that the water enters the two runners in a symmetrical manner. The resolution of the high-speed camera is 1024×256, and the flow pattern is stored at 1000 frames per second.

Fig. 3.3 demonstrates drawings of the water model experimental device. Fig. 3.4 shows an experimental acrylic device. In order to confirm the symmetry of fluid flow in the two runners, lines were drawn at the same intervals in the runners of the acrylic device. Fig. 3.5 shows a 3D model and meshes used in the numerical analysis. The generated mesh is represented in the x-y plane. The grid size is 3.4 mm. The grid domain is 100×159×115, and the number of grids is 1,828,500. As the initial pouring condition of the analysis, 1000 ml of water is indicated in the pouring basin. Slip condition is applied as the boundary condition.

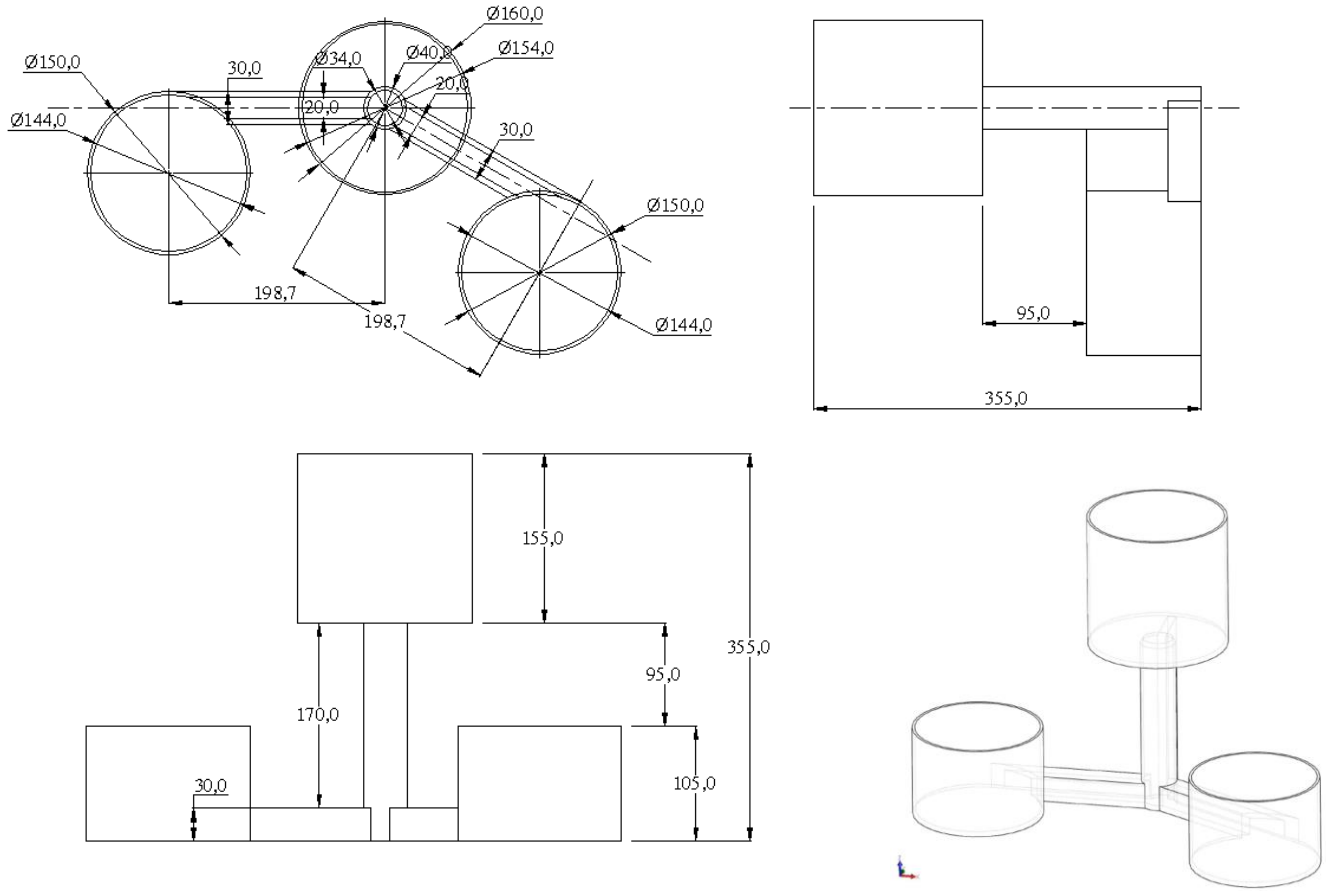

Fig. 3.3 Drawings

Fig. 3.4 Acrylic device

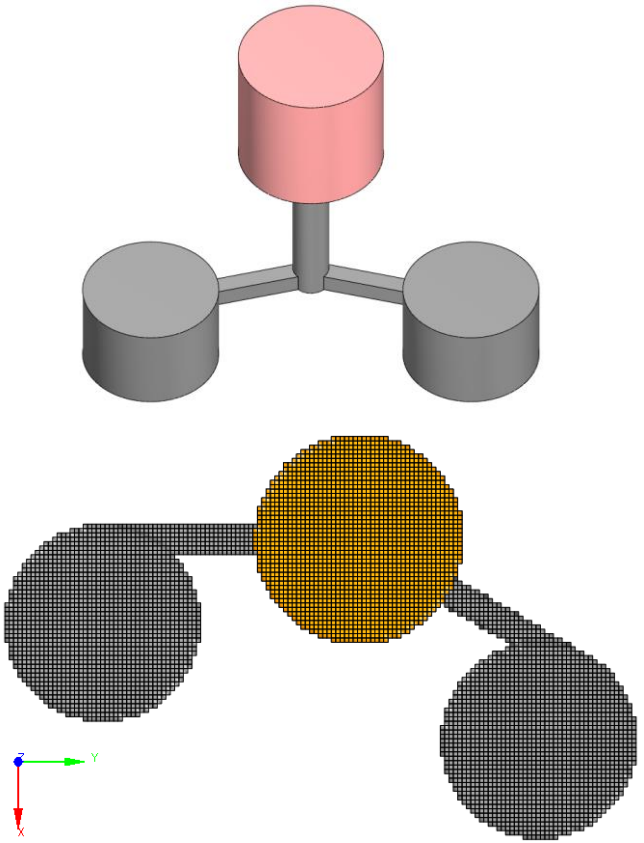

Fig. 3.5 3D model and meshes (100×159×115)

Fig. 3.6 (1-2) show the water model experimental results by pouring time. Water falling from the pouring basin passes through the sprue and enters the cavities at the same rate from two runners. Water passes through the sprue at 0.148 seconds and simultaneously enters the two cavities at 0.312 seconds. Water flows along the circular cavity and meets again near the ingate at 0.724 seconds. At 2.136 seconds, the pouring of 1,000 ml water is completed.

Fig. 3.7 (1-3) and Fig. 3.8 (1-3) show the numerical results of the water model using the conventional method and the Cut Cell method, respectively. One of the two runners symmetrical to the sprue is placed parallel to the axis and the other is inclined to the axis (see Fig. 3.5).

Fig. 3.7 (1)-(c) shows the result of the conventional method at 0.304 second. Water in the runner parallel to the coordinate axis flows faster than the water in the runner inclined to the axis. On the other hand, the result of the Cut Cell method (Fig. 3.8 (1)-(c)) shows that water flows symmetrically in the two runners. This result is consistent with the water model experimental result at 0.312 sec.

As shown in Fig. 3.8 (3), streams of water flowing along the circular cavity meets again near the ingate and water fills up at the same height in the two cavities. In Fig. 3.8 (1-3), it can be seen that the results of the Cut Cell method as a whole agree well with the water model results in a similar sequence.

The results of the conventional method are completely asymmetric, unlike in the water model (see Fig. 3.7 (1-3)). In the inclined runner, the velocity of water decreases due to the stepped grids. In the aligned runner, the grid coincides with

the original shape, so water flows without velocity decreasing. In Fig. 3.7 (3)-(a), due to the reduced velocity of water, water injected into the cavity with the inclined runner spreads out along the bottom of the cavity. The velocities in the two symmetrical runners vary. It can be seen that the final height of water in the two cavities is different after pouring water. That is unreasonable.

Fig. 3.9, Fig. 3.10, and Fig. 3.11 show the results of close-up on the runners. The results of the Cut Cell method (Fig. 3.11) show that water flows simultaneously in the two runners but the results of the conventional method (Fig. 3.10) do not.

The water model experimental results and the numerical results of the two methods are compared. The results of the Cut Cell method were in good agreement with those of the water model. On the other hand, the results of the conventional method in the Cartesian grid are not more accurate than those of the Cut Cell method.

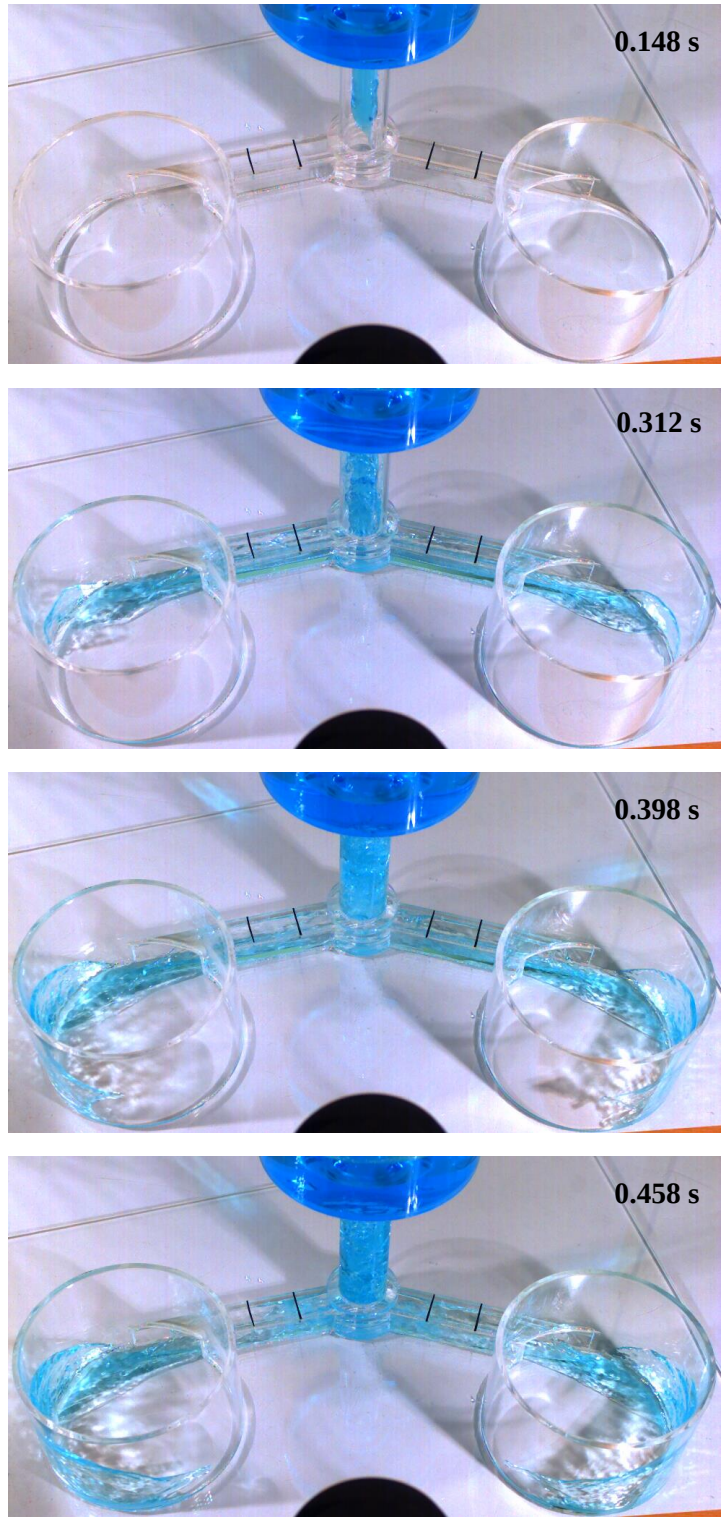

Fig. 3.6 Experimental results of water model according to pouring time (1)

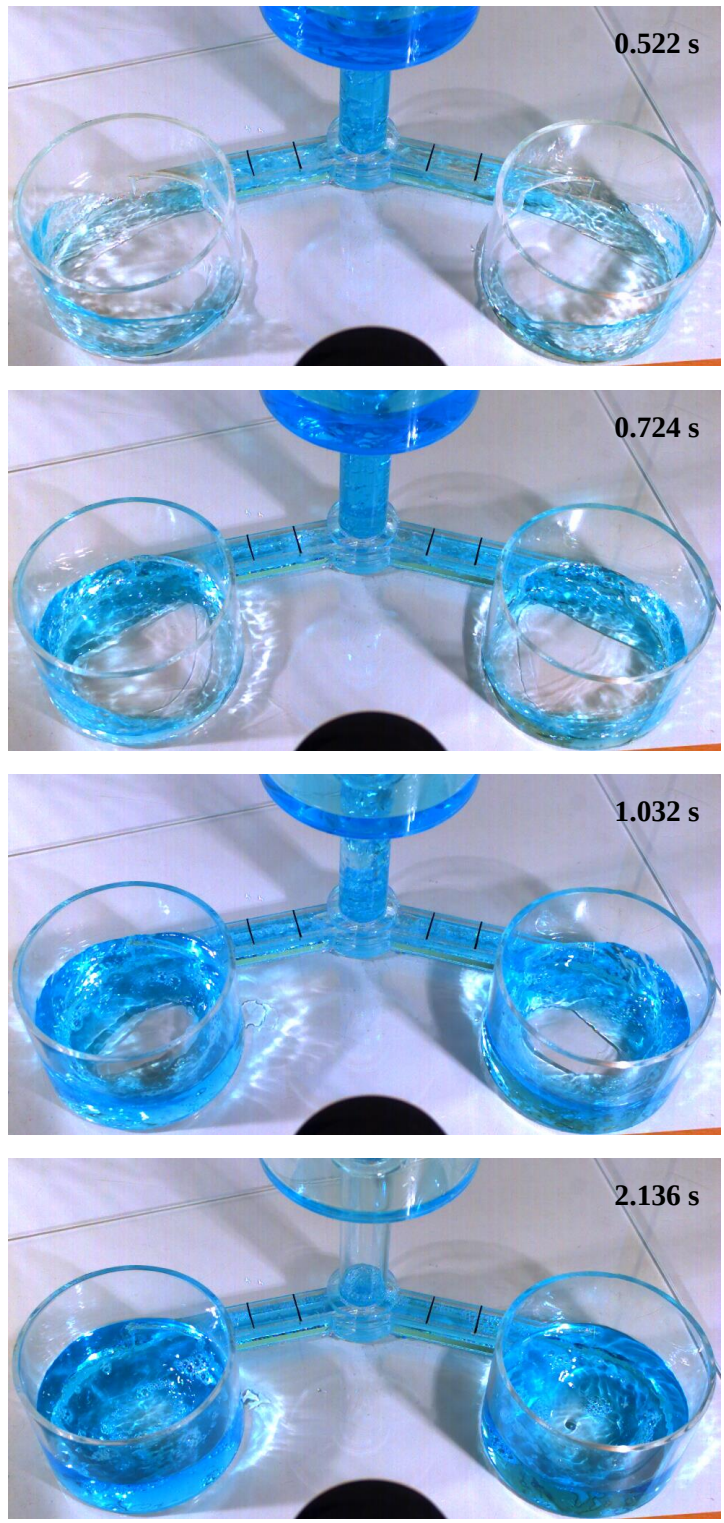

Fig. 3.6 Experimental results of water model according to pouring time (2)

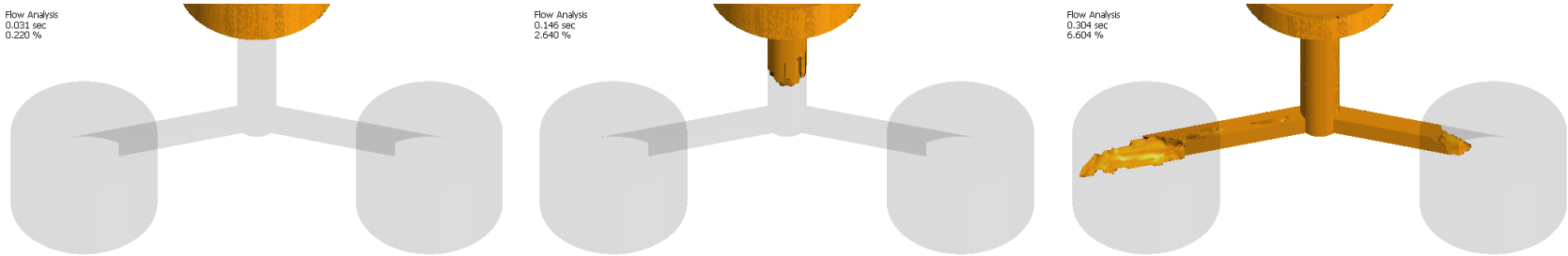

(a) 0.031 s **(b) 0.146 s** **(c) 0.304 s**

Fig. 3.7 Results of the conventional method according to pouring time (1)

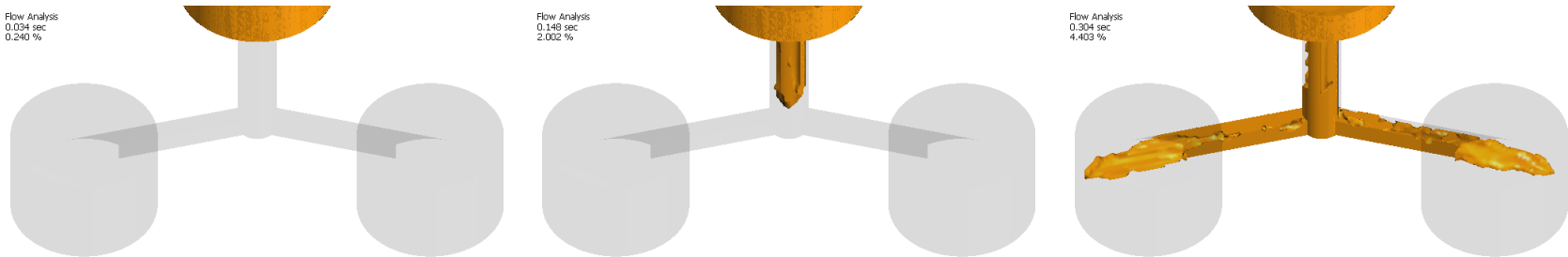

(a) 0.034 s **(b) 0.148 s** **(c) 0.304 s**

Fig. 3.8 Results of Cut Cell method according to pouring time (1)

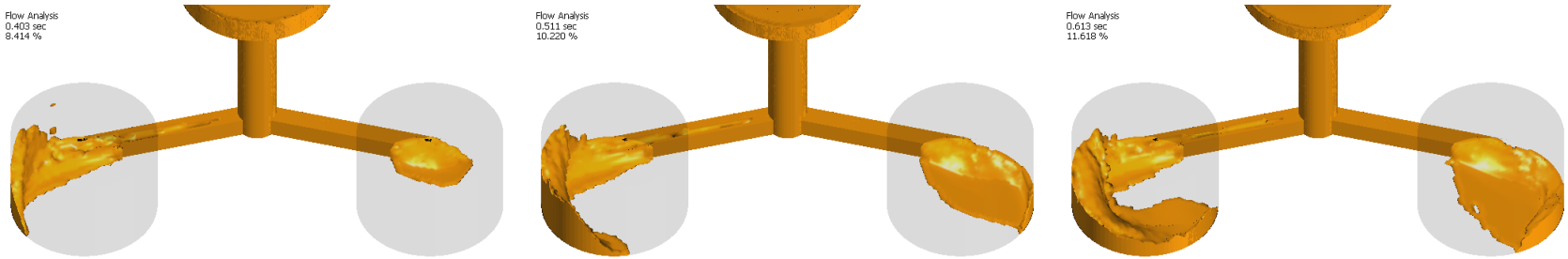

(a) 0.403 s **(b) 0.511 s** **(c) 0.613 s**

Fig. 3.7 Results of the conventional method according to pouring time (2)

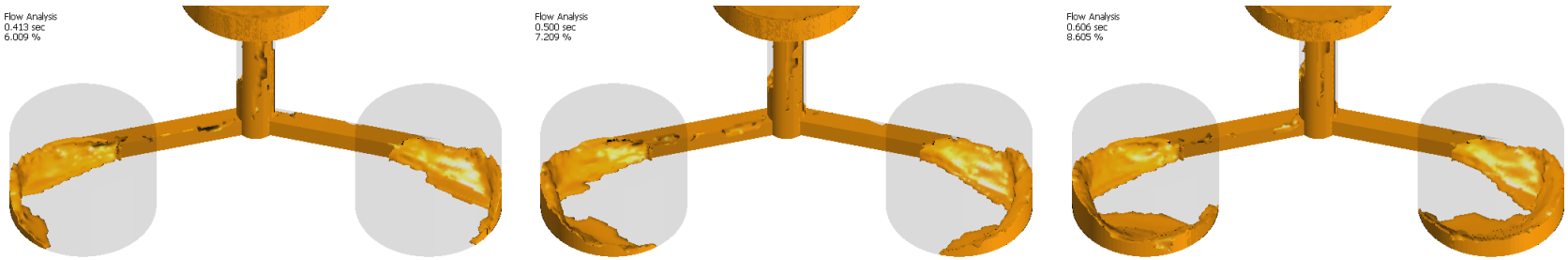

(a) 0.413 s **(b) 0.500 s** **(c) 0.606 s**

Fig. 3.8 Results of Cut Cell method according to pouring time (2)

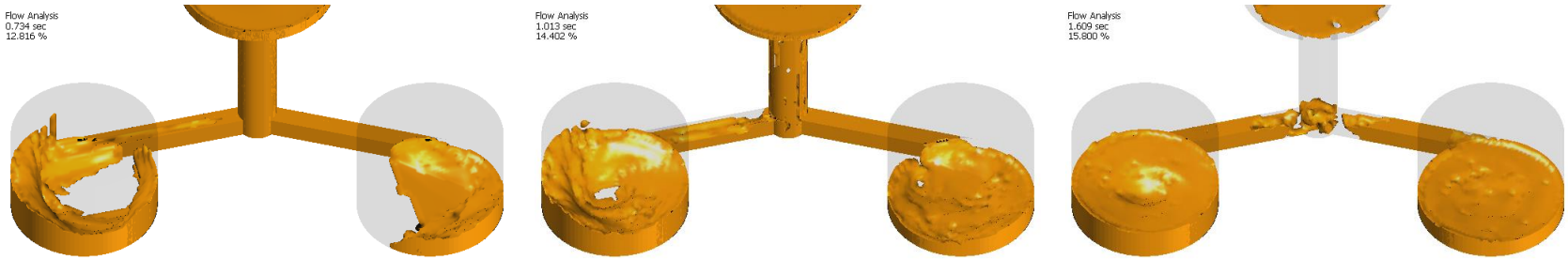

(a) 0.734 s **(b) 1.013 s** **(c) 1.609 s**

Fig. 3.7 Results of the conventional method according to pouring time (3)

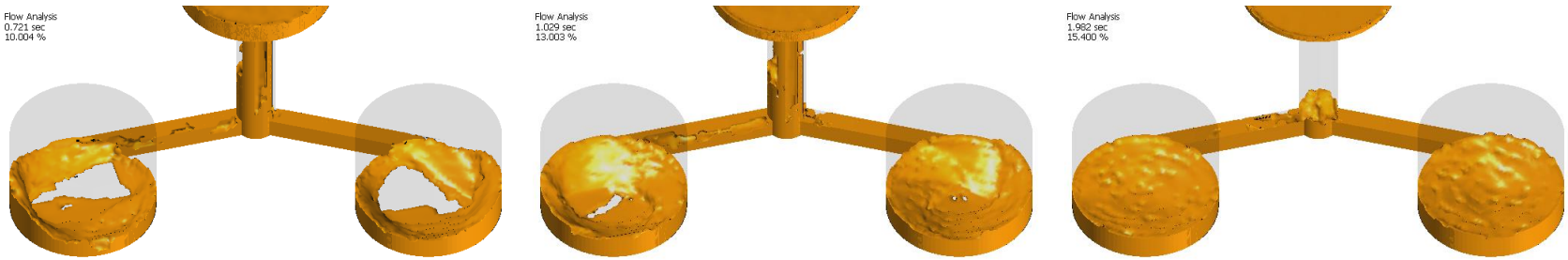

(a) 0.721 s **(b) 1.029 s** **(c) 1.982 s**

Fig. 3.8 Results of Cut Cell method according to pouring time (3)

Fig. 3.9 Close-up results of water model experiment in the runner

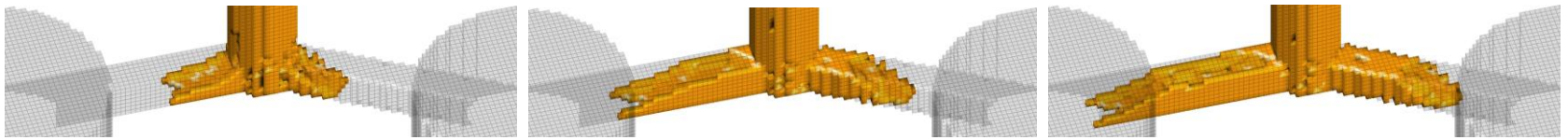

Fig. 3.10 Close-up results of the conventional method in the runner

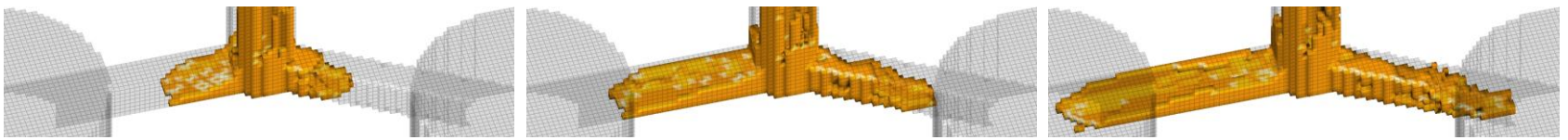

Fig. 3.11 Close-up results of Cut Cell method in the runner

■ **Case 2**

The second water model is a gravity casting shape in which three ingates are placed in a sloped runner. The device is fabricated according to a typical gating system design that is designed to pour molten metal sequentially from the Ingate 1 into the cavity [1]. Water enters into the three ingates through a sloping runner. Water should first flow into the ingate (Ingate 1), which is farthest from the pouring basin. As in the Case 1 described above, 3000 ml of water is filled in the pouring basin. The resolution of the high-speed video camera is 1024×1024, and the flow pattern is stored at 125 frames per second.

Fig. 3.12 is drawings of the water model experimental device. Fig. 3.13 shows an experimental acrylic device. Fig. 3.14 shows a 3D model and meshes used in the numerical analysis. The grid size is 3.54mm. The grid domain is 140×51×141, and the number of grids is 1,006,740. As the initial pouring condition of the analysis, 3000 ml of water is indicated in the pouring basin. Slip condition is applied as the boundary condition.

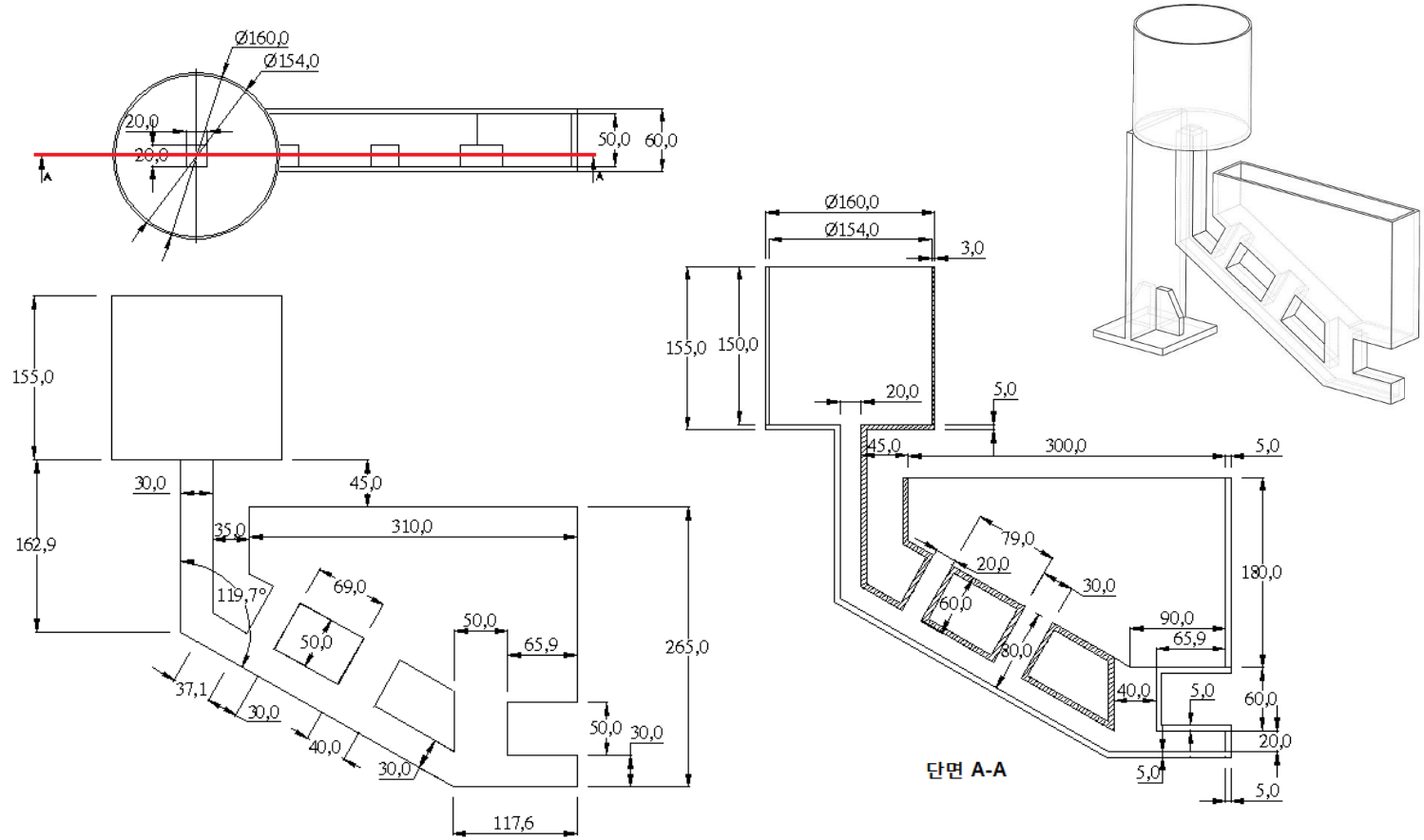

Fig. 3.12 Drawings

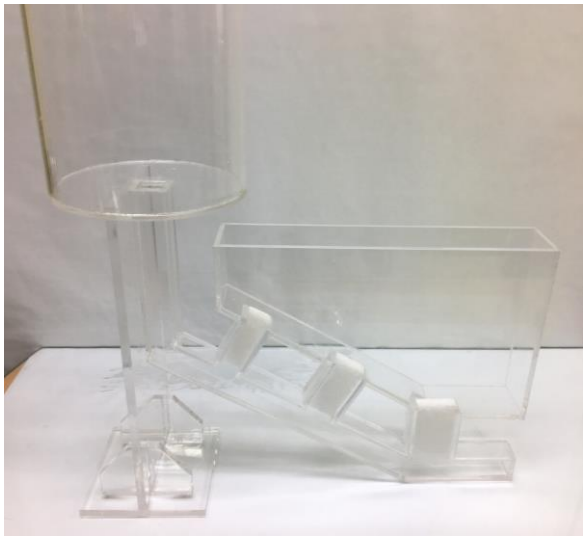

Fig. 3.13 Acrylic device

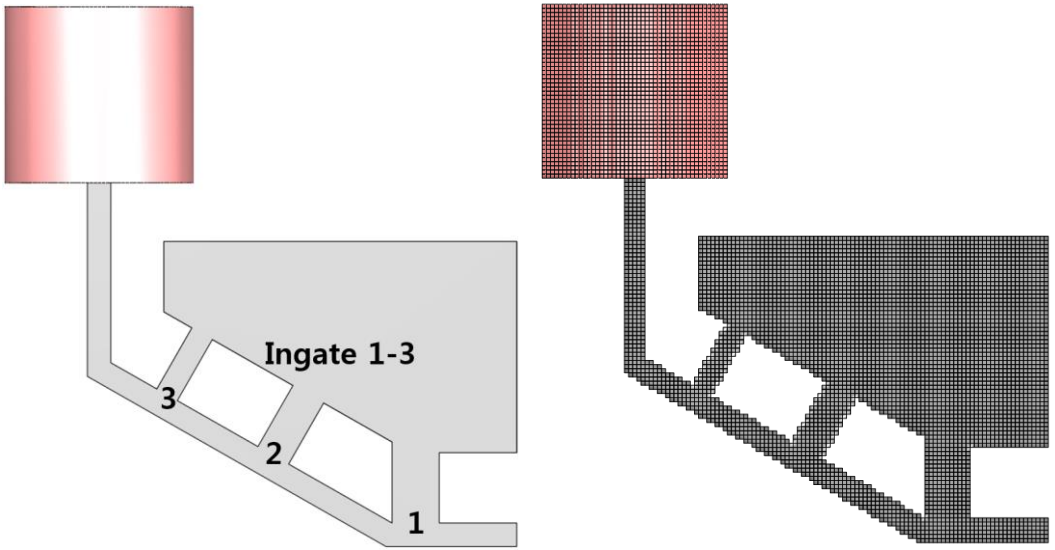

Fig. 3.14 3D model and meshes (140×51×141)

Fig. 3.15 presents the results of the high-speed camera photograph of the water model experiment. Based on the gating system, the poured water reaches the runner extension at the end of the runner, and flows into the cavity through the Ingate 1 at the farthest from the pouring basin. At 1.037 seconds, water flows into the Ingate 2. From 2.12 seconds, water flows into the Ingate 3 as can be seen.

Fig. 3.16 shows the numerical results of the water model using the conventional method and the Cut Cell method. Fig. 3.16 (left) shows the result of the conventional method and Fig. 3.16 (right) shows the results of applying the Cut Cell method.

From the results of the Cut Cell method, water takes 0.781 seconds to reach the runner extension. On the other hand, the result of the conventional method shows that water flows into the Ingate 3 near the pouring basin, thus not meeting the intended purpose of the gating system design.

The result of the Cut Cell method shows that water flows into the Ingate 1 at 0.914 seconds. For the same point of time, water reaches the runner extension by the conventional method. By the Cut Cell method, water flows into the cavity through the Ingate 2 at 1.313 seconds, as in the case of the water model. On the other hand, by the conventional method, water enters the cavity in the order of the ingates adjacent to the pouring basin. By the Cut Cell method, water begins to flow in the Ingate 3 at 2.11 seconds. After 2.775 seconds, results from both methods show water entering from all the three ingates.

The runner inclined to the Cartesian grid is expressed in a stepped grid. In the Cartesian conventional method without cut-cell, the velocity of water decreases by the stepped grid at the inclined runner. Unlike the design intent of the gating system, numerical error lead to fluid flowing first into Ingate 3. Since the stepped grids lead to deceleration, the total filling rate is about 4% slower than that of the Cut Cell method.

The numerical results using the Cut Cell method are qualitatively consistent with the water model experimental results. In conclusion, use of the Cut Cell method for casting flow analysis in Cartesian grid system improves accuracy compared to the existing method.

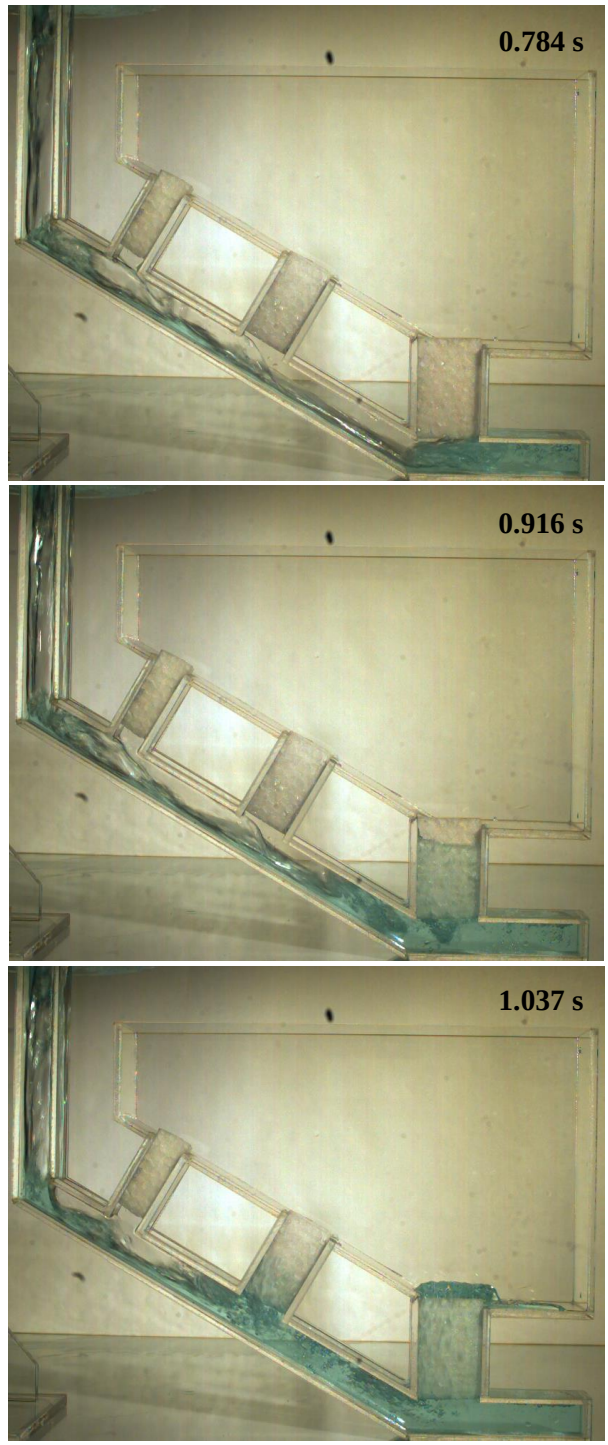

Fig. 3.15 Experimental results of water model according to pouring time (1)

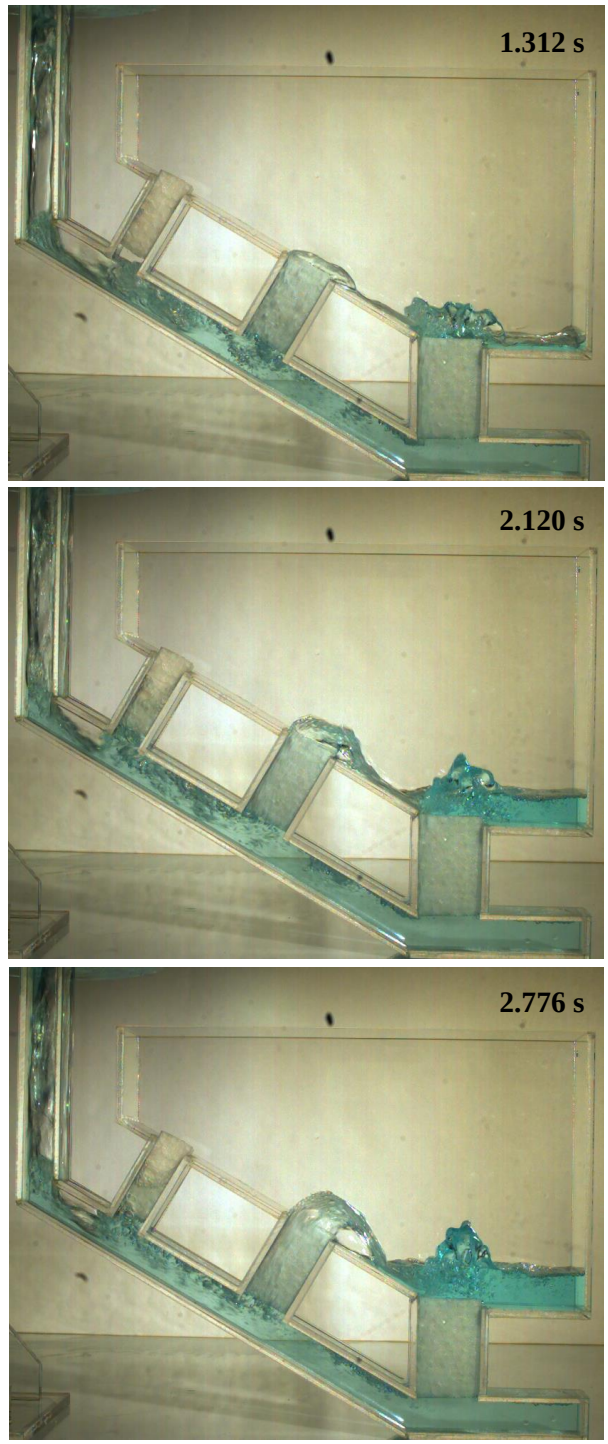

Fig. 3.15 Experimental results of water model according to pouring time (2)

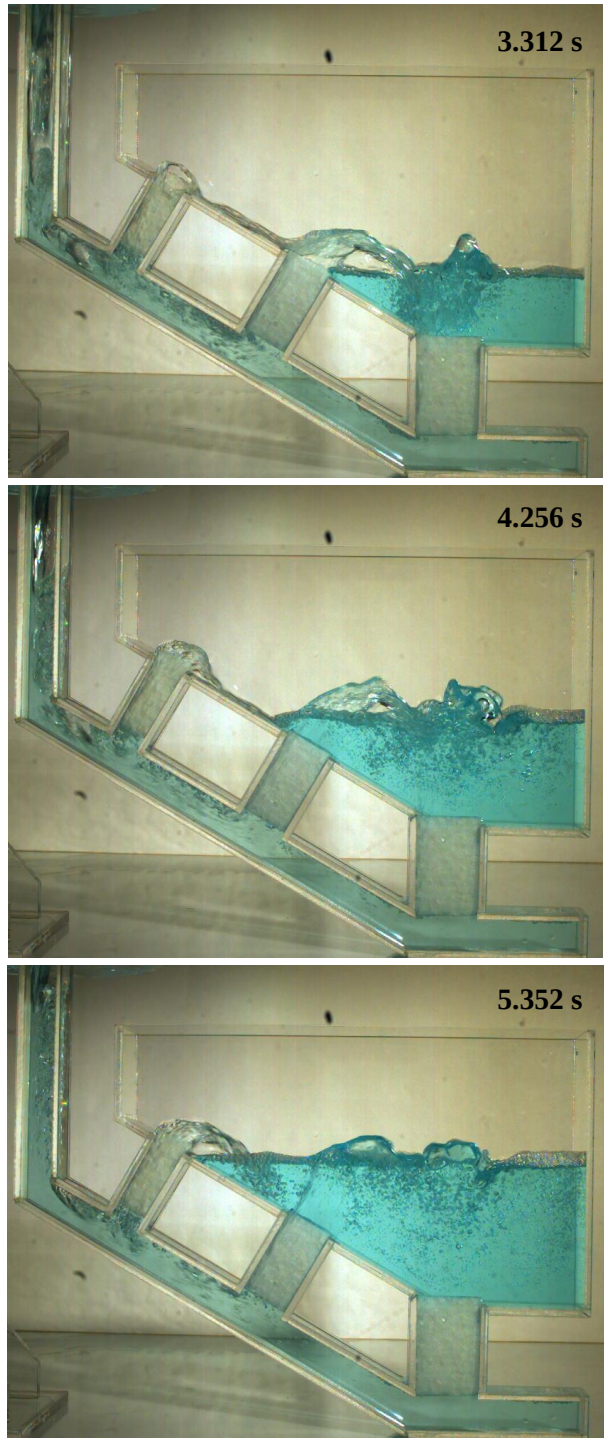

Fig. 3.15 Experimental results of water model according to pouring time (3)

Fig. 3.16 Results of the conventional (left) and Cut Cell (right) methods (1)

Fig. 3.16 Results of the conventional (left) and Cut Cell (right) methods (2)

Fig. 3.16 Results of the conventional (left) and Cut Cell (right) methods (3)

3.1.3 Comparison with BFC results

In order to verify the accuracy of the developed Cut Cell method, the simulation results of the Cut Cell method and BFC system are compared. In the BFC system, flow analysis is performed using a two-phase flow module of COMSOL Multiphysics Software. The two-phase flow module of COMSOL uses Phase Field and Level Set methods. A body-fitted grid is generated and Level Set method is used to track free surfaces for the analysis of casting flow. The analysis conditions are the same as those used in the Cut Cell method.

Fig. 3.17 and 3.18 describe the generated body-fitted meshes. The models of Case 1 and Case 2 used in the water model experiments are analyzed. The meshes generated by the body-fitted method are consistent with the original shapes, unlike the Cartesian grids of Fig. 3.5 and 3.14. The number of grids of BFC is 174,765 and 62,614, respectively. Fig 3.19 shows the results of the water model experiment, the Cut Cell method, and the COMSOL by the same filling sequence as Case 1. Because the body-fitted grid is used, the flow in the two runners has the same speed. This is in agreement with the results of the Cut Cell method using a Cartesian grid. Fig 3.20 shows the experimental results and simulation results for Case 2. Unlike in the Cartesian grid, the sloping runner of Case 2 is not represented as a stepped grid in the body-fitted grid. The result of COMSOL shows that water flows into the cavity through the Ingate 1 first as intended by the gating system design, as in the cases of the water model and the Cut cell method.

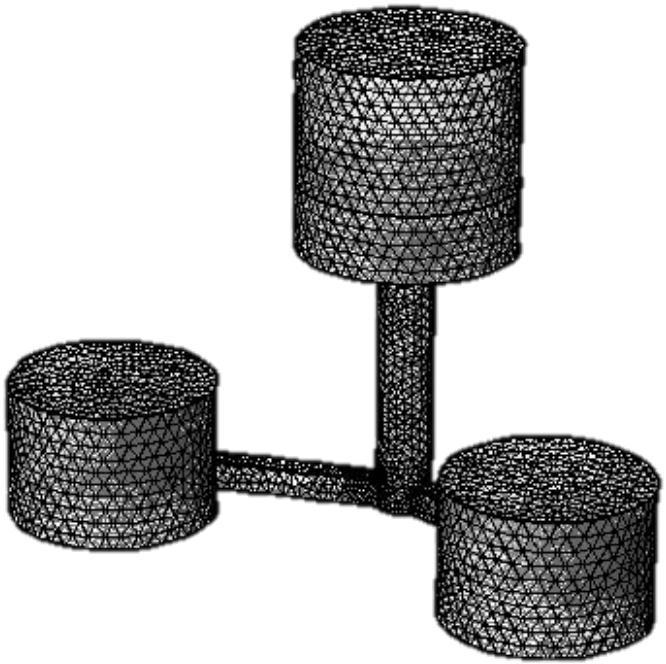

Fig. 3.17 Meshes of BFC for Case 1

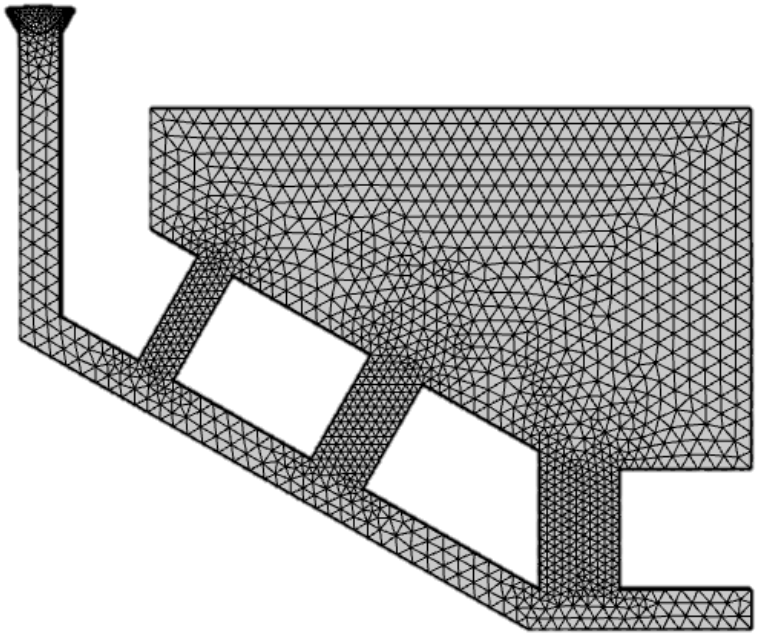

Fig. 3.18 Meshes of BFC for Case 2

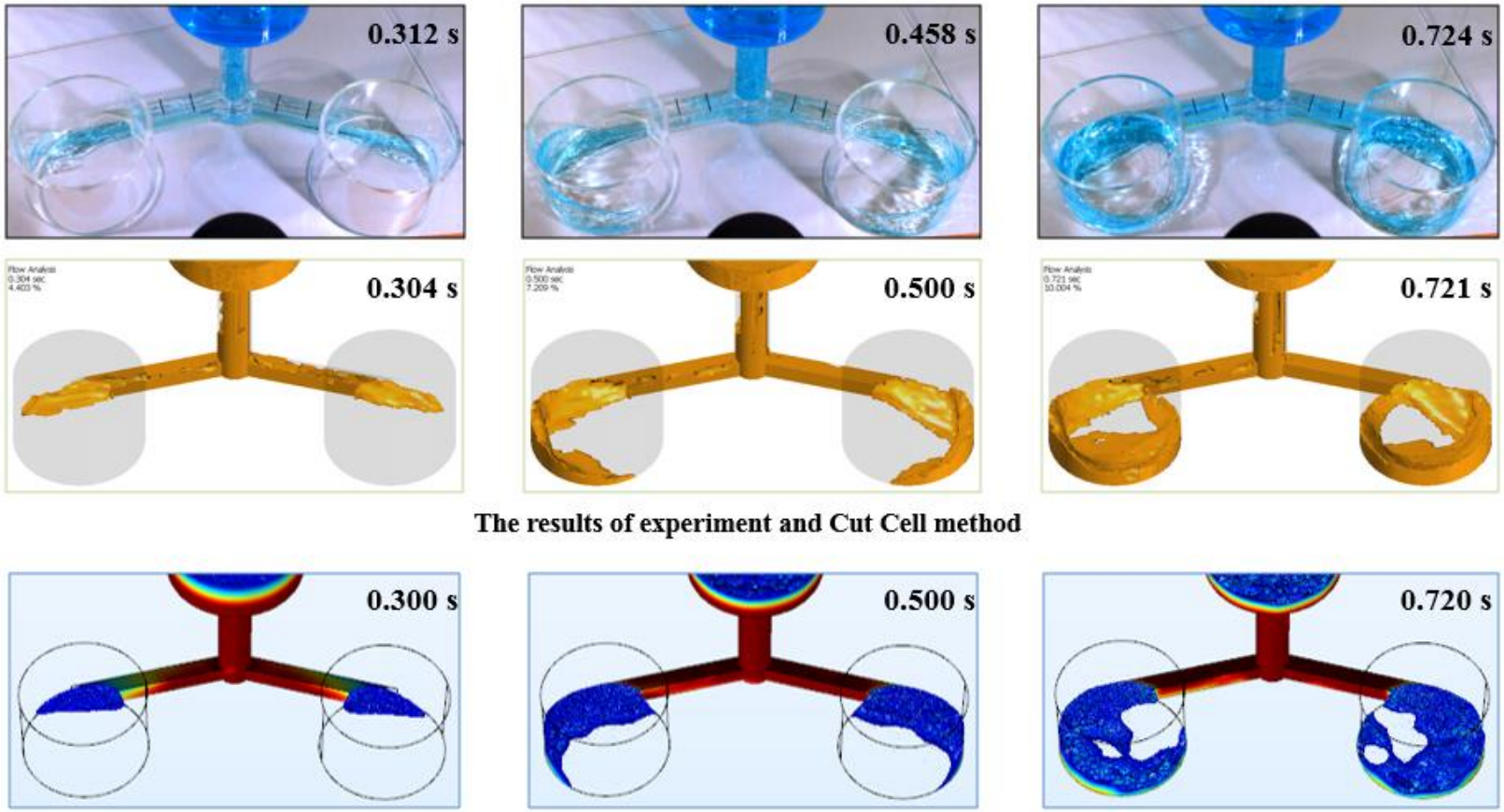

Fig. 3.19 Comparison of simulation results for Case 1

Results of experiment

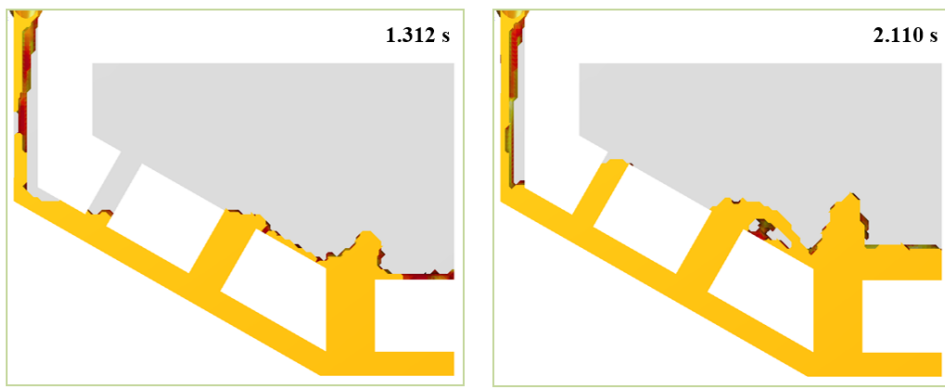

Results of Cut Cell method

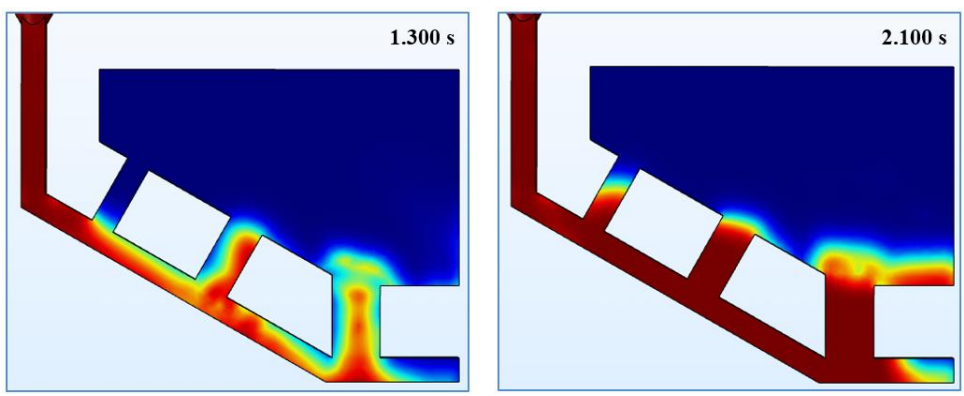

Results of BFC method

Fig. 3.20 Comparison of simulation results for Case 2

3.2 Comparison with experimental results by Mampaey

Mampaey et al. [32] compared casting experiments and numerical simulation for various gating systems. Behavior of liquid metal using transparent heat resistant window was recorded using x - ray. They implemented a numerical scheme based on an orthogonal curvilinear coordinates that employ a structured non-orthogonal mesh. The experimental models for each gating system used the same mold cavity. One had a stair shaped gating system and the other had a curved gating system with the same height and width. Mampaey reported that the behavior of casting flow was completely different depending on the gating system even for the same mold cavity.

In order to verify the developed numerical method, the numerical results of the Cut Cell method and Mampaey's casting experimental results are compared. The experimental data and the working conditions used for the experiment and the numerical analysis are shown in Table 3.1 and 3.2. Dimensions of the physical models are described in Fig. 3.21 [53].

Fig. 3.22 shows the experimental results of the stair shaped gating system according to filling sequence. The time required for filling the mold cavity was 3.906 seconds. Therefore, the pouring time of 3.906 seconds is used in the numerical analysis. In the stepped gating system, the flow takes a zigzag direction, causing energy loss. Molten metal flow is coming up quietly. Fig. 3.23 shows the results of the Cut Cell method. The flow behavior with filling sequence is similar to that depicted by the experimental results.

Fig. 3.24 shows the experimental results of the curved gating system according to filling sequence. The final filling time is 1.311 seconds. Fig. 3.25 shows the numerical results of the Cut Cell method. Fig. 3.24 and 3.25 match well qualitatively. The time taken to fill is shorter in the curved gating system compared to the stepped gating system. Molten metal passes through the ingate at a high velocity, and reaches the top of the mold cavity.

The present results are compared with the casting experimental results of previously reported research, and it is confirmed that the Cut Cell method applied to the mold filling simulation in the present paper is well implemented.

Table 3.1 Experimental data

Design	Filling time (s)	Time to fill the gating system (s)
Stair shaped	3.906	1.247
Curved	1.311	0.344

Table 3.2 Work conditions

		Density (g/cm3)	Viscosity(cm2/sec)
Cast iron (272000)	Liquid phase	7.272	0.00696
	Solid phase	7.272	1E30
No Bake Sand		1.5	1E30

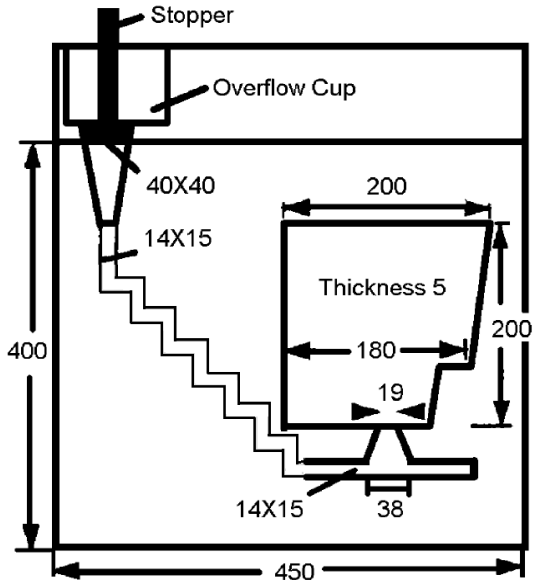

(a) A stair shaped gating system

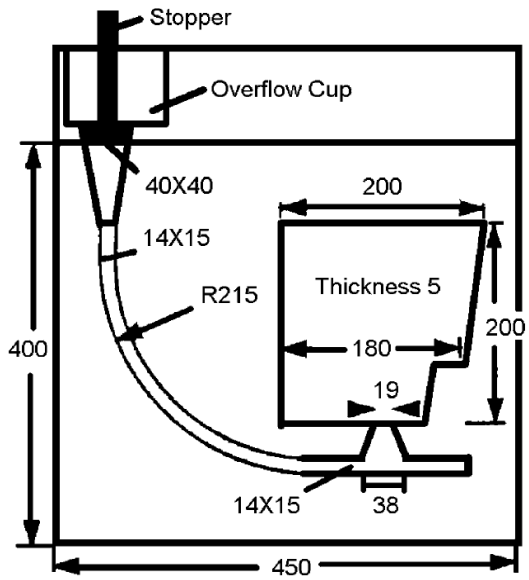

(b) A curved gating system

Fig. 3.21 Dimensions of physical models [53]

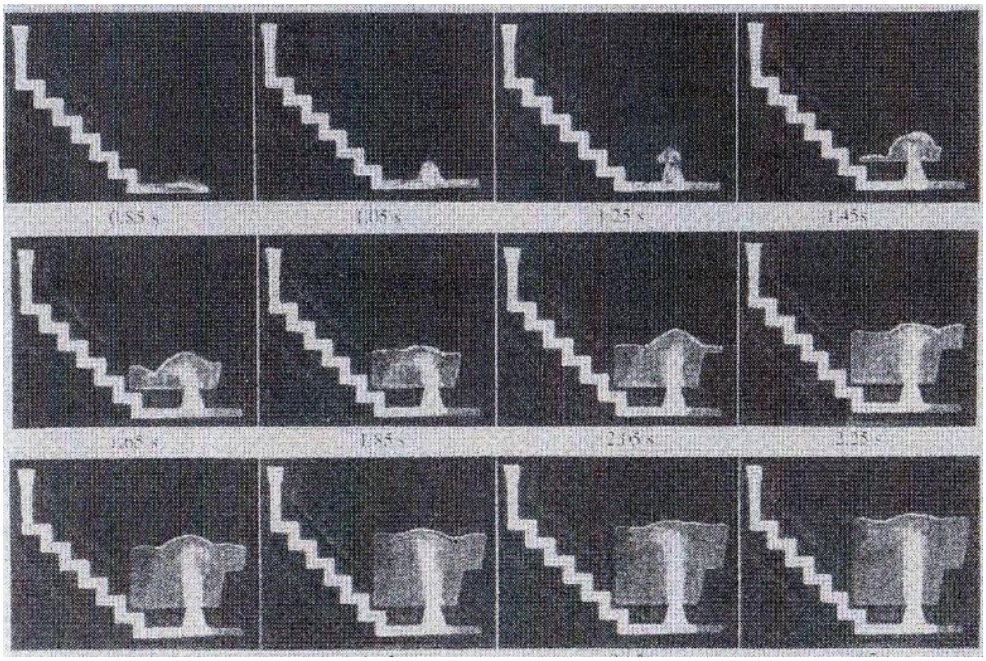

Fig. 3.22 Experimental mold filling sequence: 0.85, 1.05, 1.25, 1.45, 1.65, 1.85, 2.05, 2.25, 2.45, 2.65, 2.85, and 3.05s

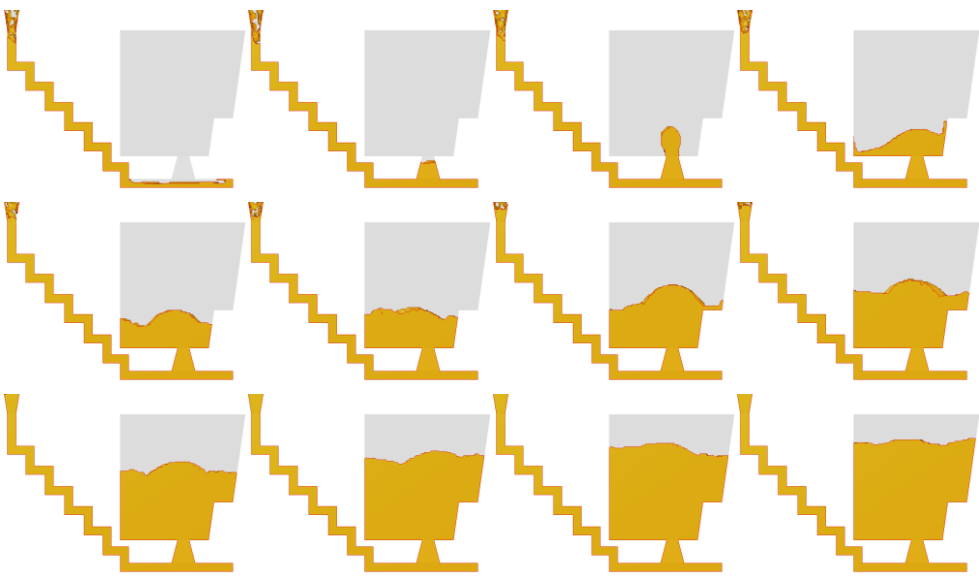

Fig. 3.23 Numerical mold filling sequence: 0.892, 1.138, 1.261, 1.445, 1.629, 1.813, 1.998, 2.182, 2.427, 2.65, 2.85, and 3.05s

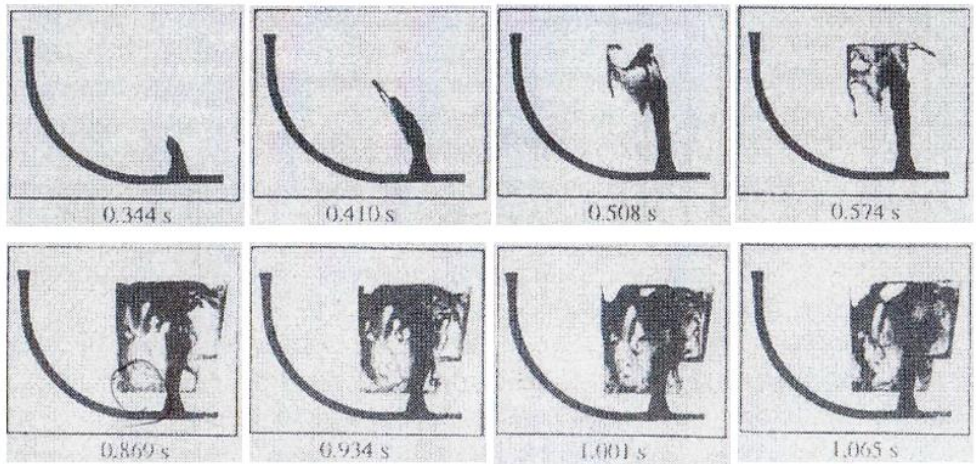

Fig. 3.24 Experimental mold filling sequence with a curved gating system: 0.344, 0.410, 0.508, 0.574, 0.869, 0.934, 1.001, and 1.065s

Fig. 3.25 Numerical mold filling sequence with a curved gating system: 0.338, 0.418, 0.506, 0.564, 0.886, 0.915, 1.001, and 1.065s

3.3 Numerical validation

The Cut Cell method compensates for energy loss when calculating the flow field in the Cartesian grid system. On the other hand, the conventional method attempts to minimize the energy loss due to shape distortions by increasing the number of grids. The rate of energy loss according to the number of grids is analyzed quantitatively with a simple model.

Fig. 3.26 describes dimensions of a sloped runner of 45°. P1 indicates an inlet, and outlet is located at the P2.

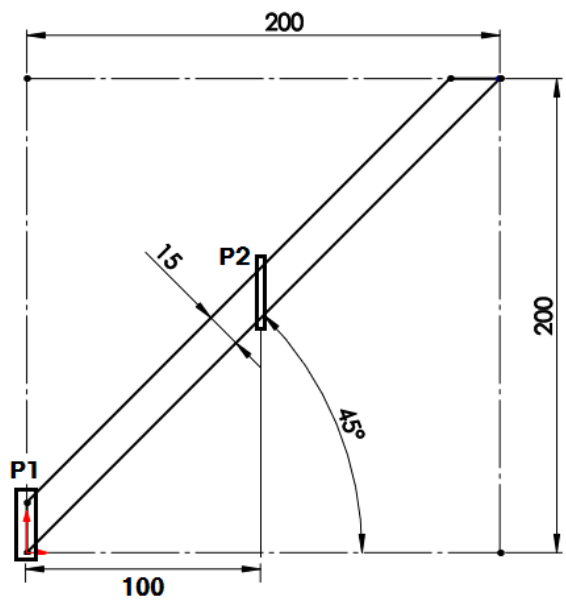

Fig. 3.26 Dimensions of a sloped runner model

3.3.1 Comparison of energy loss rate by the number of grids

The minimum number of grids is based on the thinnest area of the model and is determined by one axis direction. The number of grids used for comparison analysis is from 2 to 10 times the minimum number of grids. Fig. 3.27 represents meshes of 1 and 5 times the number of grids. Five times the number of grids indicates that the total number of grids is 125 times when all the grids are the same size. The minimum total number of grids in the present model is 9,240 and the maximum total number of grids is 9,240,000. The initial velocity is 90 cm/s in 45degrees direction.

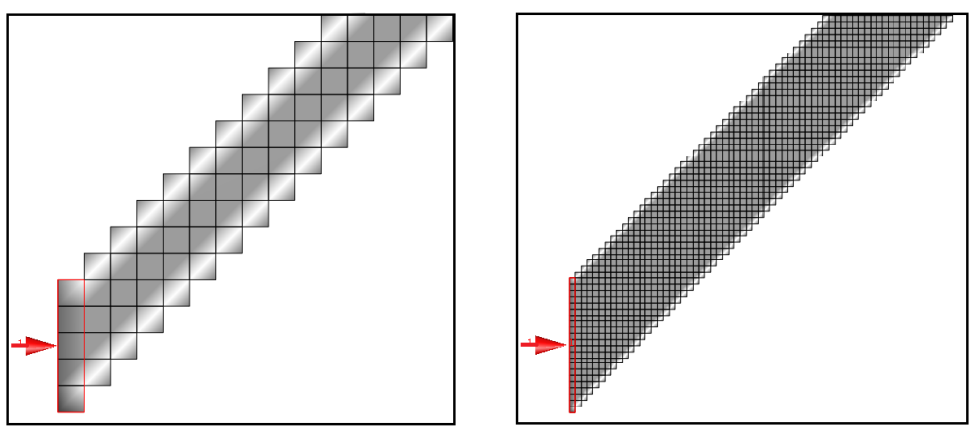

Fig. 3.27 Meshes of 1 and 5 times the number of grids

Fig. 3.28 shows the mass flow error of the two methods depending on the number of grids. By the conventional method, the mass flow error converges to 0.05 or less when the number of grids is 6 times or more. On the other hand, by the Cut Cell method, the mass flow error converges more quickly to less than 0.05.

Fig. 3.29 shows the momentum loss error of the two methods according to the number of grids. The Cut Cell method has the momentum loss of 0.1 when the number of grids is 5 times, and by the conventional method the number of grids is 8 times. Therefore, it is necessary to have the total number of grids of at least 4 times the Cut Cell method in order to use the conventional method in the Cartesian grid systems.

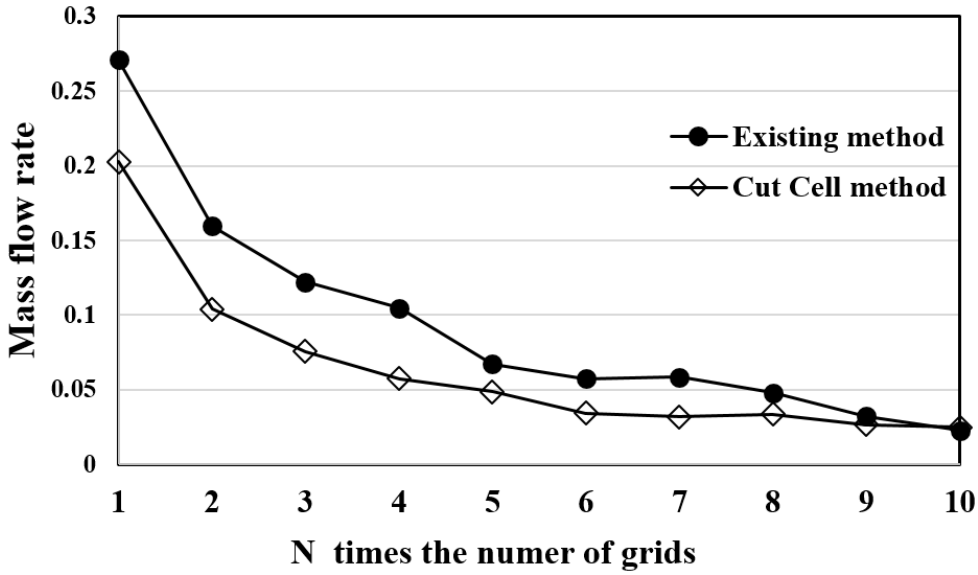

Fig. 3.28 Comparison of mass flow error by the number of grids

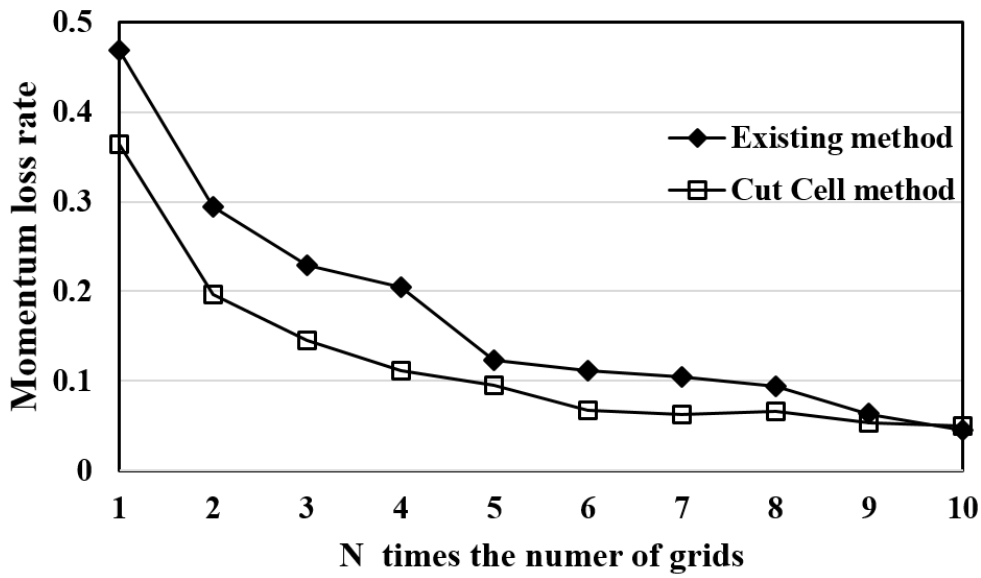

Fig. 3.29 Comparison of momentum loss error by the number of grids

3.3.2 Effects of pouring rate change

The rate of momentum loss is calculated according to the pouring rate. Fig. 3.29, 3.30, and 3.31 show the momentum loss at the pouring rates of 90, 30, and 180 cm / s, respectively, and the conventional method and the Cut Cell method are used. It can be seen that the momentum loss error of the conventional method is larger than that of the Cut Cell method. However, the difference between the momentum loss rates is almost uniform regardless of speed. Fig 3.32 shows the momentum loss rate by the conventional method according to the pouring rate. Fig 3.33 represents the result of the Cut Cell method. In Fig. 3.32 and 3.33, the momentum loss rate is almost the same depending on the number of grids regardless of speed.

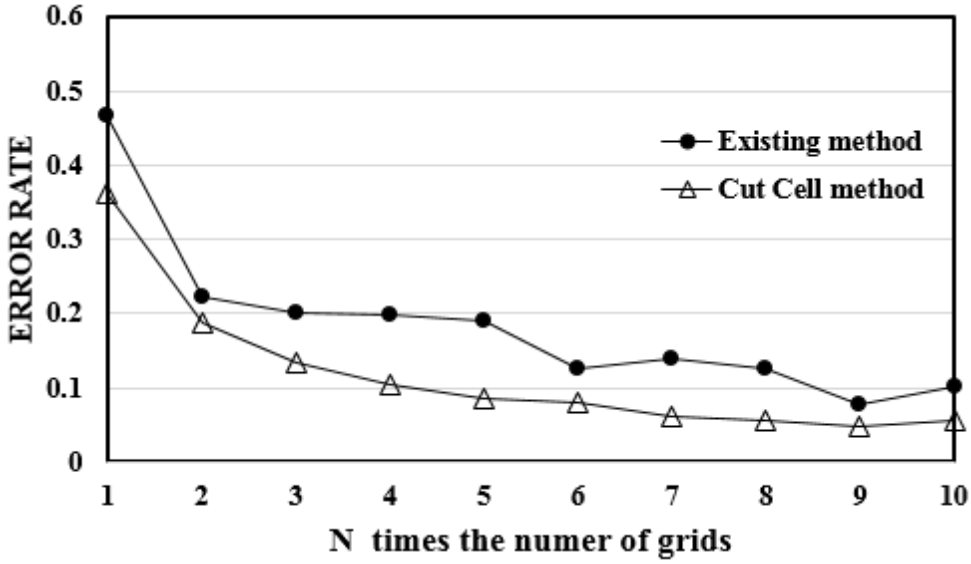

Fig. 3.30 Comparison of momentum loss at 30cm/s

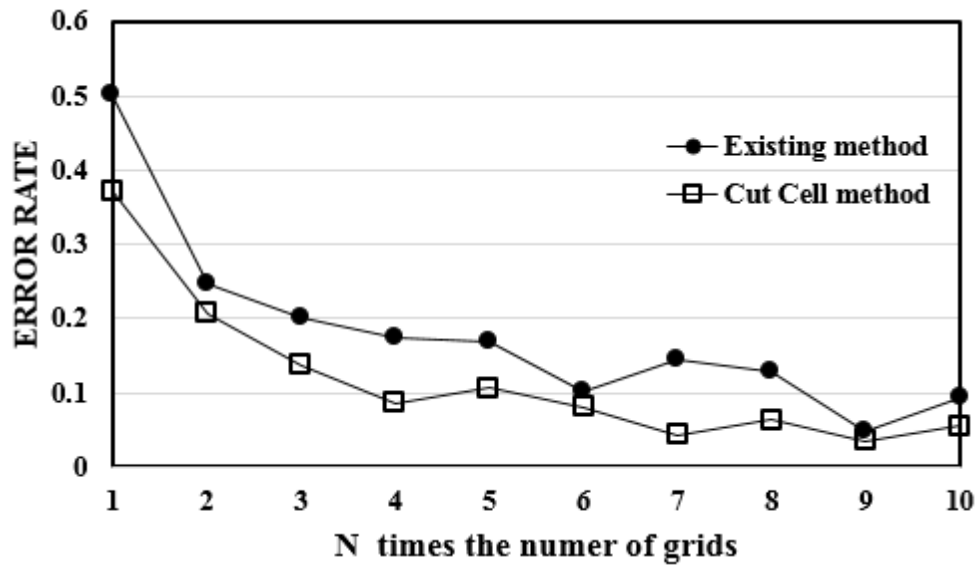

Fig. 3.31 Comparison of momentum loss at 180cm/s

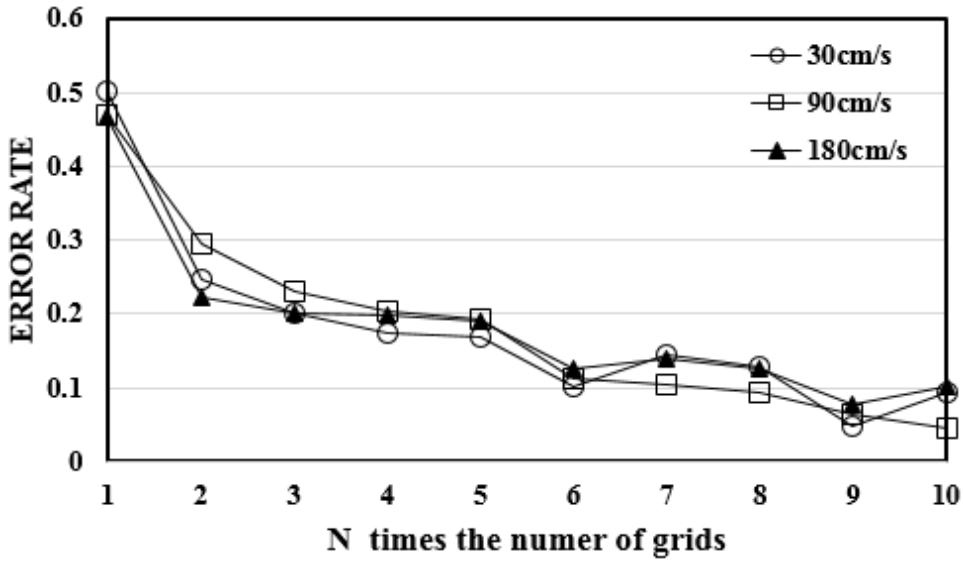

Fig. 3.32 Momentum loss of the conventional method with pouring rate

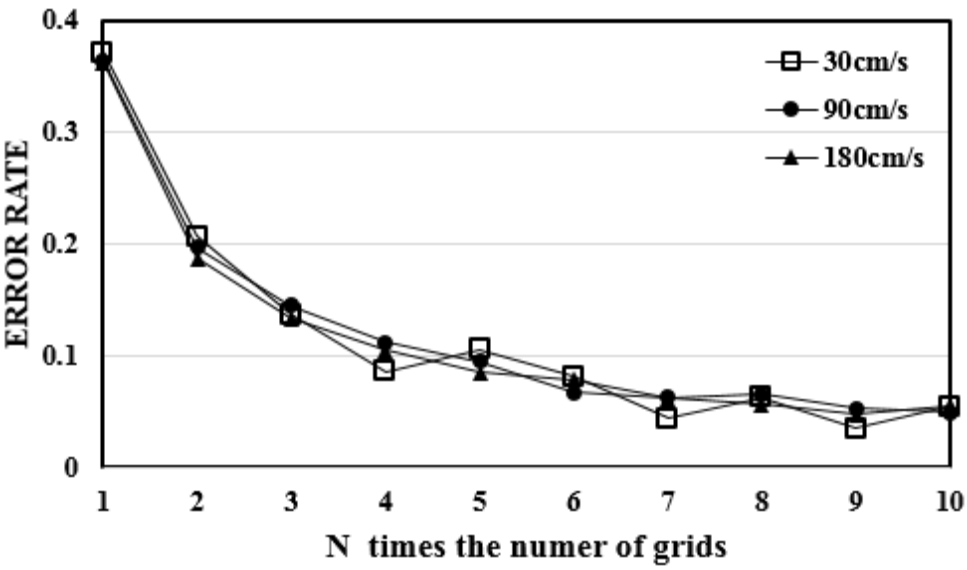

Fig. 3.33 Momentum loss of the Cut Cell method with pouring rate

3.3.3 Effects of width reduction

Fig. 3.34 is the same model as Fig. 3.26, but the width is reduced to 5 and 10mm. The rate of momentum loss is expected to increase when the flow width decreases because the ratio of cut-cells in the calculation domain increases. The change of momentum loss rate with reduction of width is investigated. The pouring rate is 90cm/s.

Fig. 3.35 compares the momentum loss of the conventional and Cut Cell methods when the width of the runner is 5 mm. The difference in momentum loss between the two methods represents large until seven times the number of grids. The momentum loss rate of the conventional method starts to become less than 0.2 from 7 times the number of grids.

Fig. 3.36 shows the results for a width of 10 mm. Momentum loss decreases sharply as the number of grids increases, unlike Fig. 3.35. By the conventional method, the momentum loss rate drops to less than 0.2 at 5 times the number of grids. On the other hand, by the Cut Cell method, the momentum loss rate becomes less than 0.2 at 3 times the number of grids. The difference in momentum loss between the two methods is also less than that of Fig. 3.35. The narrower the width of the runner, the larger the number of grids is required to reduce momentum losses.

Fig. 3.37 and 3.38 describe the momentum loss rate by width of the conventional method and the Cut Cell method, respectively. In Fig. 3.37, the difference in momentum loss rate by width is large. The 5 mm wide model shows a stable momentum loss rate when analyzed over 7 times the number of grids. Fig.

3.38 also shows the difference in momentum loss rate by width, but it is not so large compared with the existing method. This is because the Cut Cell method compensate for the energy of the cut-off portion of the Cartesian grid. Therefore, it is relatively less dependent on the number of grids.

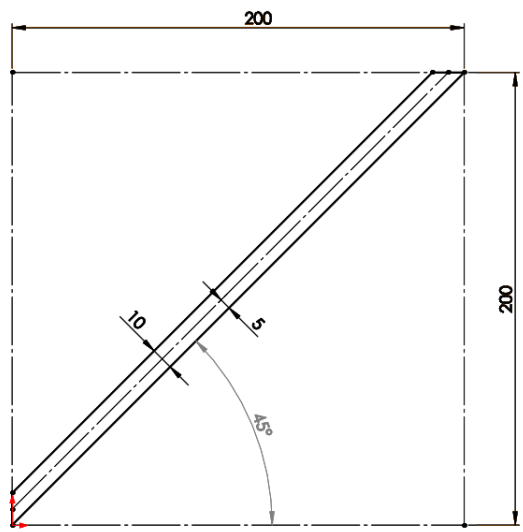

Fig. 3.34 Dimensions of sloped runners with widths of 5 and 10 mm

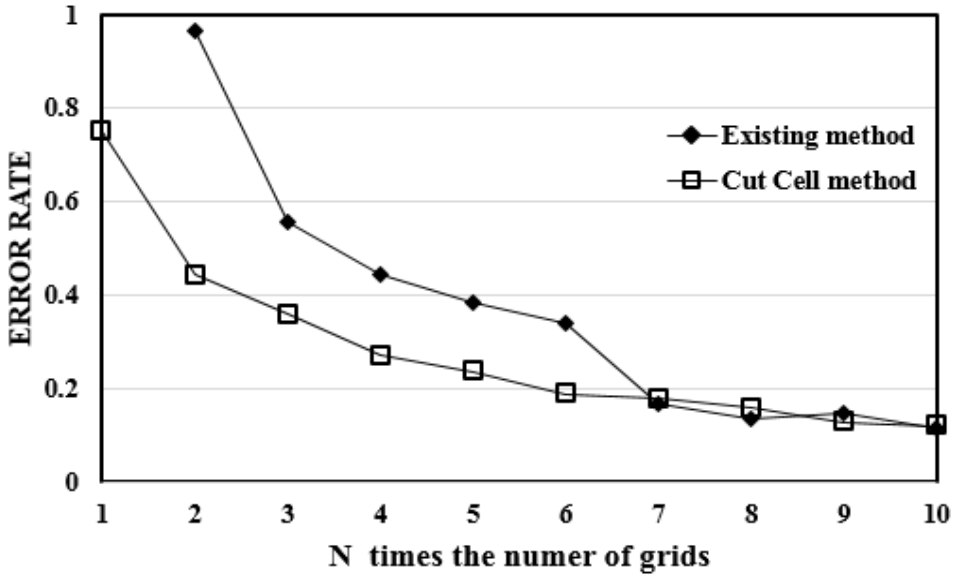

Fig. 3.35 Momentum loss of the two methods at a width of 5 mm

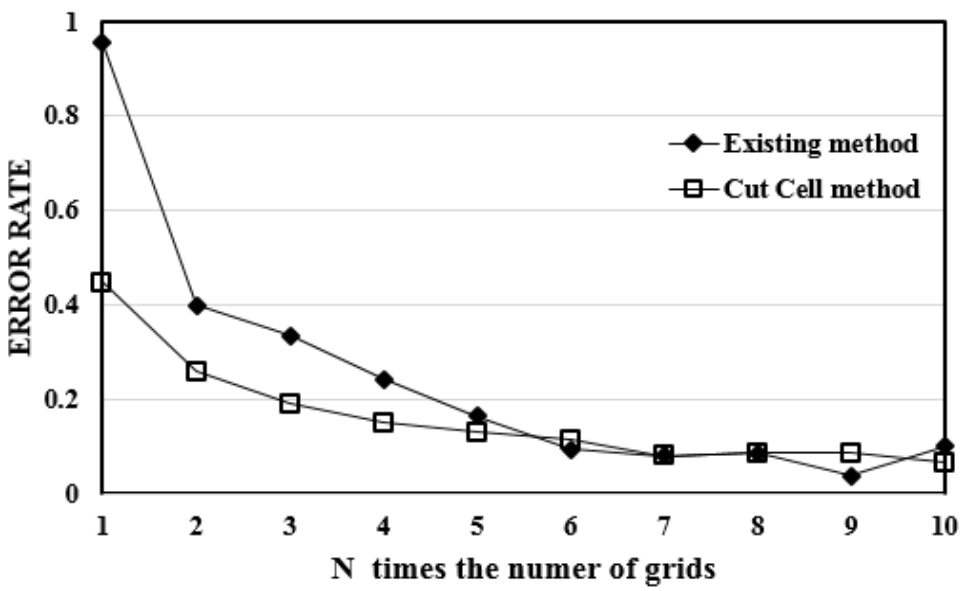

Fig. 3.36 Momentum loss of the two methods at a width of 10 mm

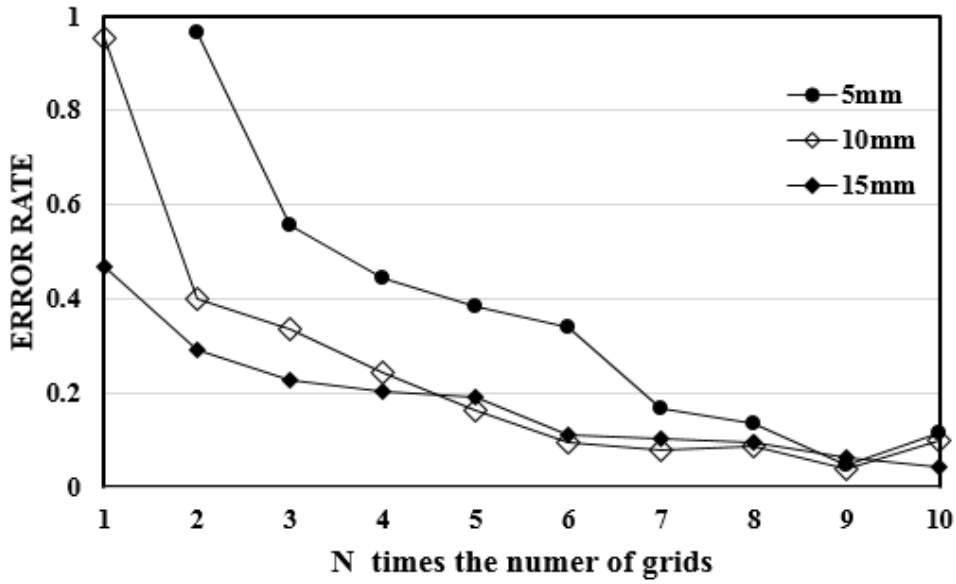

Fig. 3.37 Momentum loss of the conventional method by width

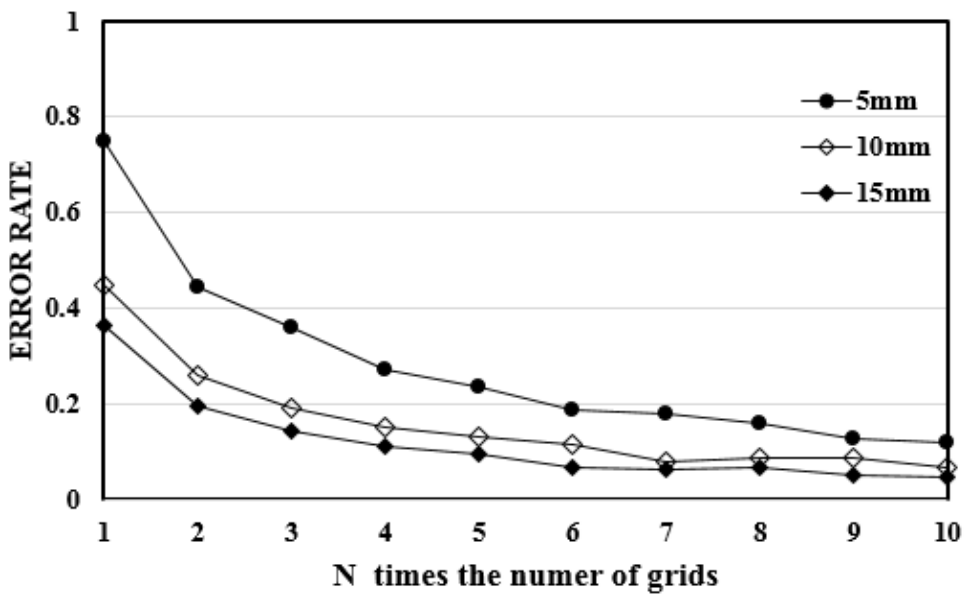

Fig. 3.38 Momentum loss of the Cut Cell method by width

Chapter 4. Simulation results and analysis

4.1 Comparison of results according to the number of grids

It is well known that the Cartesian grid generates a grid orthogonally regardless of the shape, and therefore the generated grid is not consistent with the original shape. Even distorted shapes are represented. To resolve this problem, Cartesian grid system with increased the number of grids has been used.

Casting products are usually very complicated in shape, and there are a variety of gating systems, such as curved, straight-line, and etc. Nowadays, computer performance is of an excellent level, so when it implements a numerical scheme in the Cartesian grid system, more than 10 million meshes are used. This is done to express the original shape of the product as accurately as possible. The large number of meshes mitigates the loss of energy caused by shape distortions or the obstacles in the stair step, but they do not fully compensate for the loss.

In this chapter, we compare numerical results of the two methods according to the number of meshes.

4.1.1 Model with a sloped ingate

A casting product with a sloped ingate of 45° is calculated by the die casting process. Fig. 4.1 shows a 3D model of the product. Fig. 4.2 and 4.3 show the generated grid at the x-z plane in the Cartesian grid system.

From fig. 4.2, it may be observed that the product is created with a coarse mesh. The grid domain is 24×8×38 and the total number of grids is 7,296. Since the number of grids is very small, a 45 degree slope ingate is represented as a rectangular shape.

Fig. 4.3 shows that the product is generated with a fine mesh. The grid domain is 120×40×190 and the total number of grids is 912,000. The 45° slope of the product was well expressed in the Cartesian grid system. However, enlargement shows that the sloped surfaces still have a large number of stepped shapes.

The analysis conditions are shown in Table 4.1.

Table 4.1 Analysis conditions

The material of cast	A356
The material of mold	SKD61
Pouring velocity	1000cm/s
Coarse meshes	24×8×38
Fine meshes	120×40×190

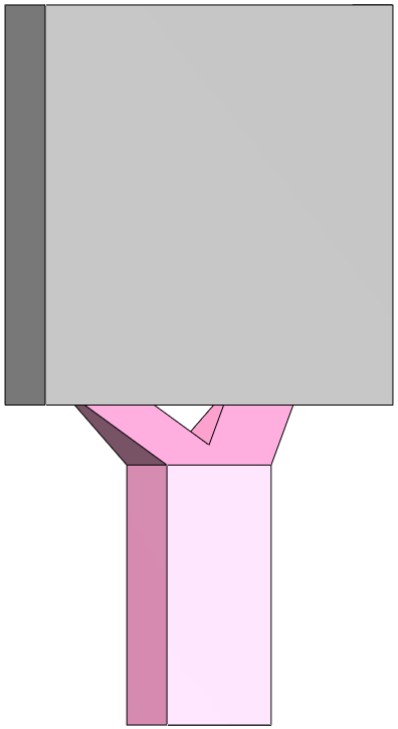

Fig. 4.1 3D model of a casting product

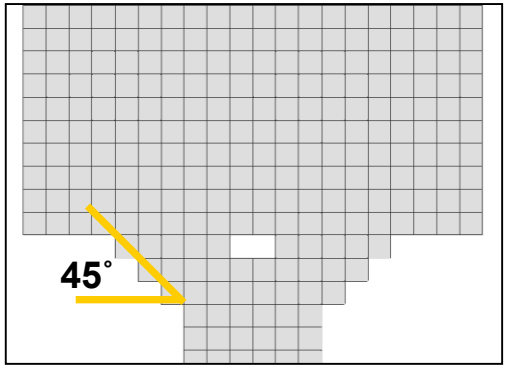

Fig. 4.2 Coarse meshes

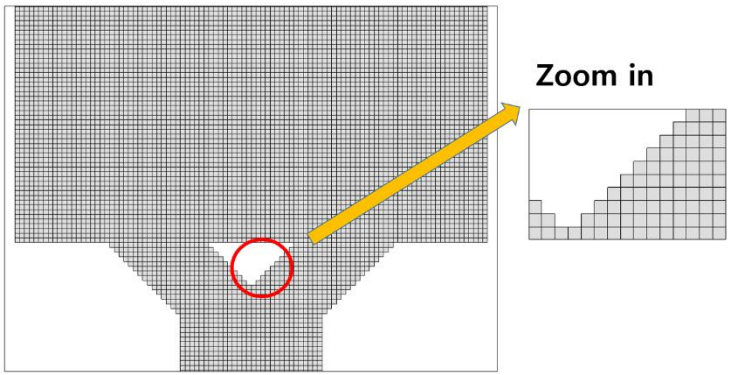

Fig. 4.3 Fine meshes

Fig. 4.4 shows the results of the conventional method by the coarse meshes according to the filling rate. An extremely small number of grids were created to compare the results according to the number of grids. Therefore, the 45° inclined ingate is represented by just a rectangle in the coarse mesh system.

At a filling rate of 24%, the molten metal passing through the ingate is seen to flow vertically. On the other hand, the Cut Cell method is represented in the same number of the coarse meshes as Fig. 4.5. As shown in Fig. 4.4, the inclined ingate is displayed as a rectangle. When the filling rate is 24%, the molten metal passing through the ingate flows exactly at an angle of 45°. In addition, the behavior of the molten metal is similar to the result at 30% of Fig. 4.4. At a filling rate of 30%, the molten metal first reaches the roof edge of the cavity. On the other hand, in Fig. 4.4 the molten metal does not reach the top of the cavity due to velocity reduction on the slope.

In order to resolve the problem of the Cartesian grid system, the number of grids was increased to 125 times (5 times in the axial direction). The results of analysis by the fine meshes are shown in Fig. 4.6. Compared with Fig. 4.4, much more accurate analysis results are obtained. However, Fig. 4.3, which enlarges the ingate area, shows the obstacles of a staircase still existing. Compared with the result shown in Fig. 4.5, it can be seen that the molten metal passing through the ingate spreads to the empty space of the cavity due to reduced velocity.

Fig. 4.7 shows the velocity color contour at 30%. Fig. 4.7 (a) shows the result of the Cut Cell method by the coarse meshes, (b) shows the result of the conventional

method using fine meshes, and (c) shows the result of the conventional method by the coarse meshes. The molten metal injected at 1000cm/s is converted to high speed after passing through the narrow ingate area compared to the gate area. The velocity of molten metal passing through the ingate is close to 3200cm/s for (a), 2400cm/s for (b) and approximately 1600cm/s for (c). Fig. 4.7 (a) represents the fastest velocity even though it is calculated by coarse meshes. The velocity results of the conventional method simulated by coarse meshes are almost two times smaller than that of the Cut Cell method. The velocity result of the conventional method by fine meshes is also smaller than that of Fig. 4.7 (a).

Problems caused by geometric distortion in the Cartesian grid system have been resolved somewhat by fine meshes rather than coarse meshes. However, the loss of momentum that occurs in a stepped grid created by a shape with an inclined or a curved surface cannot be completely mitigated.

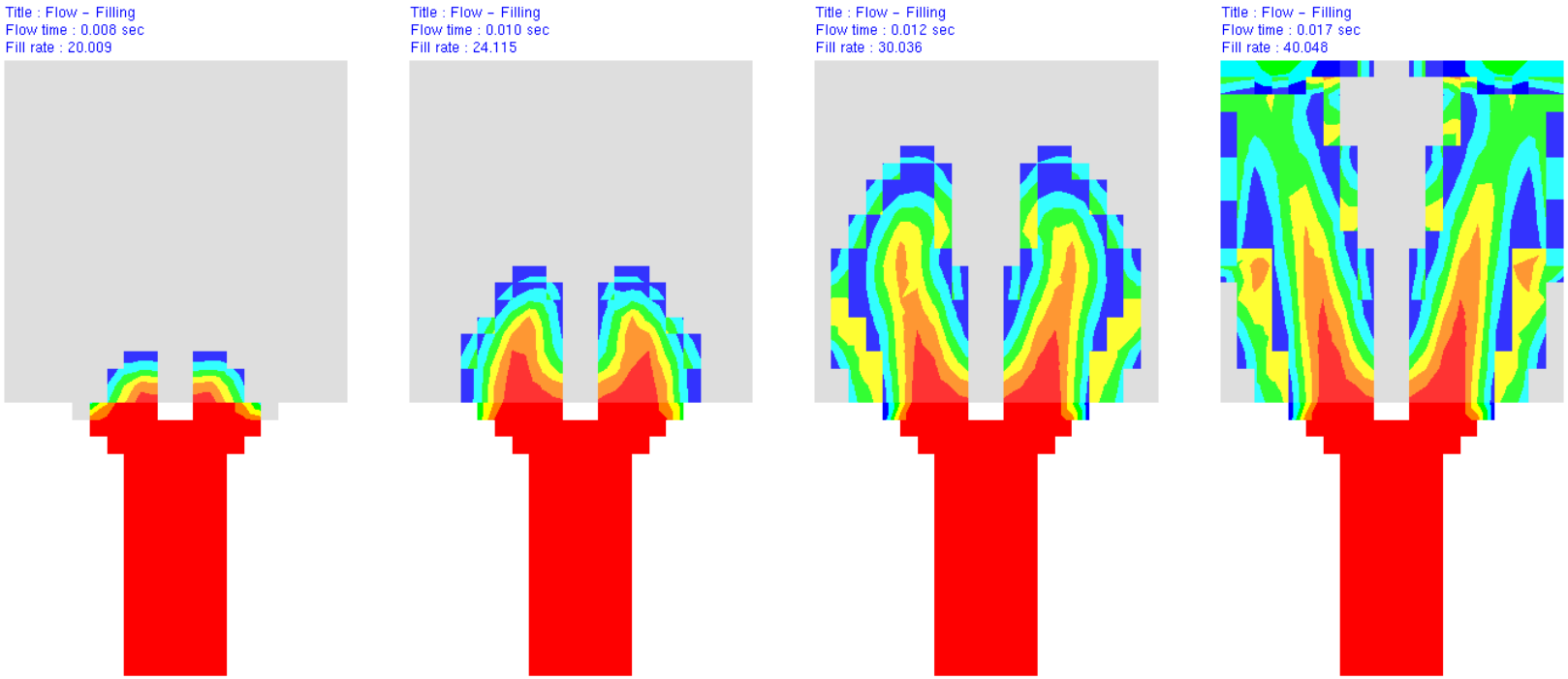

Fig. 4.4 Results of conventional method by the coarse meshes according to mold filling rate

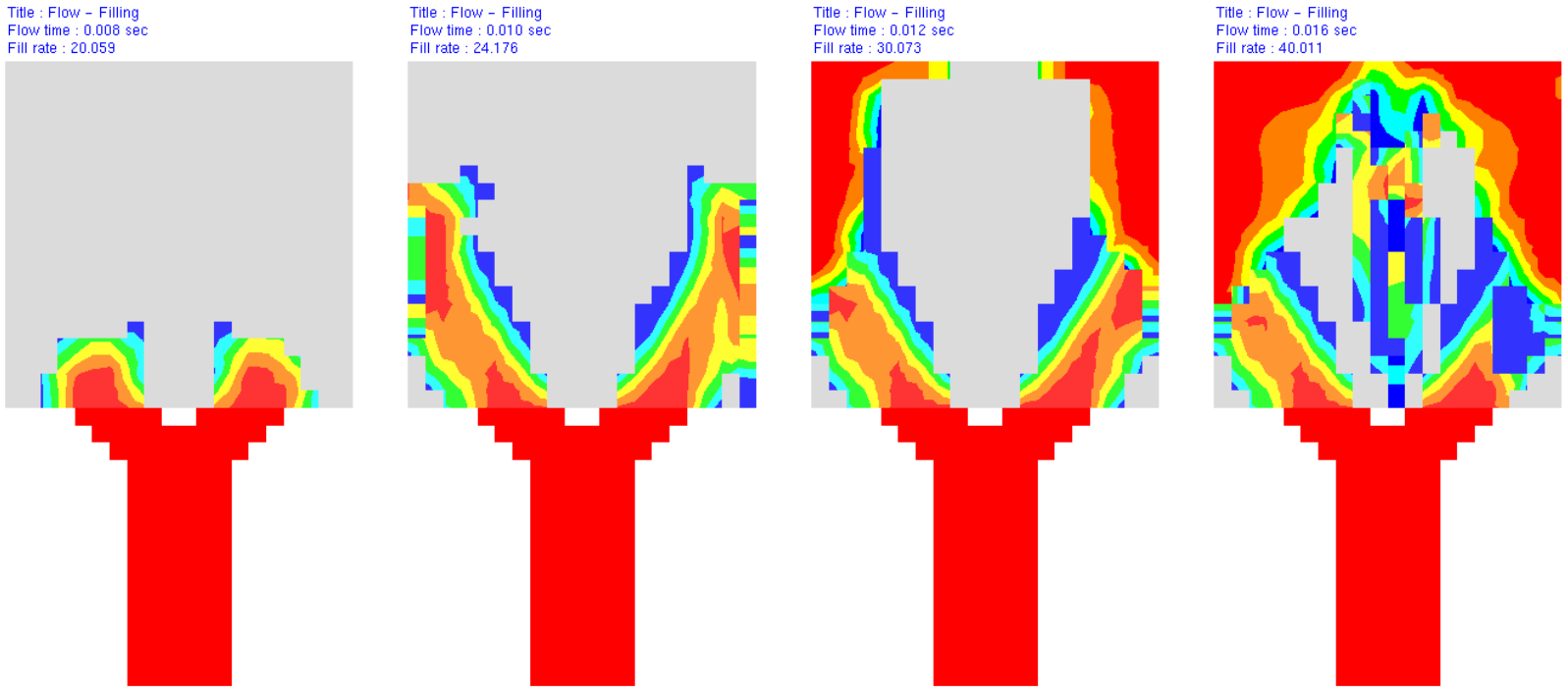

Fig. 4.5 Results of Cut Cell method by the coarse meshes according to mold filling rate

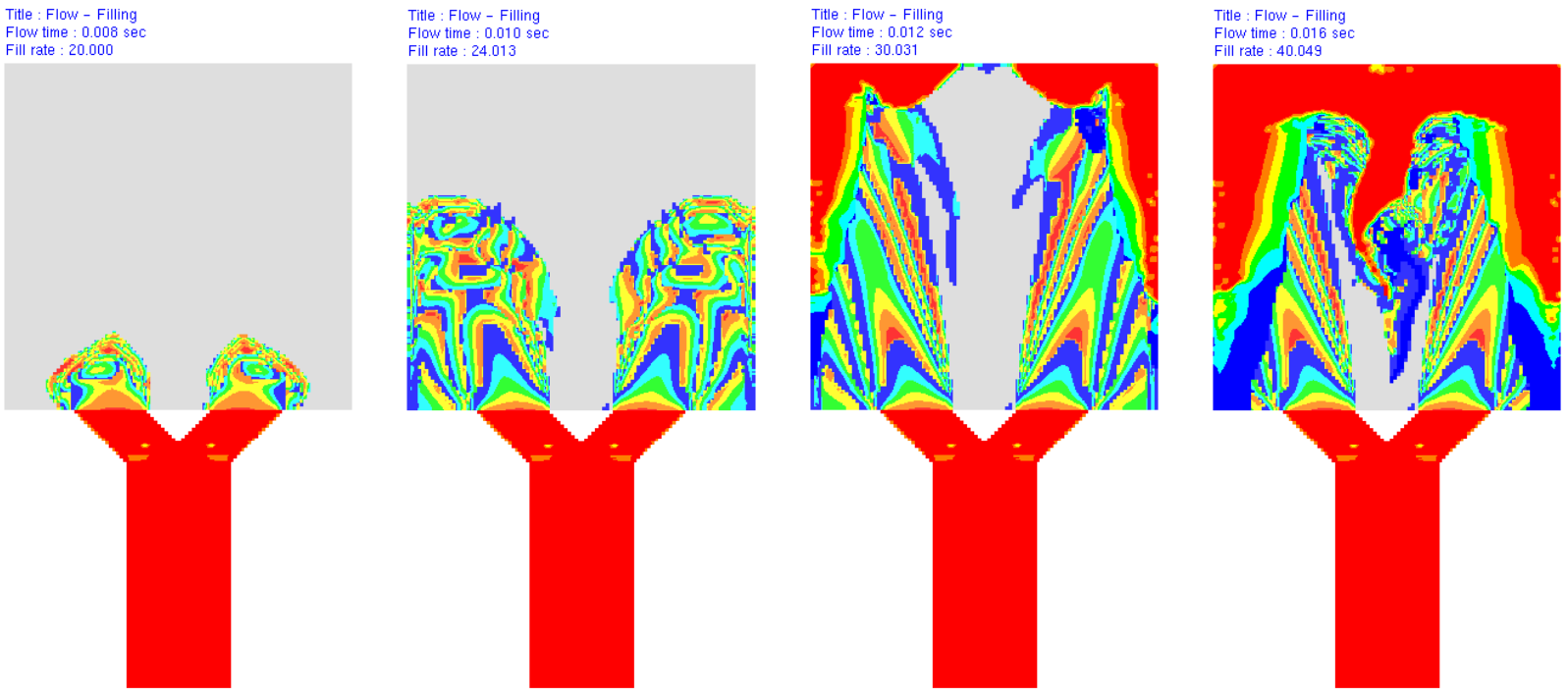

Fig. 4.6 Results of conventional method by the fine meshes according to mold filling rate

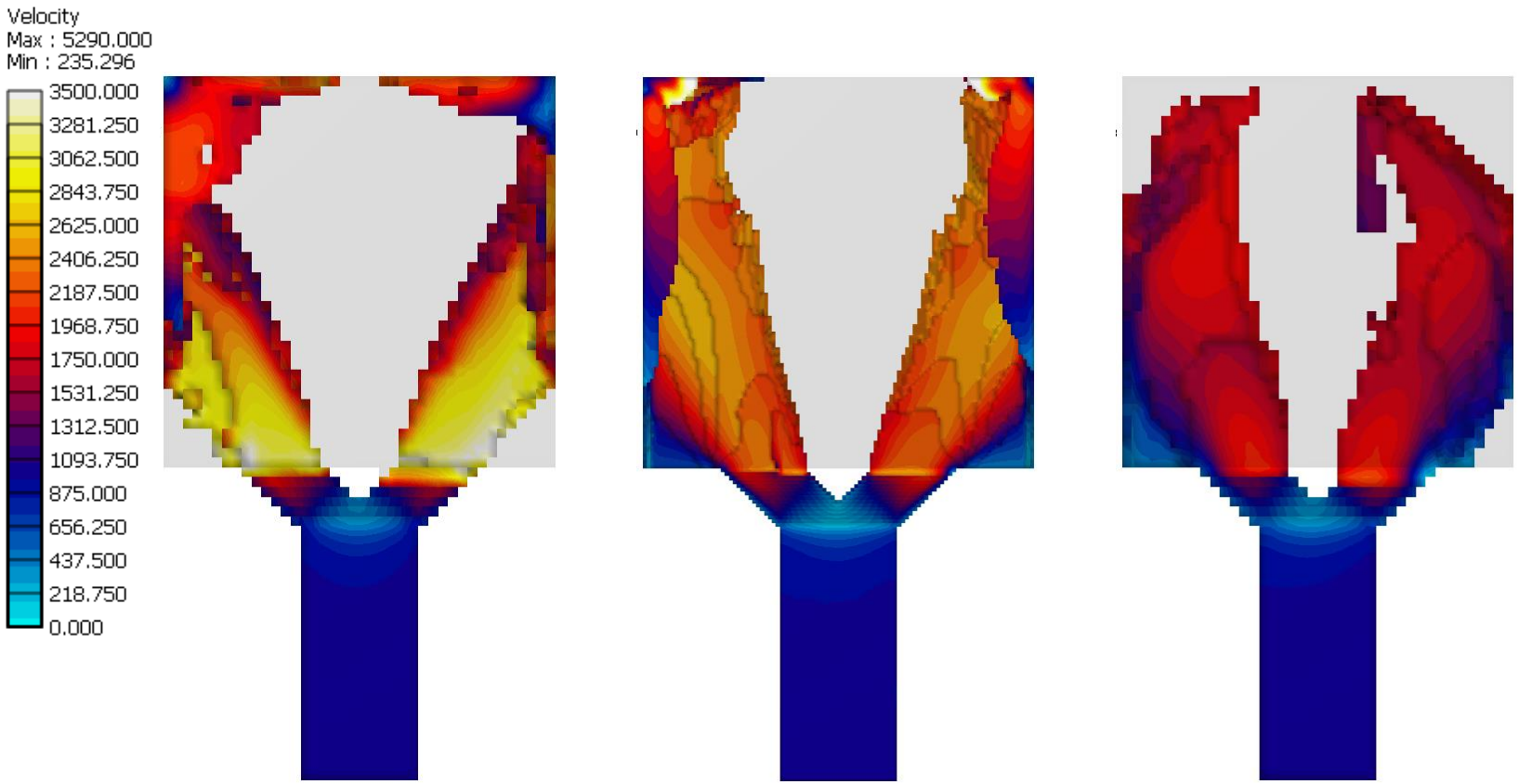

(a) Cut Cell methd by coarse mesh **(b) Conventional method by fine mesh** **(c) Conventional method by coarse mesh**

Fig. 4.7 The velocity color contour of two methods at 30 %

4.1.2 Model with a circled mold cavity

The following is a sand mold casting process model of a concave ball in a cone crusher that is mainly used in civil engineering construction sites. Fig. 4.8 shows a 3D model of the product. Fig. 4.9 and 4.10 show the generation of a grid in the Cartesian grid system. Fig. 4.9 shows that the product is created as a coarse mesh with a grid domain of 60×80×22 and a total grid size of 105,600. Fig. 4.10 shows that the product is represented by a fine mesh, with a grid domain of 120×160×44 and a total number of grids of 844,800. As can be seen in Fig. 4.9, a curved surface is represented as a stepped shape by the Cartesian grid. Fig. 4.10, which represents the meshes generated by increasing the number of grids, is closer to the actual shape of the product than Fig. 4.9. However, when a curved surface is partially enlarged, it can be seen as having stepped grids.

The analysis conditions are shown in Table 4.2.

Table 4.2 Analysis conditions

The material of cast	A356
The material of mold	FURAN
Pouring velocity	100cm/s
Coarse meshes	60×80×22
Fine meshes	120×160×44

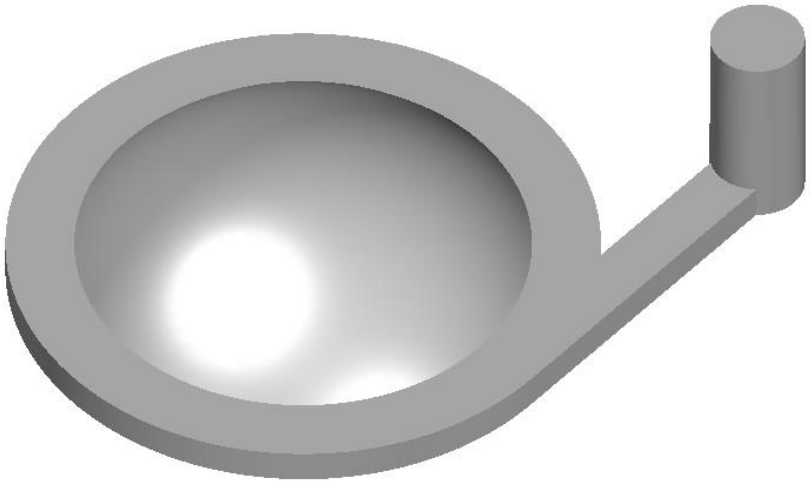

Fig. 4.8 3D model of a casting product

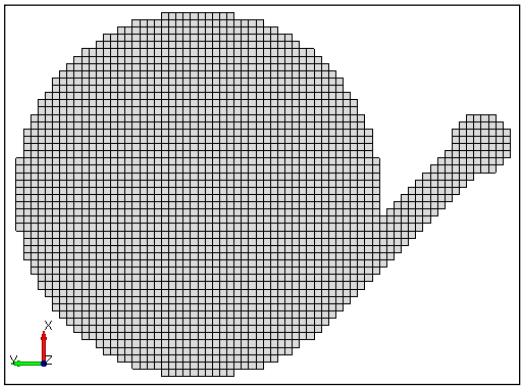

Fig. 4.9 Coarse meshes

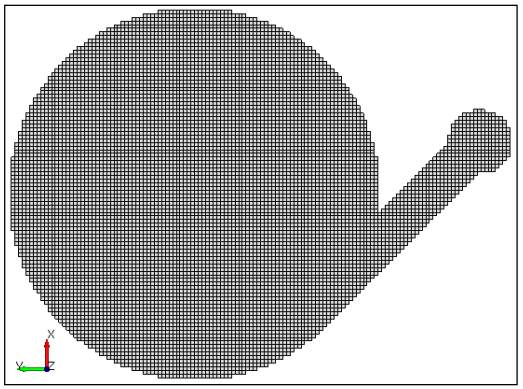

Fig. 4.10 Fine meshes

Fig. 4.11 and 4.12 show the results of the existing and the Cut Cell methods by the coarse meshes according to the filling rate, respectively. The poured molten metal passes through a sprue and enters the cavity through a runner.

As shown in Fig. 4.11, the molten metal meets the stepped grids on the surface of the cavity and does not flow along the circle, but merely overlay the top surface of the concave ball. On the other hand, Fig. 4.12 shows that the molten metal fills along the circle irrespective of the step-like grid. At a 50% filling rate, the Cut Cell method shows that the melt flows along the circular surface and then returns to the ingate. In the conventional method, however, the poured molten metal has not yet reached the ingate. There are many differences in the two results. It can be seen that the filling behavior of the molten metal is different, and the collision area and the final void region of the molten metal where gas porosity defects may occur are also different.

As seen in chapter 4.1.1, the problem can be solved by generating 8 times the total number of grids (2 times in the axial direction) in order to study the analytical results when the number of grids is increased in the Cartesian grid system. Fig. 4.13 and 4.14 show the results of the two methods using fine meshes. In the case of the Cut Cell method, the results of Fig. 4.12 and Fig. 4.14 are similar regardless of the number of grids. In the case of the conventional method results, the number of grids is increased, so that the result of Fig. 4.13 is more accurate than Fig. 4.11. However, the problems associated with computing by the Cartesian grid system are not clearly

improved. The molten metal still flows into the upper surface of the concave ball and the velocity of the front filling is slower than velocity shown by the Cut Cell method.

Fig. 4.15 shows the velocity contour of the two methods at a filling rate of 50% in the z-direction cross section. These are the results by the fine meshes. The velocity contour of the Cut Cell method (Fig. 4.15 (b)) shows an average of 225cm/s while the velocity contour of the existing method (Figure 4.15 (a)) is an average of 125cm/s. In the Cartesian grid system, it can be seen that the conventional method has a decrease in the velocity at the surfaces of the curved and sloped shape.

Fig. 4.16 shows the velocity vector by enlarging a part of the concave ball. In the Cut Cell method, the velocity vector is displayed along the circle despite the stepped gird but in the conventional method, the velocity vector is displayed in the direction perpendicular to the stepped grid.

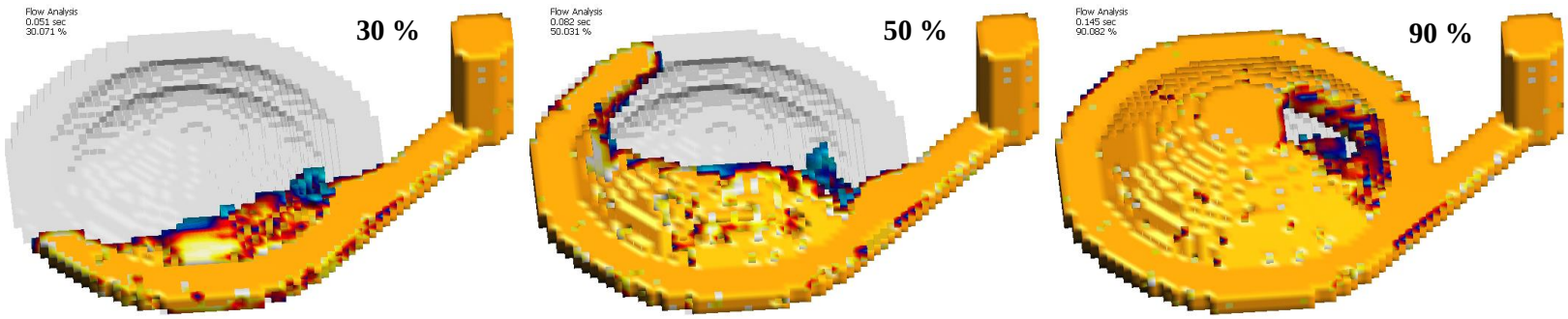

Fig. 4.11 Results of conventional method by the coarse meshes according to mold filling rate

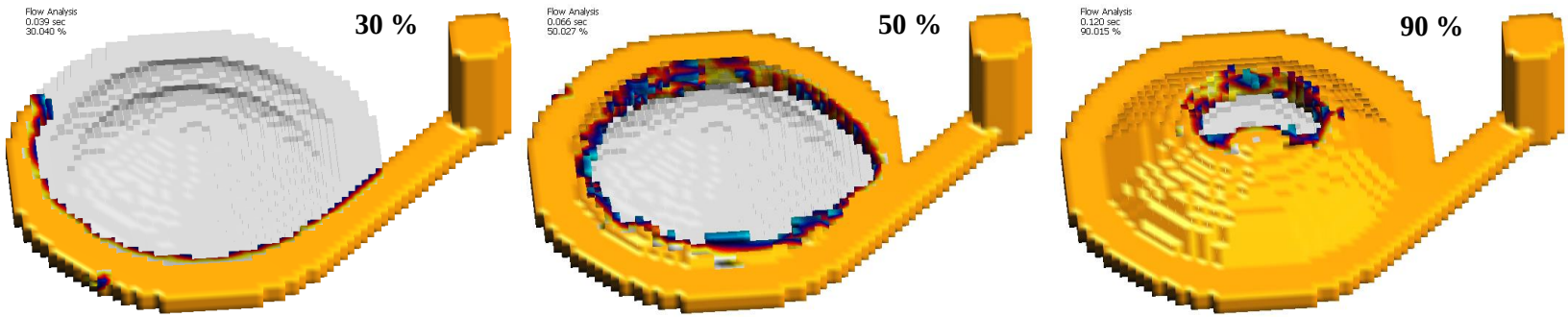

Fig. 4.12 Results of Cut Cell method by the coarse meshes according to mold filling rate

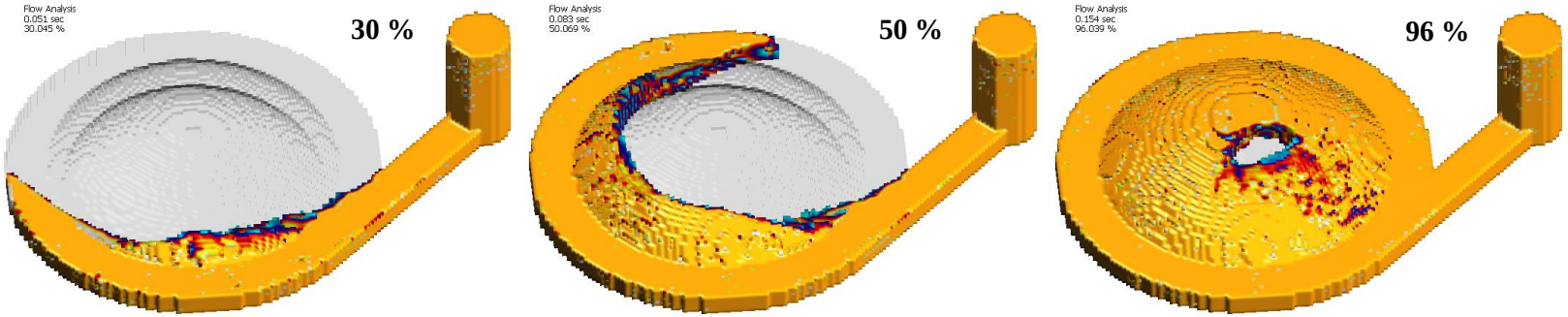

Fig. 4.13 Results of conventional method by the fine meshes according to mold filling rate

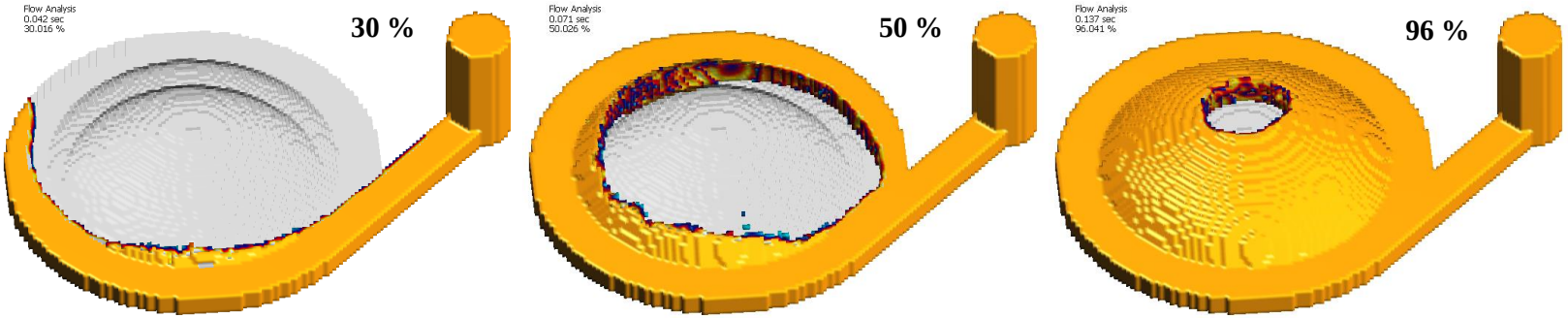

Fig. 4.14 Results of Cut Cell method by the fine meshes according to mold filling rate

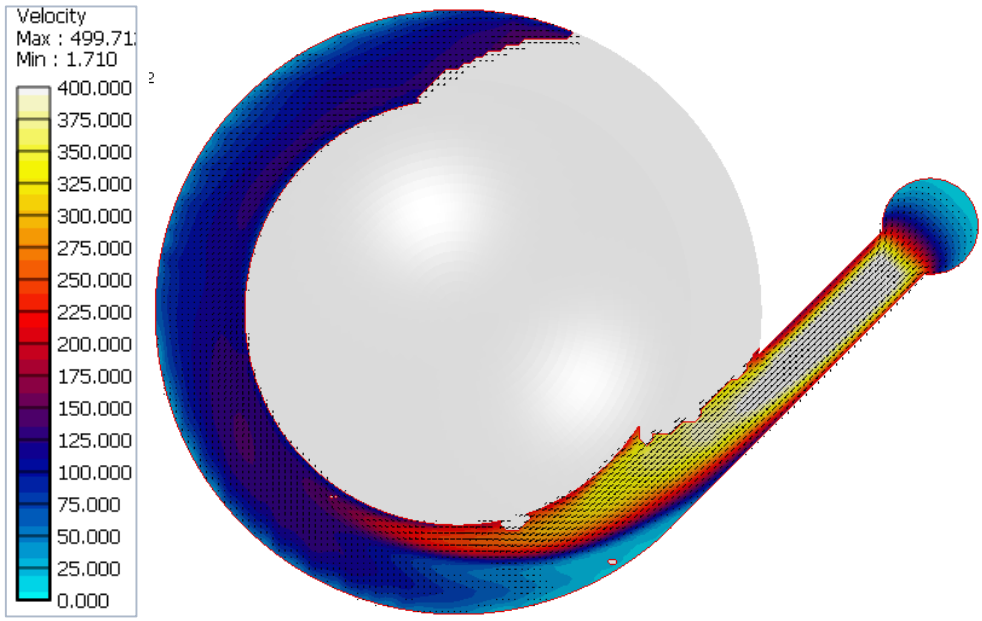

(a) Conventional method

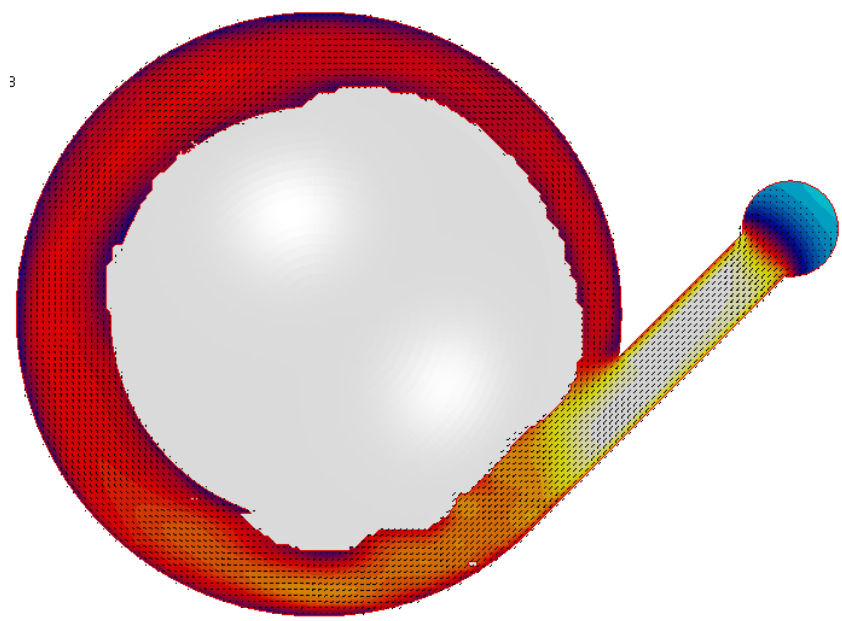

(b) Cut Cell method

Fig. 4.15 Comparison of the velocity contour with the two methods at 50 %

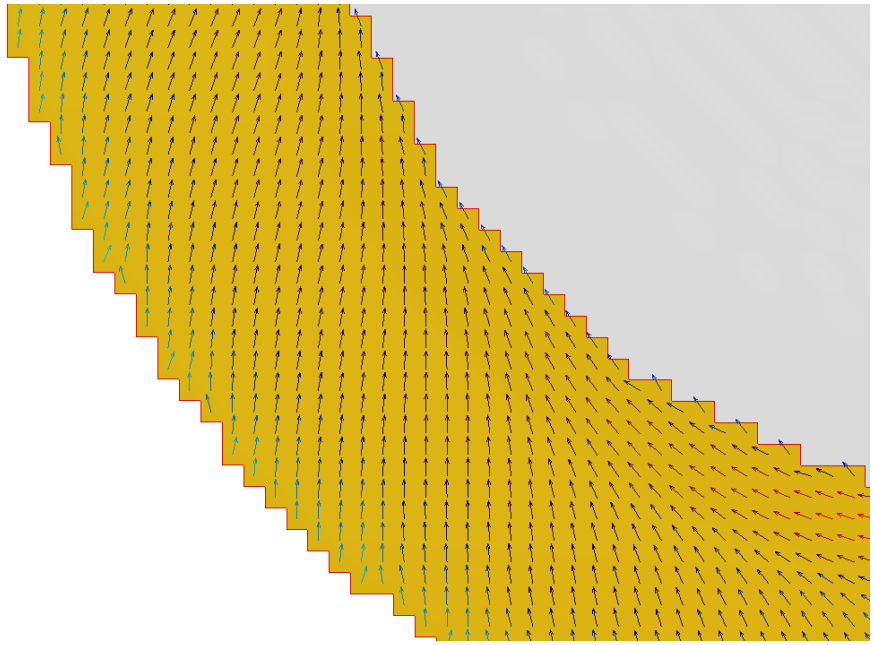

(a) Conventional method

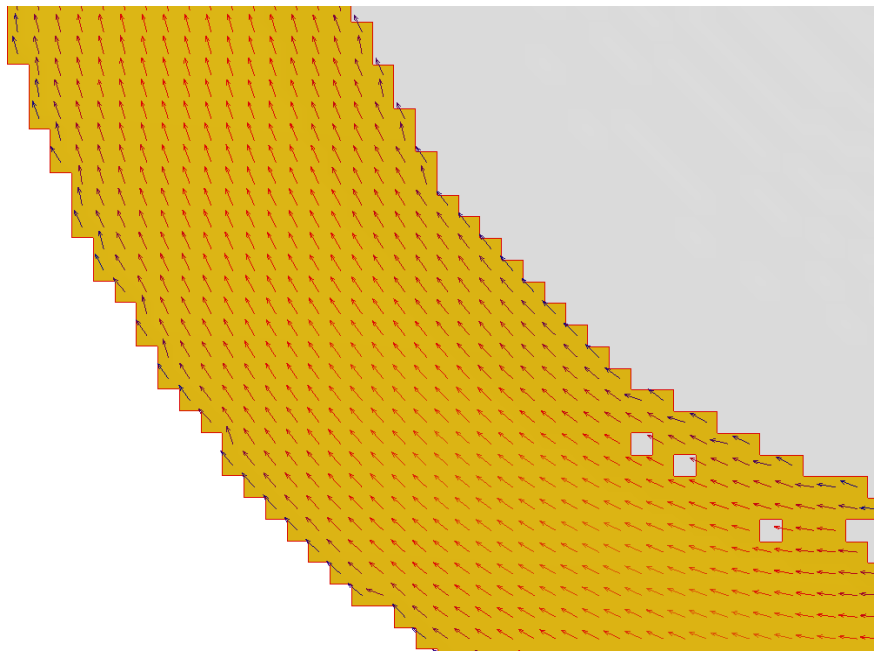

(b) Cut Cell method

Fig. 4.16 Comparison of the velocity vector with the two methods at 50 %

4.2 Application of products by casting process

Casting process can be classified as a sand casting, a gravity die casting, a high pressure die casting, and a low pressure die casting depending on the type of mold and casting method [1]. The developed Cut Cell method is applied to each casting process and compared with the results of the conventional method. The materials used for casting analysis are listed in ASTM standards.

4.2.1 Sand casting

Sand casting is a casting process to be classified as the mold material. It refers to casting using molds made of molding sand. It is the most common, relatively cheap, and old casting method. Casting of most metal alloys is possible from small to large, regardless of the pouring temperature [1].

Large cast steel product, which are parts of construction equipment, was simulated as a sand casting process. Fig. 4.17 shows a 3D model of the product. The molten metal passes through the sprue aligned on the grid and is poured into the product through three runners. Each runner lies at the same angle. Only one of three runners is placed perpendicular to the coordinate axis, creating a grid. Therefore, the other two runners are inclined to the coordinate axis, and velocity drop due to loss of momentum can be expected. The grid domain is 276×239×81 and the total number of grids is 5,343,084. In order to calculate the conventional method more accurately, the number of grids is doubled. The fine grid domain is 350×303×103 and the total number of grids is 10,923,150. The analysis conditions are shown in Table 4.3.

Table 4.3 Analysis conditions

The material of cast	A27-65-35
The material of mold	Green Sand
Pouring velocity	50 cm/s
Meshes	276×239×81
Fine meshes	350×303×103

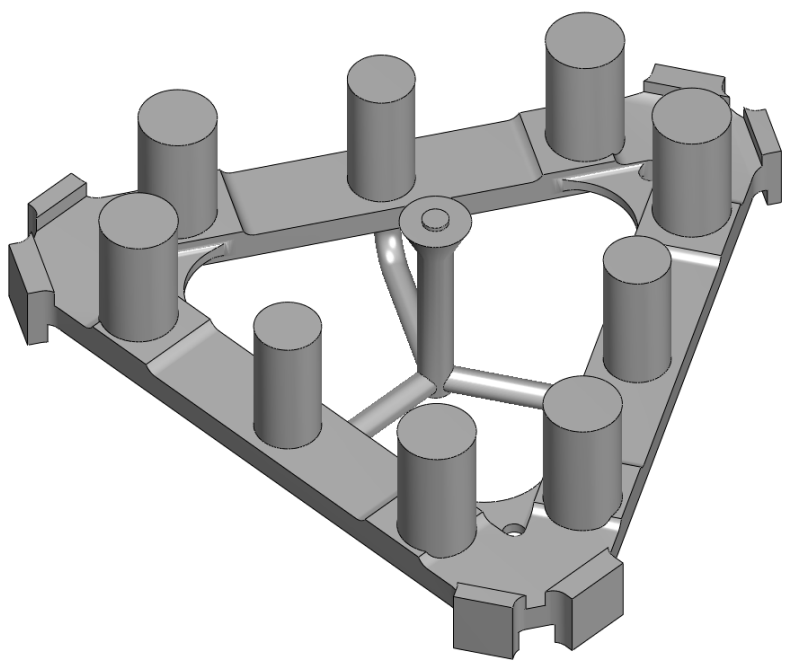

Fig. 4.17 3D model of a casting product

Fig. 4.18 and 4.19 represent the numerical results of the conventional method (a) and the Cut Cell method (b) according to the mold filling rate (1, 8, 12, 14, 19, and 70%). As can be seen in Fig. 4.18 (a), more molten metal flows through the runner aligned to the y-axis at a 1% filling rate. At 8 and 12 %, the molten metal flows slowly into the product between the inclined runners, so that the molten metal is not uniformly filled in the product. In the case of the conventional method at a 14% filling rate, it can be seen that the edge of the product between the inclined runners does not filled unlike the other two places. On the other hand, as shown in Fig. 4.19 (b), which is the result of the Cut Cell method, the product is uniformly filled with the molten metal from three runners. At 70%, in the results of two methods, the product has already been filled with the molten metal, and then risers are filled with the molten metal.

Fig. 4.20 shows the results of doubling the number of grids and simulating it with the conventional method. Due to the large number of grids, the shape is more accurately represented. However, the inclined runners still have step grids. The results in Fig. 4.20 are improved in accuracy from the results of the conventional method in Fig. 4.18 and 4.19, but there is no significant difference. The molten metal is still not evenly filled on the edge of the product.

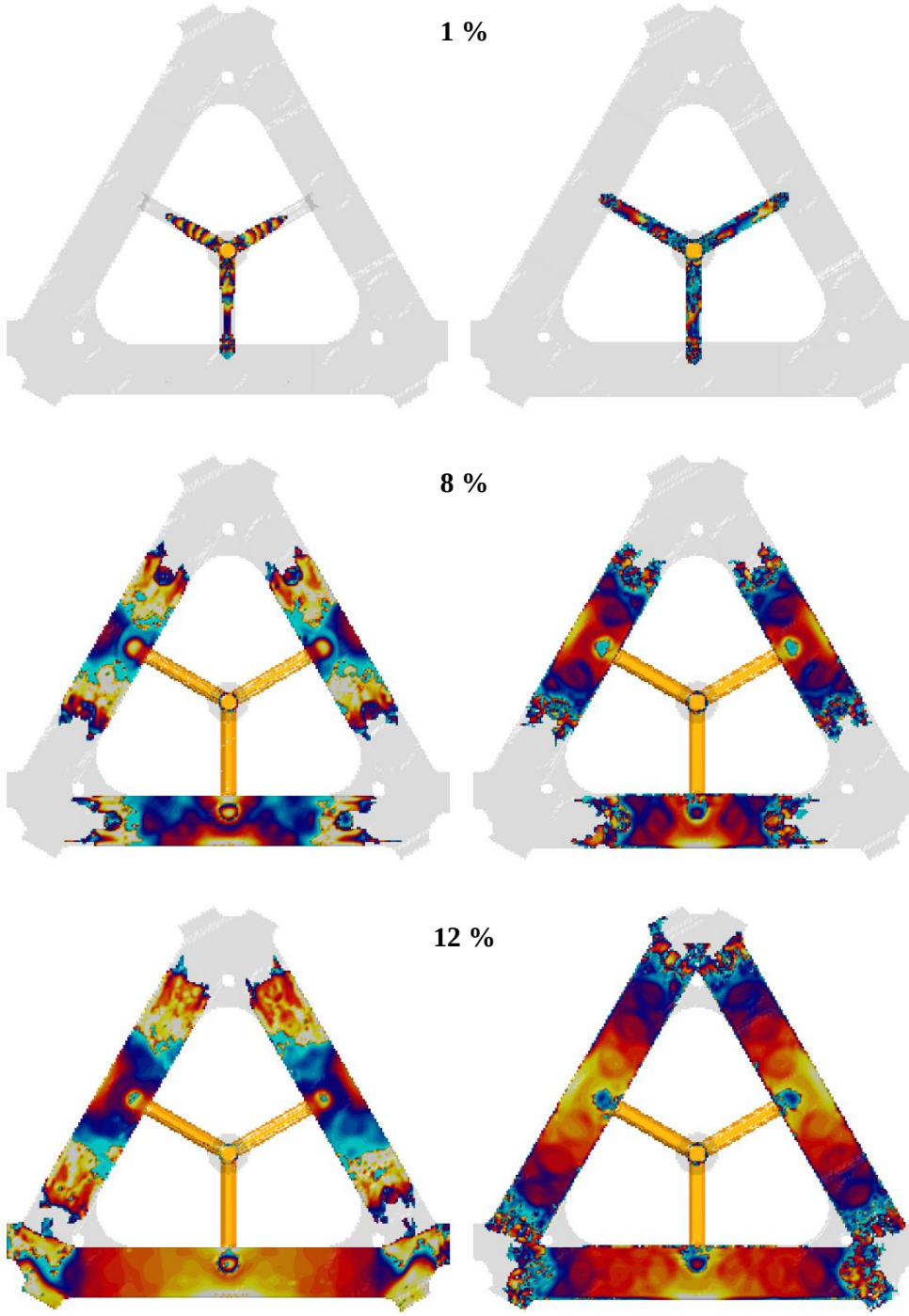

(a) Conventional method **(b) Cut Cell method**

Fig. 4.18 Results of the two methods according to the filling rate (1)

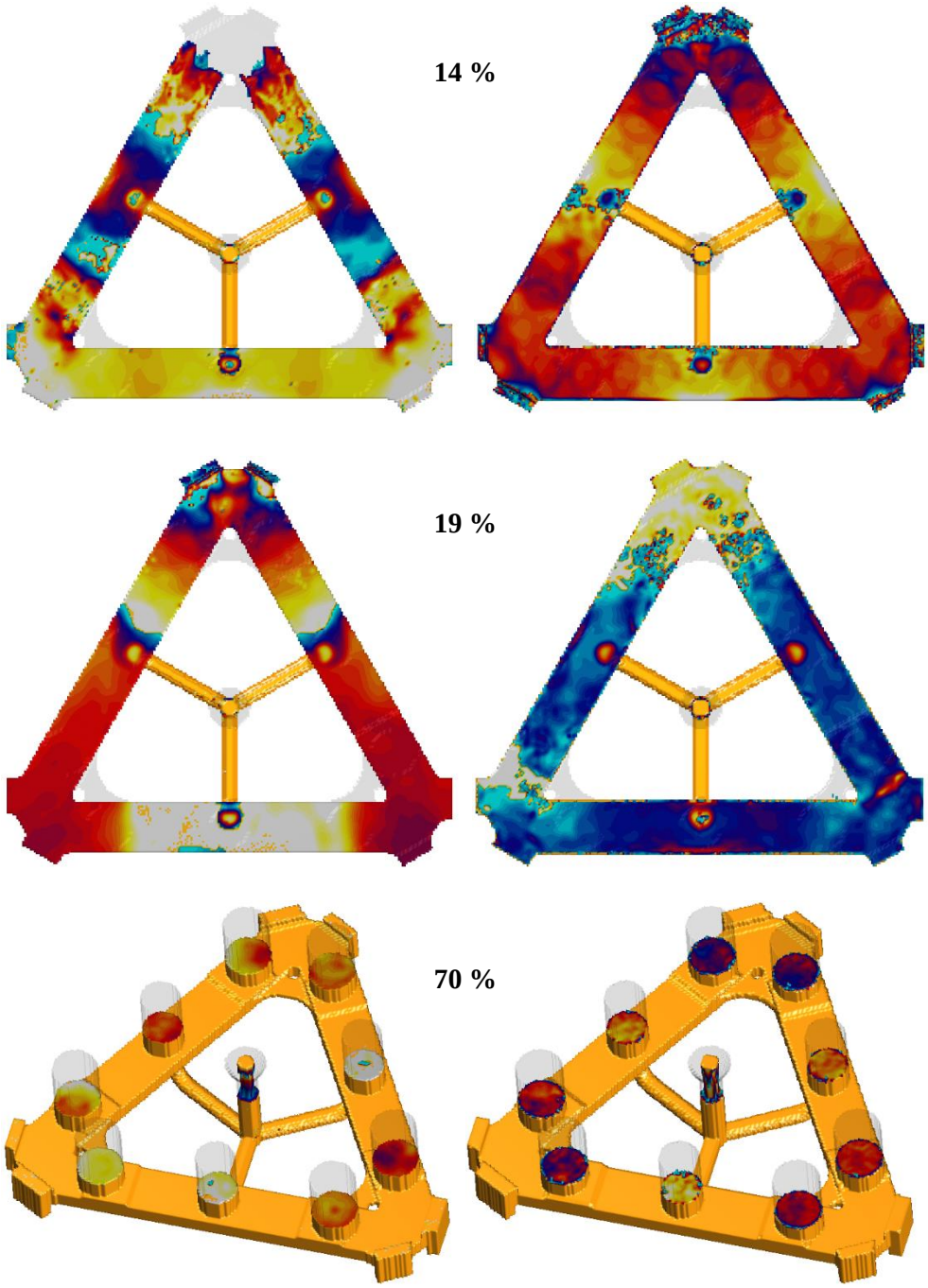

(a) Conventional method **(b) Cut Cell method**

Fig. 4.19 Results of the two methods according to the filling rate (2)

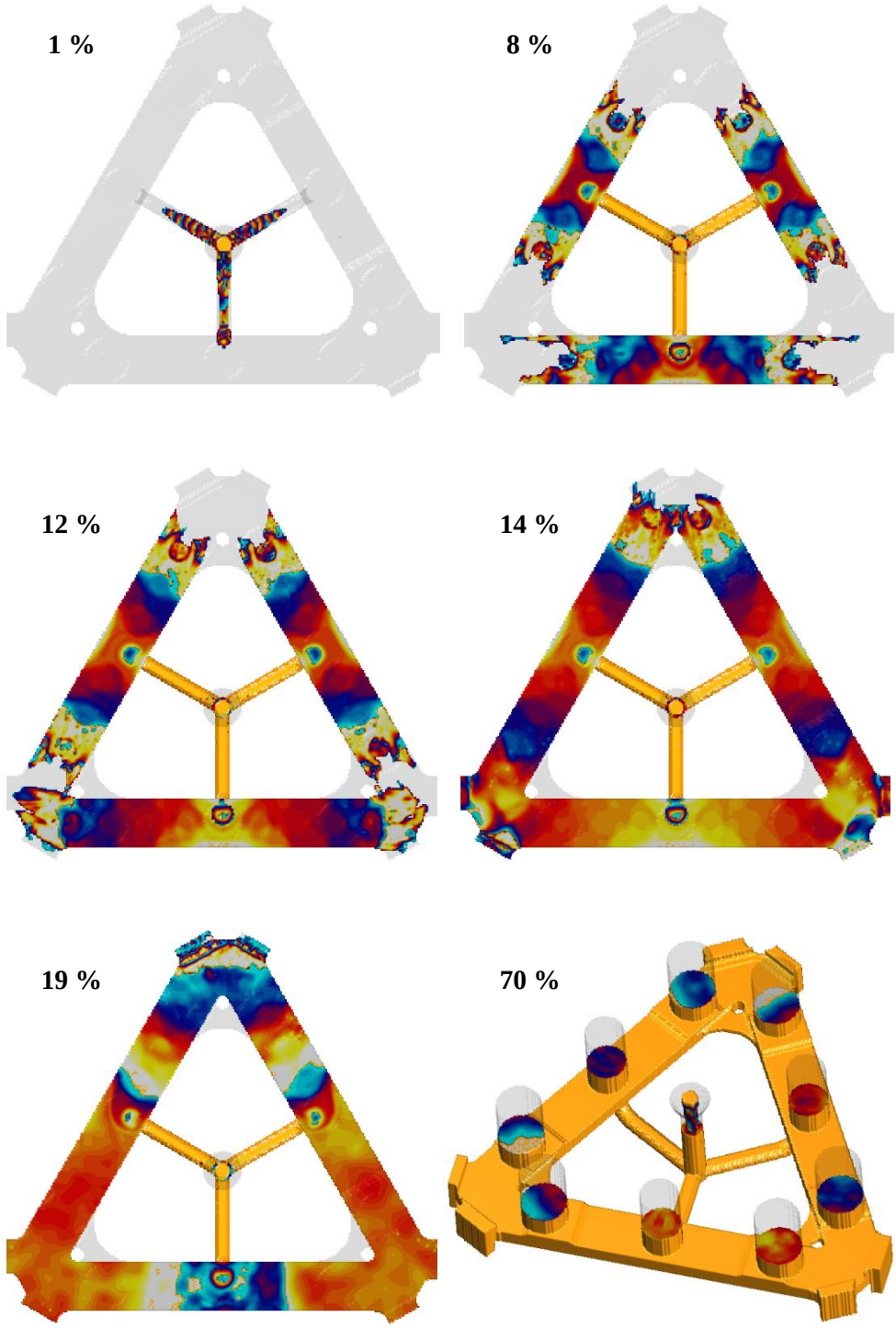

Fig. 4.20 Results of the conventional method by the fine meshes

4.2.2 Gravity die casting

Gravity die casting is a metal casting process. Gravity die casting uses a metal-made reusable mold, commonly called permanent mold casting. Compared to sand casting, the mechanical properties are improved and stable casting surface can be obtained [1].

The propeller used in general yacht was performed as a gravity die casting process. Since the thickness of the blade of the propeller is thin and the flow distance of the molten metal is long, the molten metal solidifies during mold filling so that misruns defect easily occurs.

Fig. 4.21 is a 3D model of the propeller. The grid domain is 190×190×113 and the total number of grids is 4,079,300. The fine grid domain is 300×300×178 and the total number of grids is 16,020,000.

The analysis conditions are shown in Table 4.4.

Table 4.4 Analysis conditions

The material of cast	A356
The material of mold	H13
Pouring velocity	60cm/s
Coarse meshes	190×190×113
Fine meshes	300×300×178

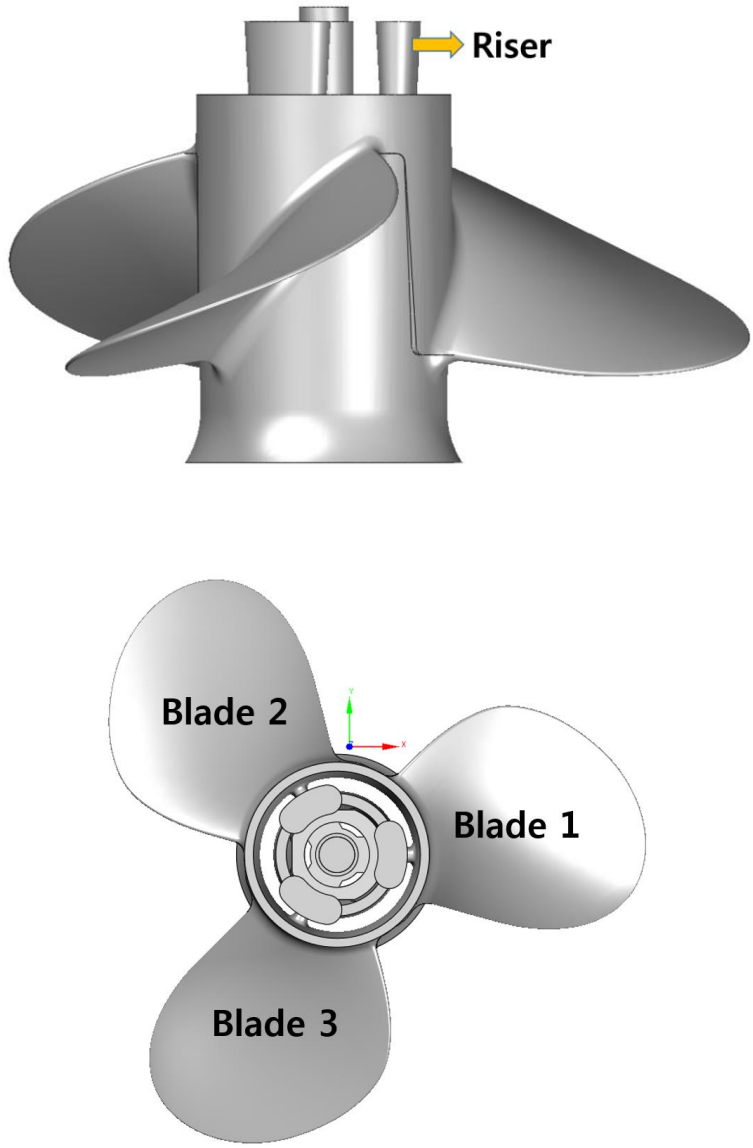

Fig. 4.21 3D model of a propeller

In Fig. 4.21, the runner of propeller is aligned on the x-axis and the other two are inclined to the coordinate axis. Blade 1 is located in the aligned runner, and Blade 3 is placed between the inclined runners. Fig. 4.22 is the numerical results of the two methods shown in the x-y plane. As a result of the conventional method, the amount of flow injected through the inclined runners is the smallest, so that the molten metal is filled later in the Blade 3 compared to the other blades. On the other hand, the results of the Cut Cell method show that the three blades are uniformly filled with molten metal. When the filling rate is 60%, however, the results of both methods are similar.

Fig. 4.23 shows the velocity contour. At 30%, the velocity contour of Blade 1 is similar in both methods. However, in the case of the conventional method, in Blades 2 and 3, the velocity is reduced to half of the Cut Cell method, and Blade 3 is insufficiently filled. The flow pattern is qualitatively similar from above 40% filling rate. However, at 60% of the velocity contour, the velocity of the conventional method is half the velocity of the Cut Cell method.

Fig. 4.24 is the results of quadrupling the number of grids to calculate the existing method more accurately. Increasing the number of grids gives a more accurate representation of the shape in the orthogonal grid, but does not result in a uniform filling in the blades. In Fig. 4.24 (b), the velocity contour is more similar to the velocity contour of Fig. 4.23 (b) than the result of Fig. 4.23 (a).

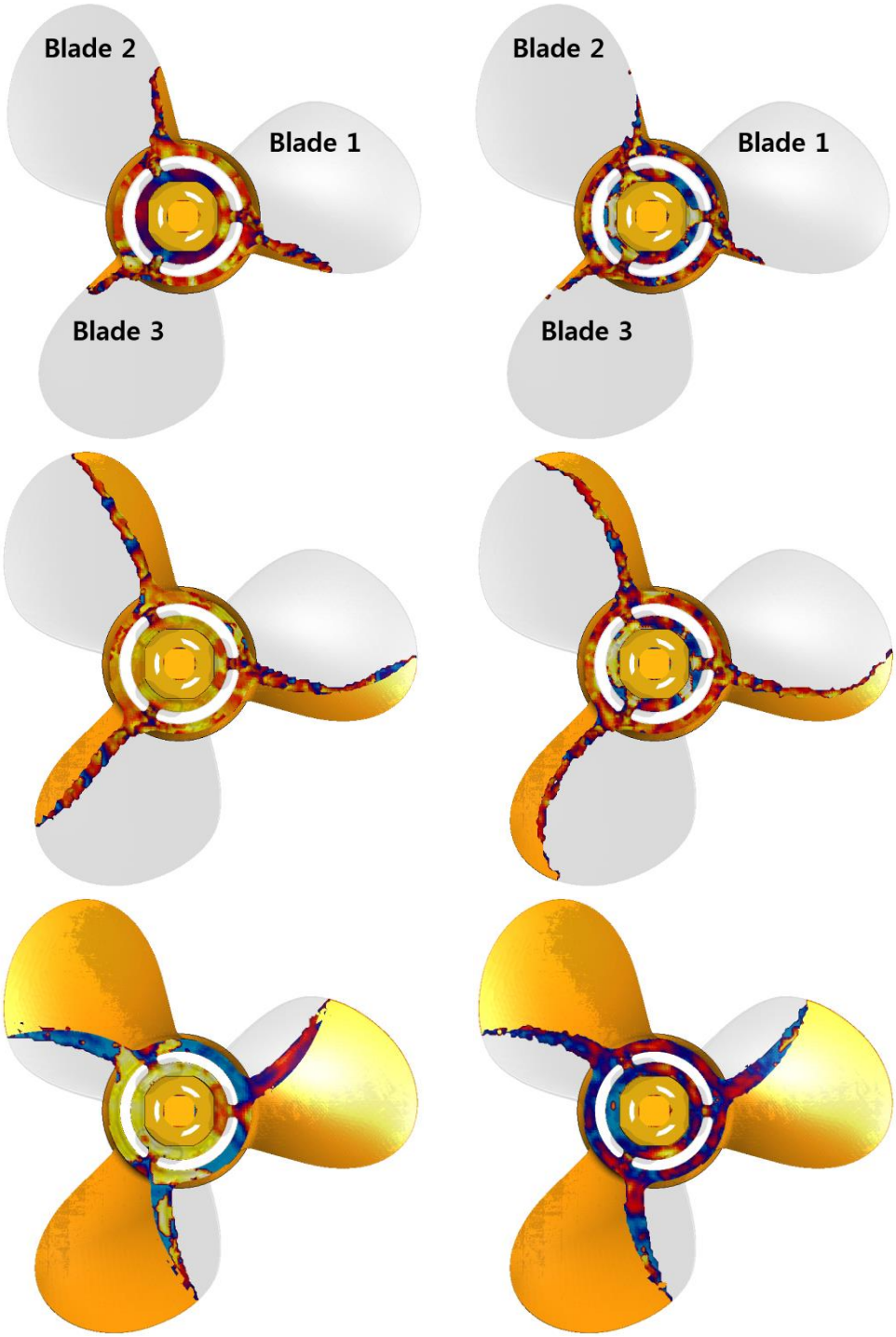

(a) Conventional method **(b) Cut Cell method**

Fig. 4.22 Results of the two methods at the 24, 30, 60 %

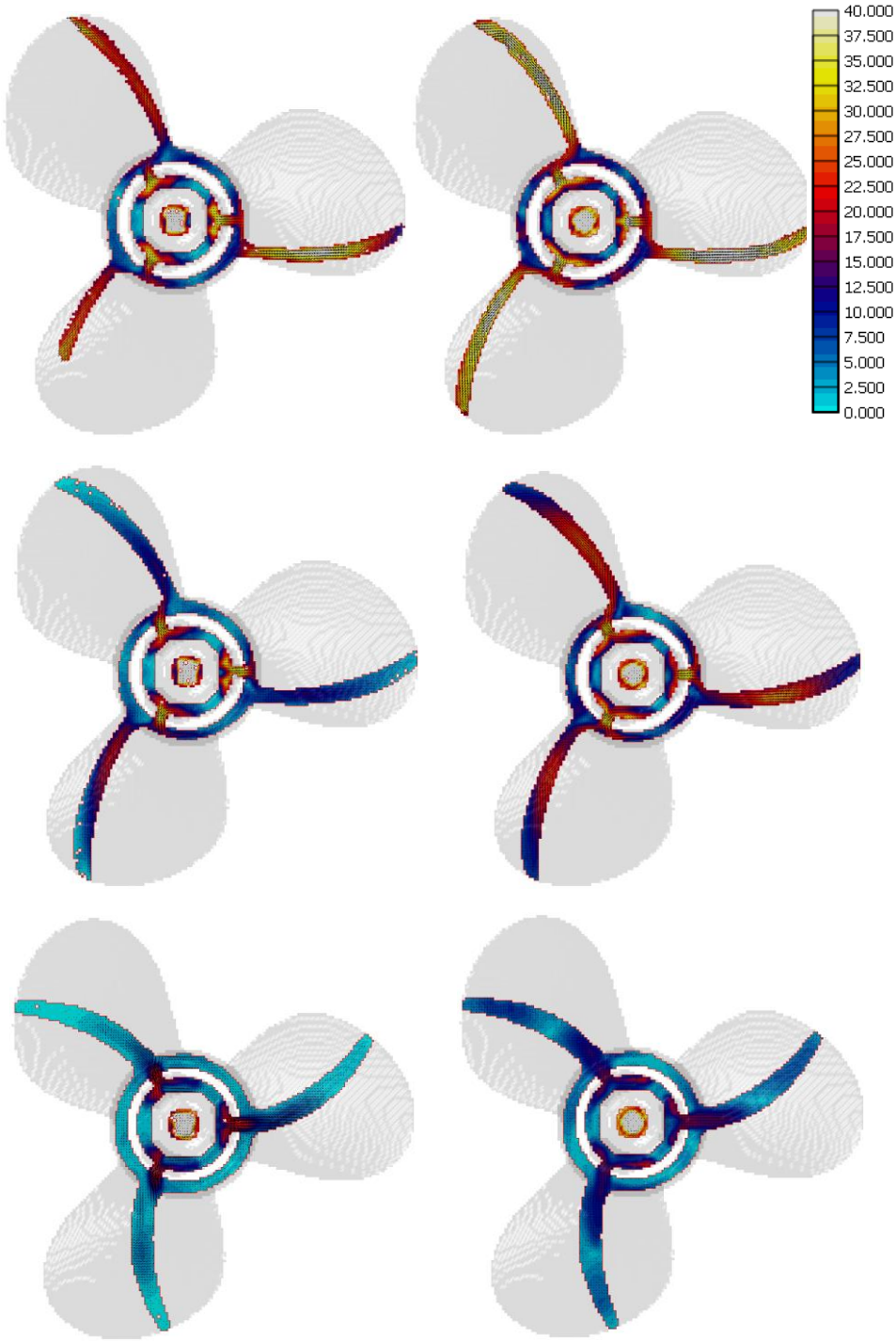

(a) Conventional method **(b) Cut Cell method**

Fig. 4.23 Velocity contour at the 30, 40, 60 %

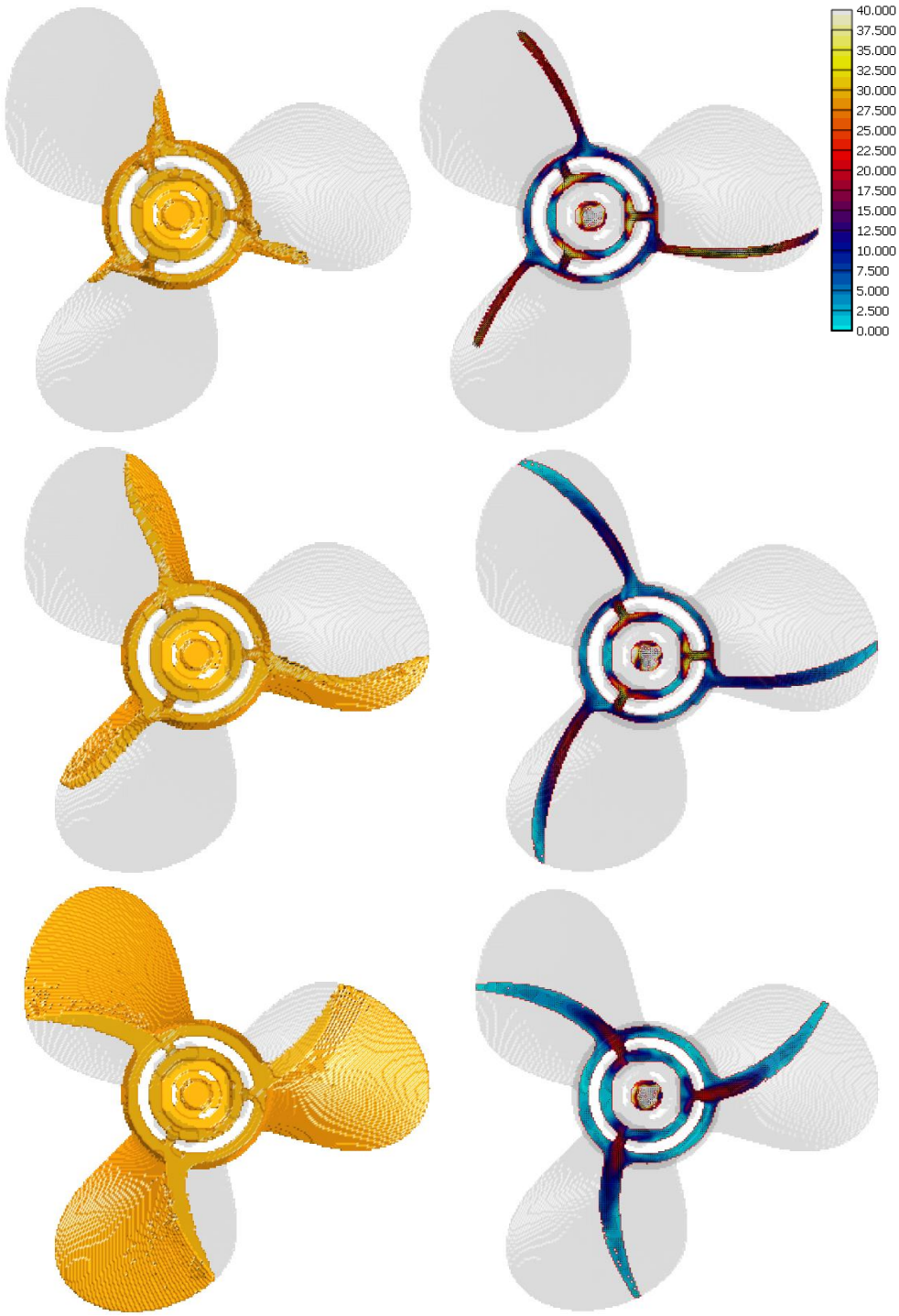

(a) Filling at the 24, 30, 60 % **(b) Velocity contour at the 30, 40, 60 %**

Fig. 4.24 Results of the conventional method in the fine meshes

4.2.3 High Pressure Die Casting

High Pressure Die Casting (HPDC) is a casting method in which molten metal is injected into a mold at high speed and high pressure. The casting surface is beautiful and mass production is possible. Due to its compact structure, it has high mechanical properties, fast production speed and light weight, and is widely used for manufacturing various parts. It is mainly used in aluminum alloy casting [2]. The major disadvantage of HPDC is that its reliability is low due to defects caused by gas porosity and shrinkage. The design of overflow and gas vent for these defect controls is very important [65].

The parts of automotive air conditioner compressor was analyzed by HPDC process. For the design of overflow and gas vent, only the product is simulated first.

Fig. 4.25 shows a 3D model of the casting product. The grid domain is 230×48×182 and the total number of grids is 2,009,280. The fine grid domain is 450×94×356 and the total number of grids is 6,493,660.

The analysis conditions are shown in Table 4.5.

Table 4.5 Analysis conditions

The material of cast	B390
The material of mold	H13
Pouring velocity	50cm/s
Meshes	230×48×182
Fine meshes	340×71×269

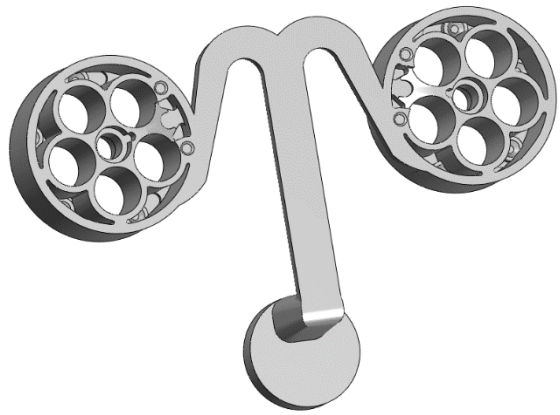

Fig. 4.25 3D model of a casting product

Fig. 4.26 shows the numerical results of the conventional method for the automotive air conditioner compressor. The sprue is aligned on the grid. The runner connected to the ingate is inclined to the grid, and shows a zigzag stair shape. When the filling rate is 60%, the molten metal passing through the ingate flows in the direction of the two arrows shown in the Fig. 4.26 (c). When it is 90%, the final filling region of the molten metal is the circle shown in the Fig. 4.26 (f).

Fig. 4.27 shows the numerical results of the Cut Cell method. At a 60% fill rate, the results are different from those in Fig. 4.26 (c). The molten metal poured in the direction of the runner has a high velocity passing through the ingate having the narrow cross-section and flows along the circular shape in the direction of the arrow shown in 4.27 (c). The molten metal injected from the direction of the runner passes through the ingate having a narrow cross-section and becomes a high velocity fluid. The molten metal then flows along the circular cavity in the direction of the arrow

shown in the 4.27 (c). When it is 90%, the final filling region of the molten metal is in the circle near the ingate marked Fig.4.27 (f).

Fig. 4.28 represents the numerical results of the conventional method in the fine meshes. In an orthogonal grid system, the number of grids of 2,000,000 is very small for simulating this castings without any special treatment, so 15 million grids are generated and analyzed. Fig. 4.28 (a) shows a similar flow pattern to Fig. 4.27 (a). At the 60% filling rate, however, as shown in Fig. 4.28 (c), the molten metal eventually flows in the direction of the two arrow shown in the figure. The final filling area also occurs at a different location from Fig. 4.27 (f).

Fig. 4.29 and 4.30 display the velocity contours in the x-z plane at 50% fill rates for both methods. Comparing the two results, the velocity contours are similar in sprue aligned in a grid. From Fig. 4.29, it can be seen that the velocity is reduced compared to Fig. 4.30 due to the step-like grid at the surface of the product. It can be seen that the velocity contour of the melt in the cavity is generally faster than that of Fig. 4.31.

Fig. 4.31 draws the velocity vector in the x-z cross section. As can be seen the velocity vector of the Cut Cell method, the velocity vector is displayed in parallel with the direction of runner. On the other hand, in the conventional method, the velocity vector exists in a zigzag shape of the surface. The velocity vector with the direction of +z is displayed at the top of the product.

(a) 40% filled **(d) 70% filled**

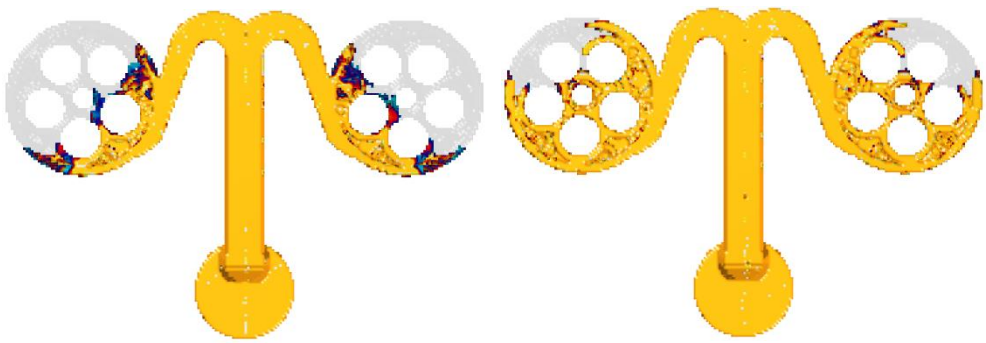

(b) 50% filled **(e) 80% filled**

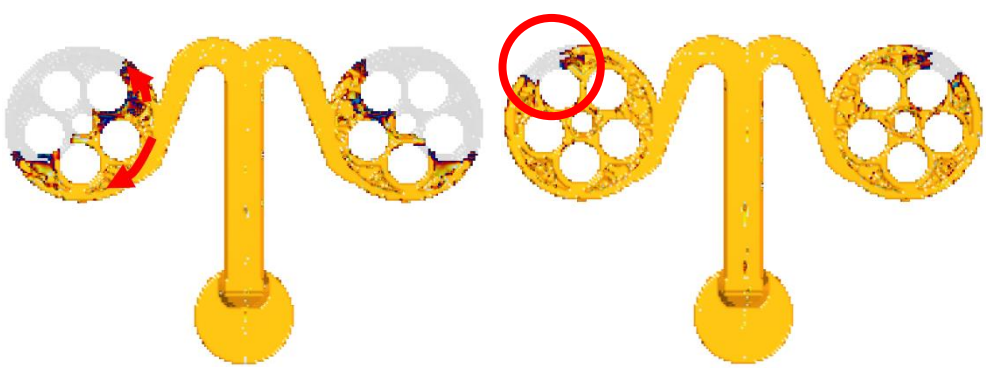

(c) 60% filled **(f) 90% filled**

Fig. 4.26 Results of conventional method for air conditioner compressor

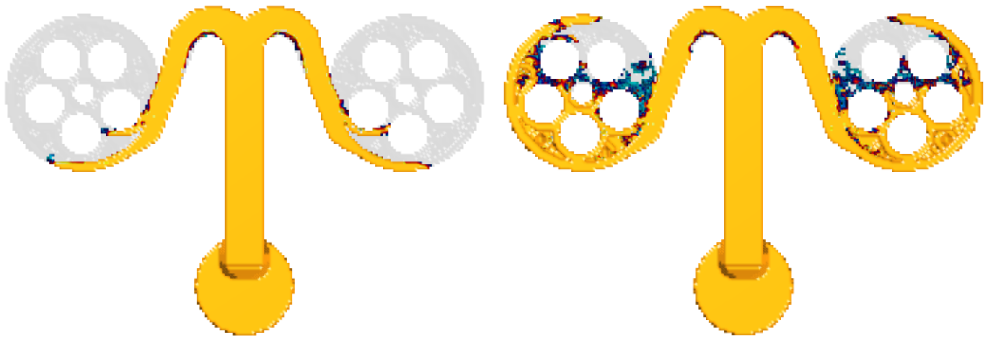

(a) 40% filled **(d) 70% filled**

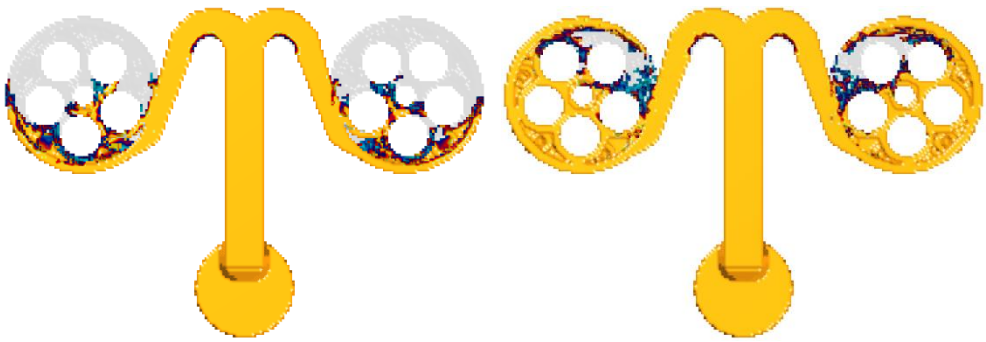

(b) 50% filled **(e) 80% filled**

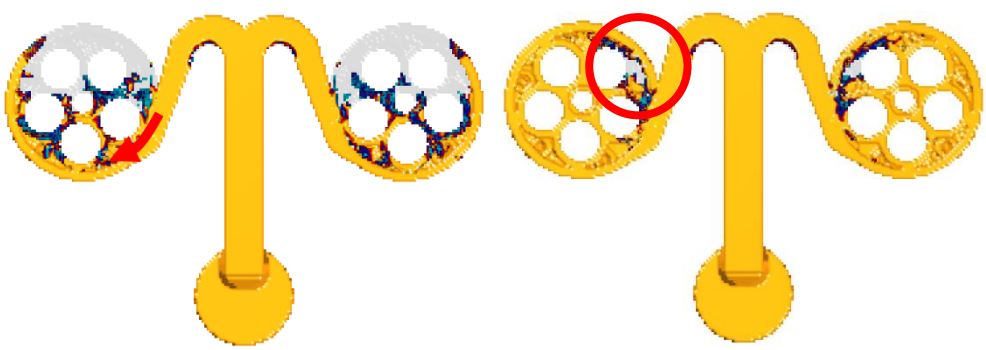

(c) 60% filled **(f) 90% filled**

Fig. 4.27 Results of Cut Cell method for air conditioner compressor

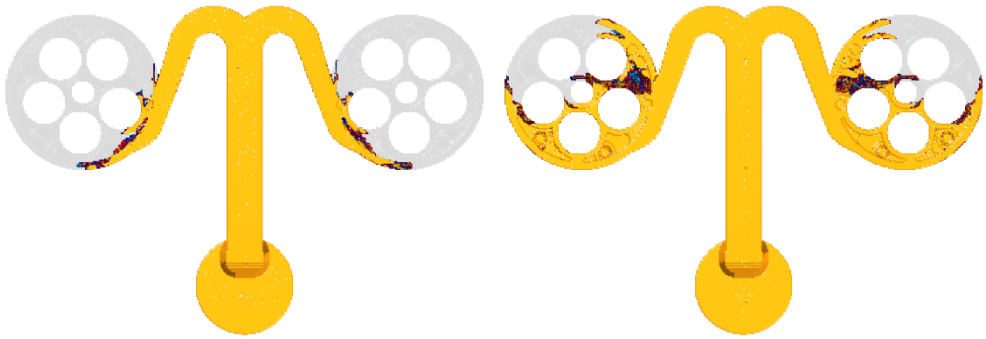

(a) 40% filled **(d) 70% filled**

(b) 50% filled **(e) 80% filled**

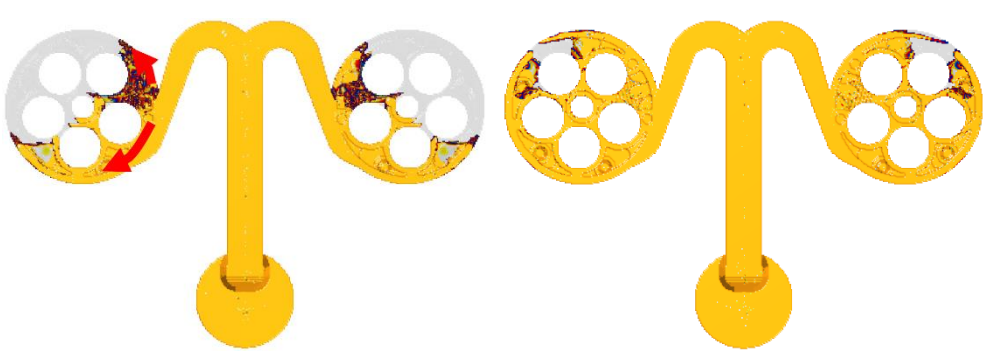

(c) 60% filled **(f) 90% filled**

Fig. 4.28 Results of conventional method in the fine meshes

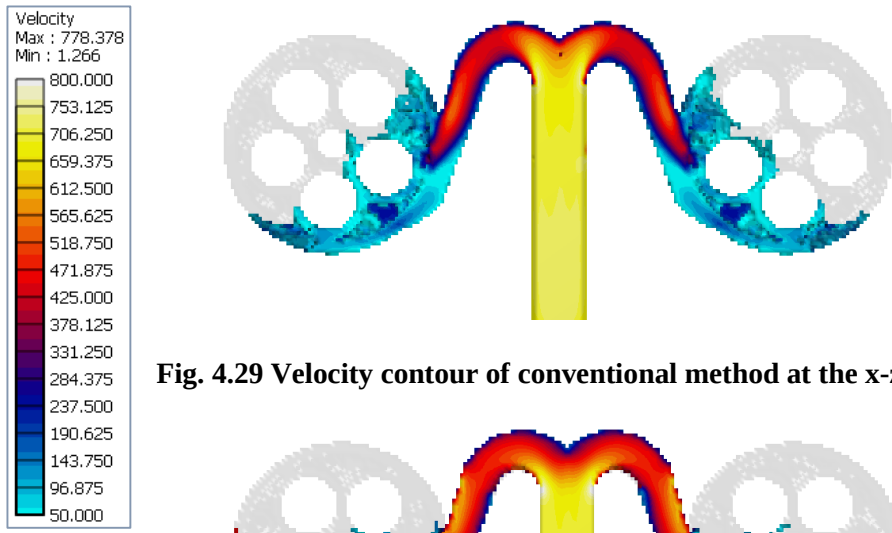

Fig. 4.29 Velocity contour of conventional method at the x-z plane

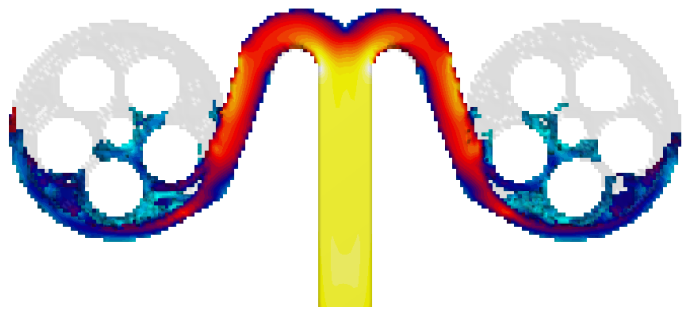

Fig. 4.30 Velocity contour of Cut Cell method at the x-z plane

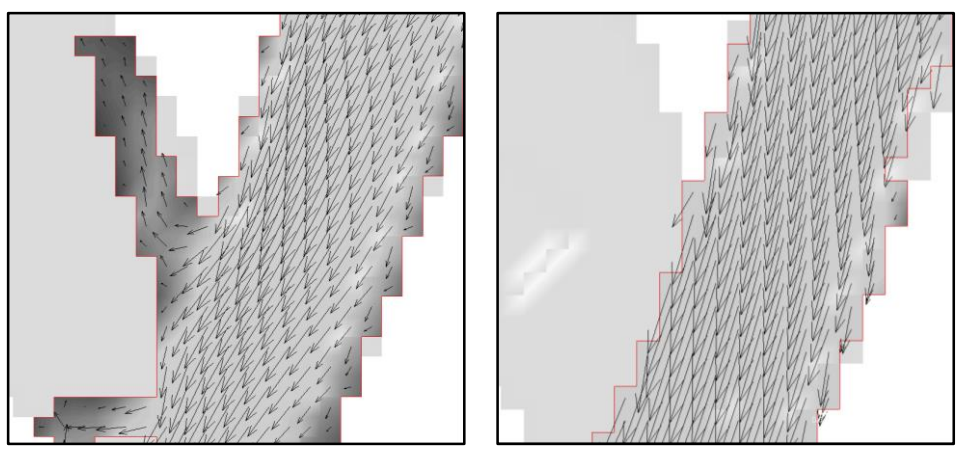

(a) Conventional method **(b) Cut Cell method**

Fig. 4.31 Velocity vector at the cross section of the x-z plane

In the High Pressure Die Casting (HPDC) process, the final filling area is isolated and gas porosities are likely to be concentrated. Therefore, overflow is installed in the final filling area to discharge the fluid to prevent porosity defects. Fig. 4.32 is the practical castings of an automotive air conditioner compressor with the gating system. Fig. 4.33 and 4.34 demonstrate the gating system design based on the results of the Cut Cell method and the existing method, respectively. A completely different design is made for the same castings.

Fig. 4.35 shows the results of casting flow simulation using the Cut Cell method including two types of the gating system. In Fig. 4.35 (a), the overflow is located where the melt flows along the product. During mold filling, the flow first escapes to the overflow and there is still an empty space. Air remaining in the final filling area cannot escape, so there is a high possibility that gas porosity defect occurs at the position.

On the other hand, as shown in Fig. 4.35 (b), an overflow is located above the ingate. The molten metal injected into the ingate flows along the product and returns to the ingate again. The molten metal containing air in the unfilled space is finally discharged to the overflow, thereby preventing gas porosity defects. If the Cartesian grid system is analyzed without the Cut Cell method, it is possible to design an incorrect casting plan as shown in Fig. 4.34. In this case, the analytical accuracy cannot be relied upon.

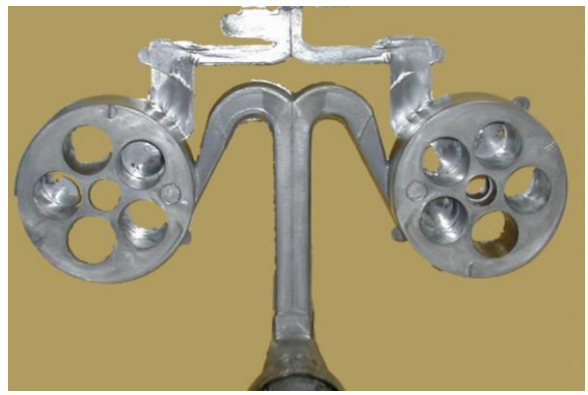

Fig. 4.32 Real castings of an automotive air conditioner compressor

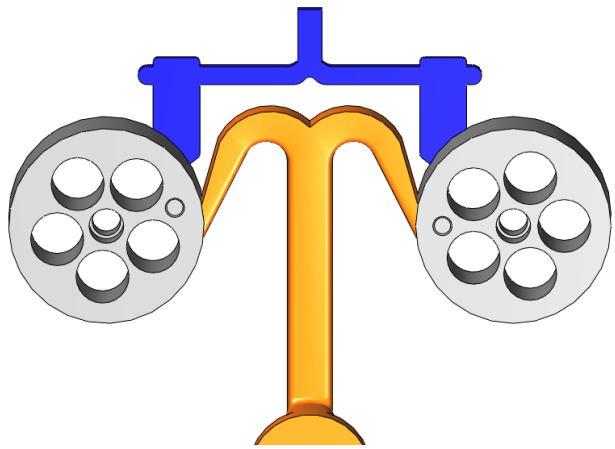

Fig. 4.33 Casting design based on the result of Cut Cell method

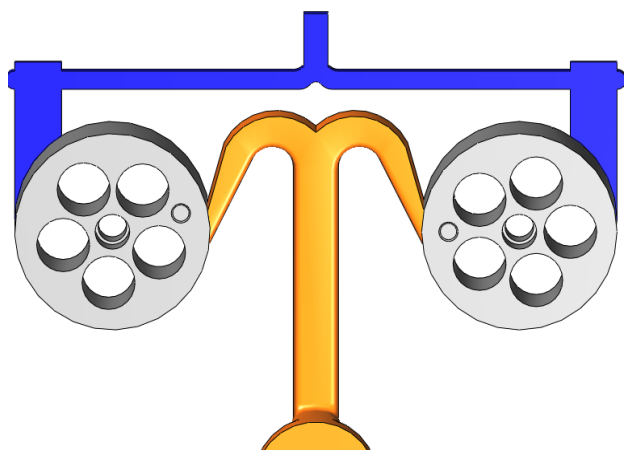

Fig. 4.34 Casting design based on the result of conventional method

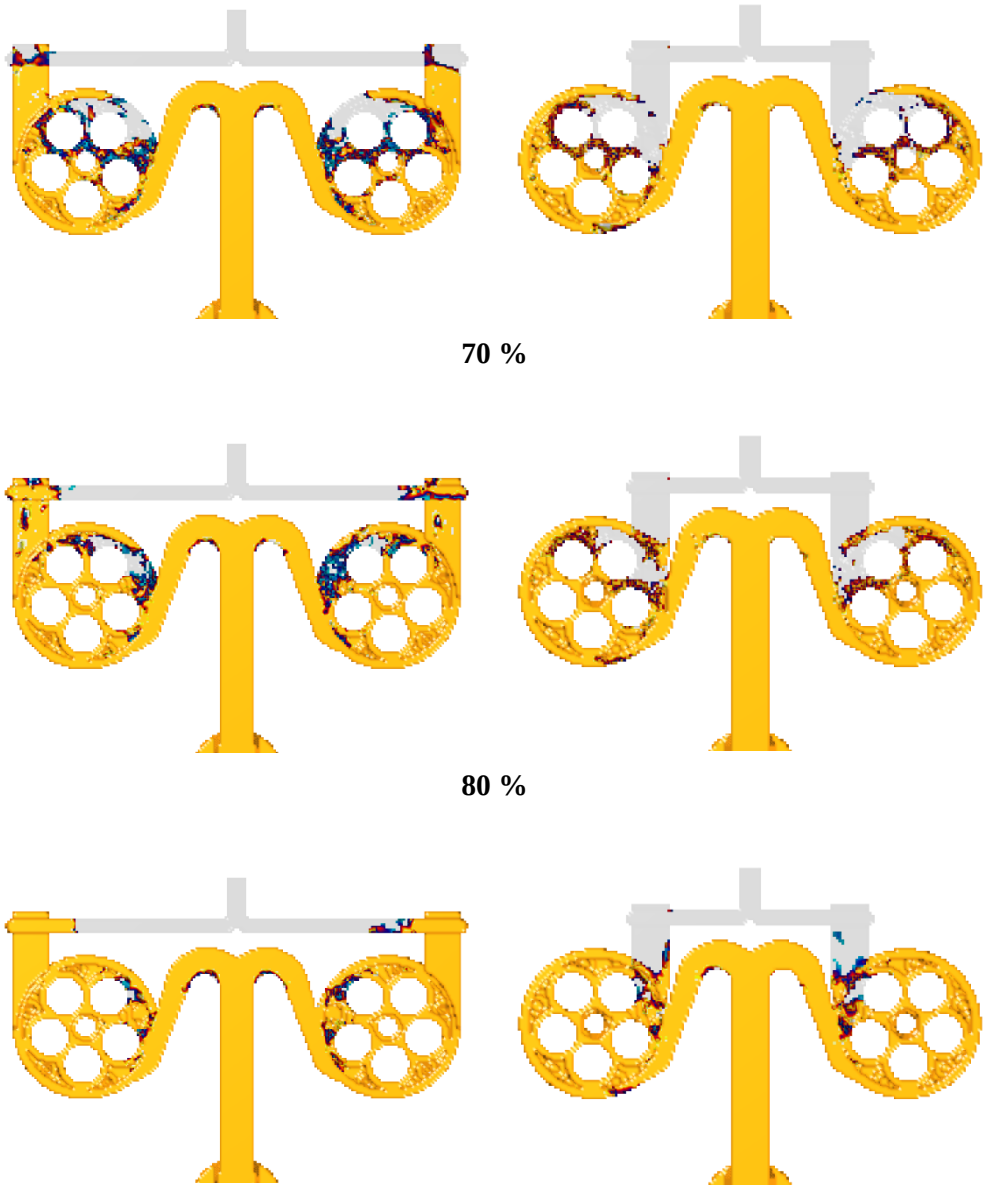

Fig. 4.35 Simulation results of Cut Cell method by the casting design

4.2.4 Low Pressure Die Casting

Low Pressure Die Casting (LPDC) is a casting method in which the molten metal is pushed upward in a direction opposite to gravity through stoke. LPDC is similar to the gravity die casting method, but it differs from pushing the molten metal in the opposite direction of gravity and controlling the pouring velocity. LPDC is easy to produce good castings and has high reliability of mechanical strength, but productivity is not very good [2]. A typical case of LPDC is an automotive aluminum alloy wheel.

Fig. 4.36 shows a 3D model of the wheel. The grid domain is 180×180×122 and the total number of grids is 3,952,800.

Pressurized conditions of LPDC and the analysis conditions are shown in Table 4.6 and 4.7, respectively.

Table 4.6 Pressurized conditions

Time (s)	Pressure (g/cm2)
0	0
7	180
14	220
24	540

Table 4.7 Analysis conditions

The material of cast	A356
The material of mold	H13
Meshes	180×180×122

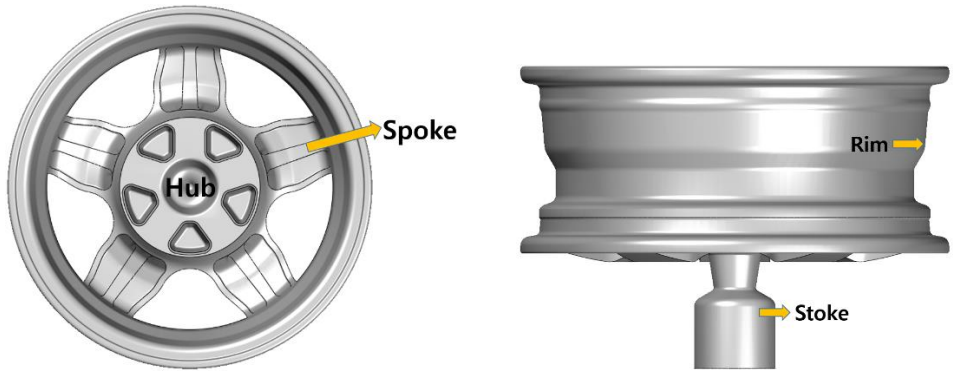

Fig. 4.36 3D model of an aluminum alloy wheel

Fig. 4.36 shows a 3D model of the wheel. The grid domain is 180×180×122 and the total number of grids is 3,952,800.

Fig. 4.37 shows the numerical results of the two methods of aluminum alloy wheels according to the filling rate. The flow filling pattern of the conventional method and the Cut Cell method is very similar. At the same filling rate, the filling time is initially faster for the Cut Cell method, but at a 90% filling rate, they become almost similar. LPDC has a very slow filling rate in which the flow is filled against gravity. The flow is pushed up stoke aligned to the axis. The flow reaching the hub passes through the spokes and rises vertically in the rim. The wheel's rim has a circular surface, but the flow velocity is slow and the flow direction is aligned to the grid, so there is no noticeable difference between the two methods.

Fig. 4.38 shows the flow velocity contour in the center section of the rim in the x-z plane. When the filling rate is 12%, the molten metal reaches the hub. At that time, the velocity contour of the two methods are very similar in stoke. When it is

30%, the molten metal is poured into the spoke. Spoke is inclined to the z-axis and is directed downward. The molten metal reaching the hub accelerates. The velocity of the molten metal in the spoke gets fast. In the Cut Cell method, it is about 60 cm/s whereas in the conventional method, it is about 35-40 cm/s. When it is 70%, the molten metal is filled in the rim. The velocity contours of both methods are very similar. At this time, the velocity at rim is 5-10 cm/s and very low velocity.

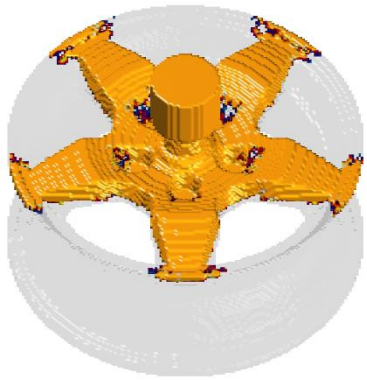

30 % (7.289 s)

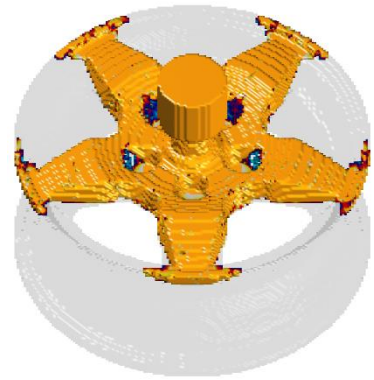

30% (7.137 s)

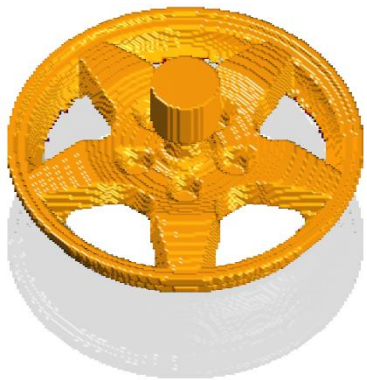

60 % (8.343 s)

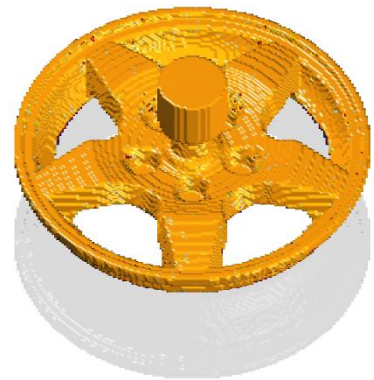

60% (7.996 s)

90 % (11.680 s)

90% (11.964 s)

(a) Conventional method **(b) Cut Cell method**

Fig. 4.37 Results of the two methods according to the filling rate

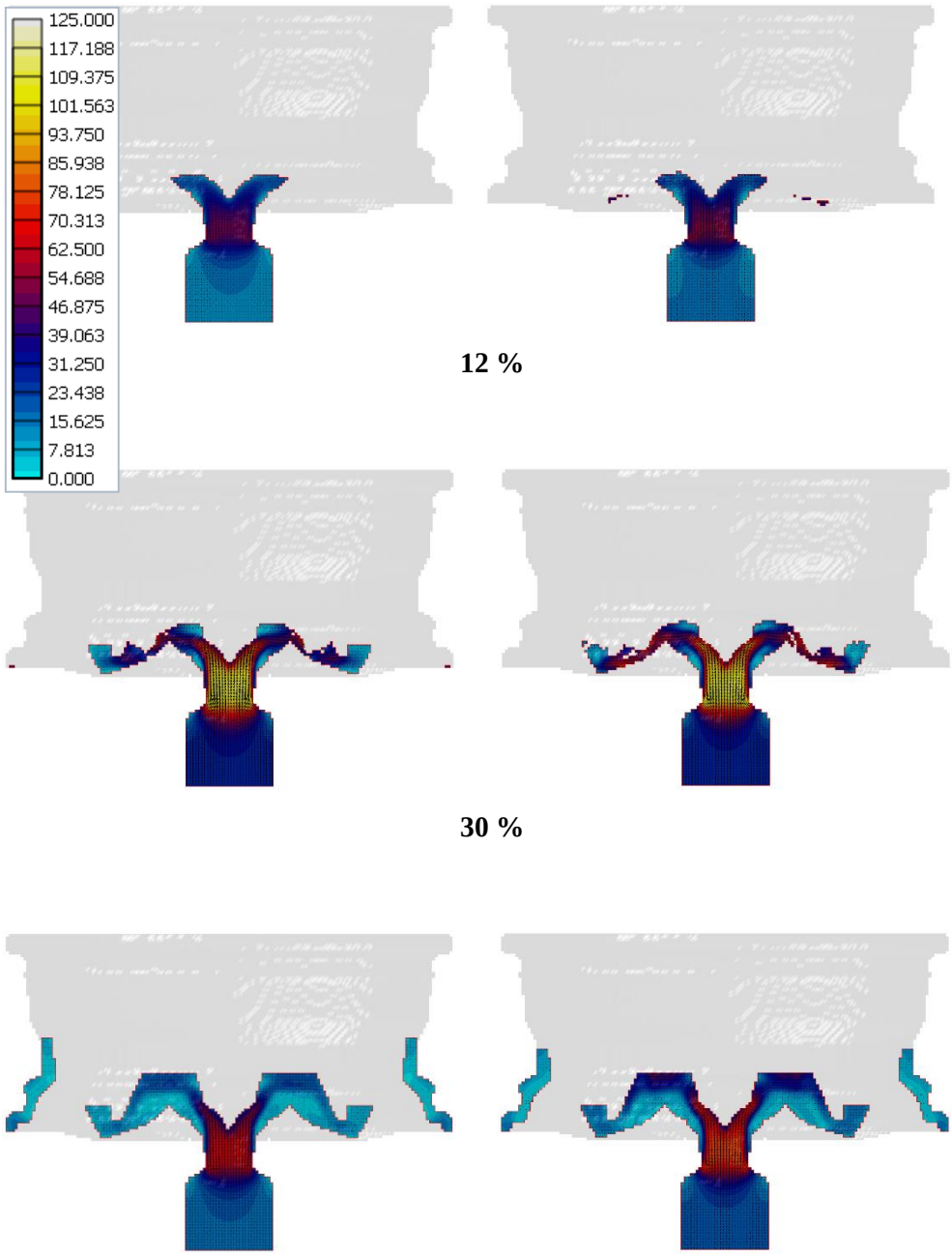

(a) Conventional method **(b) Cut Cell method**

Fig. 4.38 Velocity contour of the two methods at the 12 %, 30 % and 70 %

4.3 Computational time

The computational time is compared to examine the efficiency of the Cut Cell method. Table 4.8 shows the computational time of the conventional method, the Cut Cell method, and the conventional method by the fine meshes for the models analyzed in Chapter 4. Comparing all the analysis cases, the Cut Cell method by the same meshes took longer time to calculate. In general, numerical analysis in a conventional Cartesian grid system, that is, without the Cut Cell method, requires a large number of grids in order to minimize geometric distortions. If the shape is complex, it is usually required to generate 10 to 20 million grids.

In Chapter 4.1, the numerical results and computational time according to the number of grids are considered. In the case of the Cut Cell method, the correct results can be obtained even with a very small number of grids. On the other hand, the results of the conventional method are not accurate. The computational time is increased by using the fine meshes to obtain accurate analysis results. However, the Cut Cell method is more accurate than the existing methods by the fine meshes.

In Chapter 4.2, for the minimum accuracy, the conventional method requires more than 10 million grids. In traditional methods, generating a large number of meshes ensures reasonable results. However, the computational time of the conventional method by the fine meshes was longer than that of the Cut Cell method by the coarse meshes. In the Cartesian grid system, the Cut Cell method can reduce the total number of grids and thus improve the calculation performance when the casting with many slopes and curved surfaces is analyzed.

Table 4.8 Computational time (s) for the cases

Case		The number of grids (Fine meshes)	Cut Cell method	Conventional method	Conventional method (Fine meshes)
Chapter 4.1.1	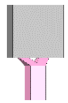	7,296 (912,000), x125	29.485	16.769	614.753
Chapter 4.1.2	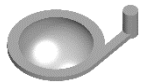	105,600 (844,800), x8	42.033	13.308	292.692
Chapter 4.2.1	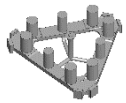	5,343,084 (10,923,150), x2	4473.49	3924.608	10778.5
Chapter 4.2.2	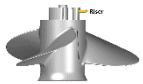	4,079,300 (16,020,000), x4	2092.44	1824.52	7154.18
Chapter 4.2.3	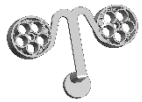	2,009,280 (6,493,660), x3	1037.56	494.483	3643.06
Chapter 4.2.4		3,952,800 (-)	1910.23	982.609	-

Chapter 5. Conclusion

Casting design is essential to produce high quality castings. Computer simulations have been widely used in the foundry industry since the development of CAE. In order to manufacture castings of sound metallurgy and accurate dimensions, it is very important to develop casting designs for the mold filling stage. Through casting flow simulation, it is possible to assess in advance whether the casting design is appropriate. In this respect, it is important to accurately perform the mold filling simulations.

Numerical techniques based on the Cartesian grid system have been studied at the beginning of casting flow simulation. It is thought that Cartesian grid system may be suitable since casting flow simulation involves free surface tracking. It is relatively easy to generate a grid using the Cartesian grid system. However, complex casting products with many slopes and curves distort the boundaries of the geometry in the Cartesian grid system. This leads to loss of momentum and unsound results. Creating a large number of grids to avoid this problem leads to poor computational performance, and cannot solve the intrinsic problems caused by stair boundaries.

BFC system provides good quality numerical results. However, grid generation is difficult and calculation efficiency is poor, so it is not feasible to apply BFC system in the field of casting flow simulation. The casting process runs very quickly from product development to completion, so computational time is an element that is just as important as the accuracy of casting flow analysis.

To solve this problem, the present study applied the Cut Cell method -based on PCT, which is used to analyze the fluid flowing around an object moving in the Cartesian grid, to the casting flow analysis.

First, experimental and numerical validations are conducted to verify the developed numerical method.

A simple casting shape acrylic device was fabricated, and the result of the water model experiment is in good agreement with the numerical result of the Cut Cell method. In addition, another experiment is carried out using a casting shape device based on the gating system design. The accuracy of Cut Cell method is confirmed by comparing the results of the conventional method and the Cut Cell method with the experimental result. The results of casting experiment conducted by Mampaey and the developed Cut Cell method are also compared, and it is confirmed that the numerical result agrees well with the practical casting flow values.

Mass flow rate error and momentum loss are measured by the number of grids and analyzed for the conventional method and the Cut Cell method. In both methods, the energy loss decreased as the number of grids increased. In the case of the conventional method, the number of grids should be at least 4 to 5 times greater than that within the Cut Cell method in order to guarantee minimal energy loss.

Second, a comparative study of the existing method and Cut Cell method is performed to see how application of the Cut Cell method affects the casting flow simulation.

Numerical results of the two methods are compared according to the number of grids. In the conventional method, the results are more accurate when analyzed using a fine grid system rather than a coarse grid system. However, the Cut Cell method likewise improved accuracy. Comparing the results of the two methods, in is seen that the results of the conventional method of fine meshes are similar to or slightly less accurate than those of the Cut Cell method using coarse meshes. The increase in the number of grids in the Cartesian grid system does not fully compensate for the loss of energy caused by shape distortion or obstacles in the stair grids.

Practical castings were implemented as a typical casting process such as sand casting, gravity die casting, HPDC, and LPDC. The developed Cut Cell method works well for each process. A comparison study of the two methods is also carried out. In the case of sand casting and gravity die casting process, the accuracy of analysis was different between the conventional and the Cut Cell methods. In the case of HPDC, use of fine meshes was not effective in correcting the simulation error of the conventional method. In the case of an automotive wheel, which is an LPDC process, there is no visible difference between the two methods, such as the flow pattern.

Finally, the computational time of the analyzed model is examined. In a coarse grid system, the Cut Cell method took a longer time than the conventional method. However, when the conventional method is simulated in the coarse grid system, analytical accuracy is low. Therefore, the conventional method should be applied with fine meshes. However, it is seen that computational time of the conventional

method with fine meshes took longer than that of the Cut Cell method with coarse meshes.

In conclusion, it is confirmed that Cut Cell Cartesian grid method without BFC is effective in obtaining more accurate casting flow analysis. However the Cut Cell method involves long computational time. Another disadvantage is the necessity of calculating a separate variable value for applying a cut-cell. There are cases where there is no visible difference between the two methods depending on the shape and the casting process. Therefore, in the analysis of casting flow, it is necessary to selectively use the conventional method or the Cut Cell method considering the accuracy and efficiency of analysis.

References

[1] Kil Hong Lee, "Casting engineering," Chosun Univ., 1st ed., Korea, 2002.

[2] J. Campbell, "Invisible macro defects in castings," Journal de Physique IV, vol. 3, C7, 1993, pp. 861-872.

[3] J. Campbell, "Castings," Butterworth-Heinemann, 2nd ed., Oxford, 2003.

[4] J. Campbell, "Castings practice: The 10 rules of castings," Butterworth-Heinemann, 1st ed., Oxford, 2004.

[5] J.M. Svoboda, "Basic principles of gating and risering," 2nd ed., American Foundrymen's Society-Cast Metals Institute, 2008.

[6] Ricardo Fuoco, "The effect of gating system design on the quality of aluminum gravity casting," Computational Materials Science, vol. 36, no. 4, 2006, pp. 457-467.

[7] M. Masoumi, H. Hu, J. Hedjazi, and M. A. Boutorabi, “Effect of gating design on mold filling,” AFS Transactions, vol. 113, 2006, pp. 185-196.

[8] M. Masoumi, S. M. A. Boutorabi, & J. Hedjazi, “Effect of gating design on melt entry velocity,” AFS Transactions, vol. 116, 2008, pp. 47-60.

[9] Mu Seong Jee, "Advanced Casting Processes," Kuhminsa, Fifth ed., Korea, 2013.

[10] I. Ohnaka, J-D Zhu, N. Sako, A. Sugiyama, and C-K Ye, "Challenging issues in computer simulation of casting," International Journal of Cast Metals Research, vol. 24, no. 3, 2011, pp. 133-138 .

DOI: 10.1179/136404611X13001912813690

[11] C. M. Choudhari, K. J. Padalkar, K. K. Dhumal, B. E. Narkhede, B. E. Narkhede, and S. K. Mahajan, "Defect free casting by using simulation software," Applied Mechanics and Materials, vol. 313-314, 2013, pp. 1130-1134.

[12] J.D. Zhu, I. Ohnaka, A. Sugiyama, T. Ohmichi, and Y. Ogino, "Modeling of mold filling in gating systems with filters," International Journal of Cast Metals Research, vol. 15, 2002, pp.161-165.

DOI: 10.1080/13640461.2003.11819477

[13] S. M. H. Mirbagheri, H. Ashuri, N. Varahram & P. Davami, "Simulation of mould filling in lost foam casting process," International Journal of Cast Metals Research, vol. 16, no. 6, pp. 554-565.

DOI: 10.1080/13640461.2003.11819635

[14] T. Sakuragi, "Mould filling simulation with consideration of surface tension and its application to a practical casting problem," International Journal of Cast Metals Research, vol. 18, no. 4, pp.202-208.
DOI: 10.1179/136404605225022946

[15] S-Y Pang, J-X Zhou, D-M Liao, L-L Chen, M-Y Zhang, and T Chen, "Two phase flow simulation of mould filling process by sharp interface boundary condition capturing method," International Journal of Cast Metals Research, vol. 24, no. 3, 2011, pp. 218-223.
DOI: 10.1179/136404611X13001922708597

[16] Abhilash Viswanath, M.V. Manu, S. Savithri, U.T.S. Pillai, "Numerical simulation and experimental validation of free surfaceflows during low pressure casting process," Journal of Materials Processing Technology, vol. 244, 2017, pp.320-330.

[17] T. X. Hou, R. D. Phelke and J. O. Wikes, "FEM simulator for efficient casting solidification modelling," AFS Transaction, vol. 100, 1992, pp. 1057-1066.

[18] S. Kulkarni and N. K. Radhakrishna, "Prediction of solidification time of cylindrical hollow casting cast in CO_2-Sand moulds by using FEA Technique," International Journal of Materials Science, vol. 2, no. 2, 2007, pp. 137-152.

[19] A. Kermanpur, S. Mahmoudi, and A. Hajipour ermanpur, "Numerical simulation of metal flow and solidification in the multi-cavity casting moulds of automotive components," Journal of Materials Processing Technology, vol. 206, 2008, pp. 62-68.

[20] C. M. Choudhari, B. E. Narkhede, and S. K. Mahajan, "Modeling and simulation with experimental validation of temperature distribution during solidification process in sand Casting," International Journal of Computer Applications, vol. 78, no.16, 2013, pp. 23-29.
DOI: 10.5120/13607-1399

[21] J.H. Hong, Y.S. Choi, H.Y. Hwang, and J.K. Choi, "Optimum design of casting mould by gas porosity prediction module in numerical simulations," Proceedings of Modeling of Casting, Welding and Advanced Solidification Processes-XI, Opio, 2006, pp. 611-618.

[22] E. Niyama, T. Uchida, M. Morikawa, and S. Saito, "Method of shrinkage prediction and its application to steel castings practice," AFS Cast Metals Research Journal, 1982, pp. 52-63.

[23] Ch. Pequet, M. Rappaz, and M. Gremaud, "Modeling of microprosity, macroporosity and pipe-shrinkage formation during the solidification of alloys using a mushy-zone refinement method: Applications to aluminium alloys," Metallurgical and Materials Transactions A, vol. 33, no. 7, 2002, pp. 2095-2106.

[24] A. P. Paine, M. Gäumann, and P. Thevoz, " Model validations of mould filling during casting and a new approach for porosity predictions," International Journal of Cast Metals Research, vol.14, 2002, pp. 377-383.

[25] A. Reis, Y. Houbaert, Z. Xu, R. V. Tol, A. D. Santos, J. F. Duarte, and A. B. Magalhães, "Modeling of shrinkage defects during solidification of long and short freezing materials," Journal of Materials Processing Technology, vol. 202, no. 1-3, 2008, pp. 428-434.

[26] Yongqin Liu, Wanqi Jie, Zhiming Gao, and Yongjian Zheng, "Investigation on the formation of microporosity in aluminum alloys," Journal of Alloys and Compounds, vol. 629, 2015, pp. 221-229.

[27] C. Zhang, Y. Bao, M. Wang, and L. Zhang, "Shrinkage porosity criterion and its application to A 5.5 Ton steel ingot," Archives of Foundry Engineering, vol. 16, no. 2, 2016, pp. 27-32.

[28] Francis H. Harlow and J. Eddie Welch, "Numerical calculation of time-dependent viscous incompressible flow of fluid with free surface," Physics of Fluids, vol. 8, 1965, pp. 2182-2189.

DOI: 10.1063/1.1761178

[29] A. Amsden and Francis H. Harlow, "The SMAC method: a numerical technique for calculating incompressible fluid flows," Technical Report LA-4370, Los Alamos National Laboratory, 1970.

[30] C. W. Hirt and B. D. Nichols, “Volume of fluid (VOF) method for the dynamics of free boundaries,” Journal of Computational Physics. vol. 39, 1981, pp. 201-225.

[31] J. F. Thompson, "A reflection on grid generation in the 90s: trends, needs and influences," International Conference on Numerical Grid Generation in Computational Fluid Dynamics and related Fields, vol. 1, Mississippi State University, 1996, pp. 1029-1110.

[32] F. A. Mampaey and Z. A. Xu, "Simulation and experimental validation of mold filling," Proceedings of Modeling of Casting, Welding and Advanced Solidification Processes-VII, 1995, Pennsylvania, pp. 3-14.

[33] J. D. Zhu and I. Ohnaka, " A new simulation method of mold filling by using regular and irregular-mixed elements," Proceedings of Modeling of Casting, Welding and Advanced Solidification Processes-IX, Aachen, 2000, pp. 428-435.

[34] J. Hetu and F. Tlica, "A Finite element method for casting simulation," Numerical Heat Transfer A, vol.36, 1999, pp.657-697.

[35] C. P. Hong, S. Y. Lee, and K. Song, "Development of a new simulation method of mold filling based on a Body Fitted Coordinate system," The Iron and Steel Institute of Japan International, vol. 42, no. 9, 2001, pp.999-1005.

[36] S. Y. Lee, N. H. Nam, D. H. Roh, S. B. Kim, and C. P. Hong, "Mold filling simulation based on the Body fitted coordinate system in an unstructured grid system," Proceedings of Modeling of Casting, Welding and Advanced Solidification Processes-XI, Opio, 2006, pp. 95-102.

[37] J. Thompson, Z. Warsi, and C. Wayne Mastin, *Numerical Grid Generation: Foundations and Applications*, Elsevier, Amsterdam, 1985.

[38] J. H. Ferziger and M. Perić, *Computaional methods for fluid dynamics*, 3rd ed., Springer, 2002.

[39] N. Weatherill and C. Forsey, "Grid generation and flow calculations for complex aircraft geometries using a multi-block scheme," AIAA-84-1665, 1984.

[40] J. Rantakokko, "Partitioning strategies for structured multiblock grids," Parallel Computing, vol. 26, no. 12, 2000, pp. 1661-1680.

[41] B.L. Muir and B.R. Baliga, "Solution of three dimensional convection-diffusion problems using tetrahedral elements and flow orientated upwind interpolation functions," Numerical Heat Transfer, vol. 9, 1986, pp. 143-162.

[42] J. Peraire, M. Vahdati, K. Morgan, and O. C. Zienkiewicz, "Adaptive remeshing for compressible flow computations," Journal of Computational Physics, vol. 72, 1987, pp. 449-466.

[43] D. De Zeeuw and K. Powell, "An adaptively refined Cartesian mesh solver for the Euler equations," Journal of Computational Physics, vol. 104, no. 1, 1993, pp. 56-68.

[44] M. Delanaye, A. Patel, B. Leonard, and C. Hirsch, "Automatic unstructured hexahedral grid generation and flow solutions," ECCOMAS CFD 2001, Institution of Mathematics and its Application, UK, 2001.

[45] D.M. Ingram, D.M. Causon, and C.G. Mingham, "Developments in Cartesian cut cell methods," Mathematics and Computers in Simulation, vol. 61, 2003, pp.561–572.

[46] P.G. Tucker and Z. Pan, "A Cartesian cut cell method for incompressible viscous flow," Applied Mathematical Modelling, vol. 24, 2000, pp. 591-606.

[47] B. Epstein, A.L. Luntz, and A. Nachshon, "Multi-grid Euler solver about arbitrary aircraft configurations with Cartesian grids and local refinement," AIAA-89-1960, 1989, pp. 312-321.

[48] R.J. Smith, "Automatic grid generation for compressible Navier-Stokes solvers in aerodynamics design for complex geometries," Ph.D. Thesis, Institute of Science and Technology, University of Manchester, 1996.

[49] G. Yang, D.M. Causon, D. M. Ingram, R. Saunders, and P. Batten, "A cartesian cut cell method for compressible flows part A: Static body problems," Aeronautical J. vol. 2, 1997, pp. 47-56.

[50] G. Yang, D. M. Causon, and D. M. Ingram, "Calculation of compressible flows about complex moving geometries using a 3D Cartesian cut cell method," Int. J. Numer. Methods Fluids, vol. 33, 2000, pp. 1121-1151.

[51] Meng-Hsuan Chung, "Cartesian cut cell approach for simulating incompressible flows with rigid bodies of arbitrary shape," Computers & Fluids, vol. 35, 2006, pp. 607-623.

[52] Pengzhi Lin, "A fixed-grid model for simulation of a moving body in free surface flows," Computers & Fluids, vol. 36, 2007, pp. 549-561.

[53] Jinho Mok, C.P. Hong, and J. Lee, "Development of a new simulation method of mold filling and solidification based on the SIMPLER algorithm," The Iron and Steel Institute of Japan International, vol. 43, no. 8, 2003, pp. 1206-1212

[54] D. B. Kothe and R. C. Mjolsness, " RIPPLE: A new model for incompressible flows with free surfaces," AIAA/NASA/OAI Conference on Advanced SEI Technologies, Cleveland, 1991.

[55] M. Jeancolas, G. C. de Lara, and H. Hanf, “Hydrodynamics study of horizontal gating systems,” AFS Transactions, vol. 70, 1962, pp. 503-512.

[56] M. N. Srinivasan and V. Kondic, “Progress in the hydraulics of gating,” The British Foundryman, 1963, pp.426-432.

[57] P. D. Webster, “Study of the flow of metals in runners,” The British Foundryman, 1967, pp. 314-319.

[58] Ho-Young Hwang, Cheol-Hee Nam, Young-Sim Choi and Jun-Ho Hong, "A study on effects of the filter on flow pattern of the traditional gating system by the water modeling experiment," Journal of Korea Foundry Society, Vol. 36, No. 6, 2016, pp. 208-214.

[59] R. Cuesta, J. A. Marato, D. Morinigo, I. de Castro, and D. Mozo, “Water analogue experiments as an accurate simulation method of the filling of gravity castings,” AFS Transactions, vol. 114, 2006, pp. 137-149.

[60] Ricardo Fuoco, Carlos S. Cabezas, Edison R. Correa, and Marcelo A. Bastos, “Study on gating system design for aluminum gravity castings using water models,” 1st International

Conference on Gating, Filling and Feeding of Aluminum Castings, 1999, pp. 65-86.

[61] P. Cleary, J. Ha, V. Alguine, and T. Nguyen, "Flow modelling in casting processes," Applied Mathematical Modelling, vol. 26, 2002, pp. 171–190.

[62] Ho-Young Hwang, Jun-Ho Hong , Young-Sim Choi, and Jeong-Kil Choi, "Three dimensional image reconstruction technologies for casting process by water modeling," Modeling of Casting, Welding and Advanced Solidification Processes - XI, France, TMS, 2006, pp. 135-142.

[63] P. Sivaraman, "Experimental stuides on flow of molten metal through gating systems using water models," International Journal of Research in IT, Management and Engineering, Vol. 5, No. 5, 2015, pp. 42-49.

[64] V. Jaiganesh and K. Prakasan, "Hydraulics, dimensional analysis and visualization of flow through unpressurized gating systems using water models," Engineering Journal, vol. 20, no. 1, 2016, pp. 135-185.

DOI: 10.4186/ej.2016.20.1.165

[65] Ki-Young Kim, "Die casting die designing (II) - Design of overflow and gas vent," Journal of Korea Foundry Society, vol. 19, no. 3, 1999, pp. 277-283.

국문초록

주조 유동 해석 분야에서 형상고정 격자의 적용은 양질의 해석결과를 얻을 수 있음에도 불구하고 격자 생성의 어려움과 낮은 효율성으로 인해 사용에 어려움이 있다. 이에 대한 대안으로 Cartesian 격자 기반 주조 유동 수치기법이 많이 개발되어 왔다. 그러나 많은 경사와 곡면을 가진 복잡한 주조 제품은 Cartesian 격자에서 형상 표현이 제대로 되지 않는다. 형상과 일치하지 않는 계단 격자는 유동 중의 운동량 손실과 잘못된 충전 거동 등, 유동해석 결과에 불건전한 결과를 초래한다.

본 연구에서는 이러한 문제를 해결하기 위해 Cartesian 격자에서 PCT(partial cell treatment)를 기반으로 하는 Cut Cell 방법을 주조 유동 해석에 적용하였다.

개발한 수치 방법은 수모델 실험 및 실제 주조 실험과의 비교를 통하여 유효성을 검증하였다. Cartesian 격자에서 기존 방법과 Cut Cell 방법을 비교 연구하였다. 격자수에 따른 두 방법의 수치 결과를 비교해보고 격자수의 증가가 직교 격자의 단점을 해결하지 못함을 확인하였다. 또한 주조 공정별로 실제 주조품을 해석해 보았다. 기존 방법에서 나타난 해석 오류가 Cut Cell 방법에서 해결되는 것을 확인하였다. 마지막으로 기존 방법과 Cut Cell 방법의 계산 시간을 비교하였다.

결론적으로, 직교격자에서 BFC 의 적용 없이 Cut Cell 방법을

사용하여 좀 더 정확한 주조 유동 해석이 가능함을 확인하였다. Cut Cell 방법은 기존의 방법보다 정확도가 향상되지만 계산 시간이 오래 걸리고, 주조품의 형상이나 공정에 따라 기존 방법과 Cut Cell 방법의 결과가 가시적인 차이가 없는 경우가 있다. 그러므로 주조 유동 해석을 할 때, 해석의 정확도와 효율성을 고려하여 직교 격자에서 기존의 방법과 Cut Cell 을 적용한 방법을 선별적으로 사용할 필요가 있다.

주요어: 주조공정, 주조유동해석, Cut Cell, 직교격자계, 정확도, 충전 패턴, 수모델 실험

학번: 2009-30173

성명: 최영심